OPTIMIZATION OF PHOTOCATALYTIC DEGRADATION OF WASTEWATER USING OXIDE AND NON-OXIDE PHOTOCATALYSTS

Caressa Munien

A dissertation submitted in fulfillment of the academic requirement for the degree of **Master of Engineering in the Department of Chemical Engineering. Green Engineering Research Group,** Faculty of Engineering and the Built Environment at Durban University of Technology

Supervisor: Prof Sudesh Rathilal

Co-Supervisor: Dr Emmanuel Kweinor Tetteh

February 2025

Preface

This master's study was experimentally conducted with the DUT's Green Engineering Research Group under the Department of Chemical Engineering, South Africa. The candidate was a full-time registered master's student under the supervision of Prof Sudesh Rathilal and Dr Emmanuel Tetteh. The study used effluent from a local South African Municipal wastewater treatment plant in Durban, Kwazulu-Natal. The dissertation has five chapters compiled and discussed with the author's published and unpublished journal papers.

Declaration

I, **Caressa Munien**, the undersigned candidate, declare that,

I. The research reported in this thesis, except where otherwise indicated, is my original work.

II. This thesis has not been submitted for any degree or examination at any other university.

III. This thesis does not contain other persons' data, pictures, graphs, or other information unless specifically acknowledged as being sourced from others.

IV. This thesis does not contain other persons' writing unless specifically acknowledged as being sourced from other researchers. Where other written sources have been quoted, then:

   a. their words have been re-written, but the general information attributed to them has been referenced.

   b. where their exact words have been used, and their writing has been placed inside quotation marks and referenced.

V. Where I have reproduced a publication of which I am an author, co-author, or editor, I have indicated in detail which part of the publication was written by myself alone and have fully referenced such publications.

VI. This thesis does not contain text, graphics, or tables copied and pasted from the Internet, unless specifically acknowledged, and the source is detailed in the dissertation and the References sections.

Caressa Munien:

Sign: Date: 20/02/2025

As the candidate supervisor, I do agree to the submission of this thesis:

Prof. Sudesh Rathilal:

Sign: Date: 25/02/2025

As the candidate supervisor, I do agree to the submission of this thesis:

Dr. Emmanuel Tetteh:

Sign: Date: 20/02/2025

Acknowledgments

I want to acknowledge God, my dear family, and my supervisors, the Acting Executive Dean, Prof Sudesh Rathilal, and Dr Emmanuel Tetteh, for this highly sacred and accomplished moment. Also, my thanks to the DUT Scholarship scheme.

Dedication

As a young female taking on the engineering field came with several challenges and fears. From working long 12-hour night shifts, shutdowns, lifting heavy machinery, working in a male-dominated environment at SAPREF Refinery, the largest crude oil refinery in sub-Saharan Africa, managing large industrial designated sites, climbing ladders whilst afraid of heights, etc. All whilst starting work experience as a 19-year-old young female. I have never given up through all the challenging times and proved my resilience and strength. It has only made me the best version of myself personally and professionally.

Therefore, taking on my master's has been a privilege and honor. Having been given this opportunity is truly a blessing to me from God. It truly reflects who I am, all my strengths, and my career thus far. It drives me even more to my highest potential; it feeds the hunger of my curious mind to discover new things and continuous growth. This study and field of wastewater treatment also gives me deep satisfaction and peace of mind, knowing that I am contributing to assisting the planet, the environment, and aquatic life to heal from all the sickness that mankind has spread over their anthropogenic activities towards remediation and sustainability. I know I am on my righteous path and wish to continue to positively influence the world while nourishing Mother Nature and her beautiful creations.

This work was dedicated to Caressa Munien.

I have conducted this study and experimental test work with utmost integrity, and I hope it has been translated with due respect.

Yours sincerely

Caressa

Abstract

Wastewater treatment is a global concern, especially in developing countries with limited access to safe and clean facilities, resulting in individuals practicing unsafe and unsustainable human practices. This poses challenges for South African wastewater treatment plants (WWTPs) due to the aging infrastructures and the use of conventional technologies. Also, recent population growth, urbanization, and industrial activities have given rise to contaminating water resources with recalcitrant organic micropollutants (OMPs). Organic micropollutants cause severe environmental pollution, imbalanced ecosystems (aquatic life), human health risks, and oxygen depletion due to accelerated chemical oxygen demand (COD). Apart from the detrimental effects of wastewater on human health and the ecosystem, the United Nations (UN) sustainability development goal of obtaining clean water and sanitation (SDG #6) by 2030 is continuously threatened. Therefore, treating wastewater for reuse in the environment with good quality comes in handy.

Against this background, photocatalysis, such as the advanced oxidation process (AOP), is reported as a promising, eco-friendly, and cost-effective technology for degrading organic contaminants (COD) into harmless compounds. However, the TiO_2-based photocatalytic process has setbacks, such as recoverability and treatability efficiency, limiting its industrial application. Therefore, this study explored oxide and non-oxide photocatalysts as alternatives to TiO_2-based photocatalytic processes for a local South African wastewater treatment. The photocatalysts considered were Titanium dioxide (TiO_2), Iron (III) oxide (Fe_2O_3), Zinc Sulphide (ZnS), and Copper Sulphide (CuS). Their applicability was conducted experimentally by evaluating and optimizing the performance of oxide (TiO_2, Fe_2O_3) and non-oxide (ZnS, CuS) photocatalysts under UV, UV-visible, and natural sunlight irradiation.

The One-Factor-at-a-Time (OFAT) approach was used on the photocatalytic system to identify the relationship between the variables that influence the photocatalytic degradation treatment of municipal wastewater. The water quality parameters considered were pH, turbidity (NTU), colour (Pt. Co), and COD (mg/L). By employing the oxides and non-oxides under a constant UV irradiation light source

and OFAT approach, the catalyst load (0.5-2.5 g/L), mixing speed (30-150 rpm), and exposure time (10-60 minutes) were investigated. Among the photocatalysts, CuS displayed the best results overall for above 50% COD removal efficiency, whilst ZnS was also efficient in removing above 50% turbidity and colour at a catalyst load of 1.5 g/L, mixing speed of 90 rpm, and UV exposure time of 45 minutes. It was established that CuS was the cheapest at R2.01/1.5g as compared to TiO_2 at R32.47/1.5g.

Subsequently, the photocatalysts were investigated using three different light sources: UV, UV-visible, and sunlight irradiation. UV-visible was the most favourable at a catalyst load of 1.5 g/L, mixing speed of 90 rpm, and irradiation time of 60 minutes. Thus, the high light intensity of UV-visible, 191,000 Lux, enhanced the photocatalytic performance of the four photocatalysts under this study, with the optimum COD removal values at 72.25%, 70.87%, 70.20%, and 46.66% for Fe_2O_3, ZnS, CuS, and TiO_2 respectively.

Furthermore, response predictive models were developed as a function of the input factors of the photocatalytic system for the treatment of municipal wastewater. This was done utilizing the response surface methodology (RSM) via the Box Behnken design (BBD) with the best-performing catalyst (CuS) and the best light source (UV-visible), at the optimal conditions of catalyst load of 2 g/L CuS, a mixing speed of 120 rpm, and an exposure time of 30 minutes with treatability desirability of 96%. The selected optimal condition was then validated experimentally, and the results obtained were agreeable with the model-predicted values at 95% confidence levels.

Moreover, a comparative study with CuS and TiO_2 was evaluated with synthetic wastewater (SW) and raw wastewater (RW) at the optimal conditions. The results by CuS demonstrated above 55% COD, turbidity, and colour removal from both the SW and RW compared to the TiO_2, which obtained below 35% removal from both SW and RW. Therefore, under the conditions investigated in this study, CuS was found to be the most cost-effective and viable photocatalyst alternative to TiO_2 for wastewater treatment. However, the techno-economic and life cycle assessment must be explored to encourage the prospects of the CuS in the water settings.

Research outputs and knowledge dissimilation

This dissertation is based on the author's published and unpublished journal papers. The candidate was the first author of all the papers and presented them at local conferences.

All publications and conferences were directly linked to this study's objectives and provided supporting information for compiling the dissertation chapters.

List of journal publications:

1. Munien, C., Kweinor Tetteh, E., Govender, T., Jairajh, S., Mguni, L. L. and Rathilal, S. 2023. Turbidity and COD removal from municipal wastewater using a TiO_2 photocatalyst—a comparative study of UV and visible light. Applied Sciences, 13 (8): 4766. https://doi.org/10.3390/app13084766

2. Munien, C., Kweinor Tetteh, E., and Rathilal, S. Kinetic and Synergistic effect of semiconductor photocatalysts for wastewater treatment: Water Practice and Technology (Ref No. WPT-D-24-00325, submitted under review)

3. Munien, C., Kweinor Tetteh, E., and Rathilal, S. Advanced oxidation processes for wastewater treatment: Challenges and prospects of TiO_2 photocatalysis: Electrochemistry Communications (Ref No. EC24-11. Submitted under review)

4. Munien, C., Kweinor Tetteh, E., and Rathilal, S. Response Surface Methodology: Optimization of photocatalytic degradation process parameters for COD removal using CuS photocatalyst and UV-vis irradiation (Ref No. ESE-2024-10-0717, submitted under review)

5. Munien, C., Kweinor Tetteh, E., and Rathilal, S. Semiconductor Photocatalytic degradation (AOPs) for wastewater treatment: A critical review highlighting the various strategies to boost the photocatalytic performances (Anticipate publication by September 2025)

List of conference papers:

1. Munien, C., Kweinor Tetteh, E., and Rathilal, S. Evaluating the performance of various semiconductor photocatalysts for municipal wastewater treatment - effects of photocatalyst type and dosage. 39th JOHANNESBURG Int'l Conference on ''Chemical, Biological and Environmental Engineering'' (JCBEE-23) Nov. 16-17, 2023, Johannesburg (South Africa) ''Birchwood Hotel & OR Tambo Conference Center, Address: 14 View Point Rd, Bardene, Boksburg, 1456, South Africa. Conference Hall'' Candlewo

2. Munien, C., Kweinor Tetteh, E., and Rathilal, S. Effect of the light source on the performance of oxide and non-oxide transition metal photocatalysts – A comparative study of UV, UV-vis and sunlight. ENERGYWATERFOODCLIMATE NEXUS INTERNATIONAL SUMMIT 2024, Jul. 1-4, 2024, Durban South Africa ‘‘Coastlands Hotel’’.

3. Munien, C., Kweinor Tetteh, E., and Rathilal, S. Investigating the effect of irradiation light source on the performance of oxide and non-oxide transition metal photocatalysts– A comparative study of UV, UV-vis, and sunlight. 41st CAPE TOWN International Conference on “Chemical, Biological and Environmental Engineering” (CCBEE-24). Nov 21-22, 2024, CAPE TOWN LODGE HOTEL & Conference center Address, 101 Buitengracht Street, Cape Town 8001, South Africa

Table of Contents

List of Figures

List of Tables

Nomenclature

ANOVA	Analysis of variance
AOP	Advanced Oxidation Process
BBD	Box-Behnken Design
COD	Chemical Oxygen Demand
DBPs	Disinfection Byproducts
DCs	Developing Countries
DOE	Design Of Experiment
EDCs	Endocrine-Disrupting Chemicals
L-SPR	Laboratory-Scale Photochemical Reactor
MW	Municipal Wastewater
NTU	Nephelometric Turbidity Units
OFAT	One Factor at A Time
OMPs	Organic Micropollutants
PDWT-CUV	Photocatalytic Degradation Wastewater Treatment using a Constant UV light source
PPCPs	Personal Care Products
RSM	Response Surface Methodology
RW	Raw Wastewater
SA	South Africa
SDG	Sustainable Development Goals
SSA	Sub-Saharan Africa
SW	Synthetic Wastewater
UN	United Nations
UV	Ultraviolet
UV-vis	Ultra-Violet Visible
WW	Wastewater
WWM	Wastewater Management
WWT	Wastewater Treatment
WWTPs	Wastewater Treatment Plants

CHAPTER ONE
INTRODUCTION

1.1 Background

Water pollution threatens the populace's health, biodiversity, and the ecological environment. A significant amount of wastewater (WW) with little to no treatment is present in the environment as a result of anthropogenic activities' continuous generation of WW (Sarwar et al. 2020; Torrens et al. 2020). Approximately 90% of WW that is generated is discharged into the environment without any treatment (Adams, Sambu and Smiley 2019). About 65% of the 850 million people who reside in sub-Saharan Africa (SSA) lack access to clean, safe drinking water. Concerns among stakeholders in the region have centered mostly on the absence of good-quality drinking water for the general public, with ineffective treatment facilities (Onu et al. 2023). Notwithstanding, most water resources, such as rivers, dams, and oceans, due to inadequate wastewater treatment facilities (failure to test, treat, and supply drinking water), are deteriorating their water quality (Toxopeüs 2019; Kretzmann 2022). Poor WW and sewage water quality are major causes of environmental contamination in the majority of African countries (Quansah, Ntaryamira and Rwemera 2018). Also, lack of improved sanitation and poor wastewater management (WWM) pose a threat to waterborne diseases such as cholera, malaria, diarrhea, hepatitis, and other water-related epidemics come with a high mortality rate in SSA (Yang et al. 2020; Mutono et al. 2021). Water quality issues affect Sub-Saharan Africa (SSA) and other developing nations practically year-round (Zhang and Shen 2019). The outbreak of waterborne diseases is caused by the infectious microorganisms that proliferate in these bodies of water (Zerbo, Delgado and González 2020).

Organic micropollutants (OMPs) found in water bodies have recently emerged as a major global issue due to their occurrence, persistence, and toxicity in aquatic environments. OMPs include industrial compounds, disinfection byproducts (DBPs), endocrine-disrupting chemicals (EDCs), pharmaceuticals and personal care products (PPCPs), pesticides, E. coli, potentially toxic elements, steroids, etc., and are employed in a wide range of settings, such as agriculture, industry, animal husbandry, medicine, and daily life (Madikizela, Ncube and Chimuka 2020). These OMPs have been found all over the world in a variety of water bodies, such as rivers, lakes, and

coastal seawaters. (Madikizela, Ncube and Chimuka 2020). Given that, OMPs are harmful to aquatic species, such as bacteria, algae, invertebrates, and fish, due to their unpredictable interactions with these creatures (Rozas et al. 2017). For instance, the formation of antibiotic-resistant bacterial strains is a direct result of drug residues and has the potential to cause serious illnesses, such as bloodstream infections, lower respiratory tract infections, and urinary tract infections (Sanganyado and Gwenzi 2019). Furthermore, even at low concentrations, long-term exposure to OMPs raises the ecological danger to aquatic life in the water environment (Guo et al. 2023). The significant effects of OMPs on aquatic life, animals, and humans require them to be removed from wastewater before being discharged into water bodies (oceans, rivers, lakes, reservoirs) (Jabbar and Graimed 2022).

To achieve the Sustainable Development Goals (SDGs #6 clean water and sanitation), all stakeholders (government, academic and research institutions, and international agencies) must collaborate proactively to reduce water-related concerns in SSA (Onu et al. 2023). Many pharmaceutical compounds have been added to the EU Water Framework Directive's Watch List, which previously included certain emerging OMPs (Gomez Cortes et al. 2022). Furthermore, the US EPA updated its Drinking Water Contaminant Candidate List 4 with several pharmaceutical compounds and Endocrine-Disrupting Chemicals (EDCs) that pose a threat to human health and the environment (Sharma, Ahmad and Flora 2018). However, the lists do not pose legal ramifications for the release of OMPs into surface waters, they help to emphasize the importance of controlling these substances in WWTP effluents (Murtaza et al. 2023).

Conventional wastewater treatment techniques have been challenged and are progressively failing to satisfy the increased demand for clean water. Some of these conventional technologies include biological treatment, physio-chemical treatment, membrane filtering, absorption, and oxidation. However, these technologies possess several drawbacks: (i) they are unable to efficiently break down and remove a wide range of organic pollutants; (ii) there is secondary pollutant generation, slurry, and sludge formation; (iii) they require pre-treatment or post-treatment steps to mineralize the pollutants found in wastewater entirely; (iv) some pollutants or contaminants require external chemicals; (v) these processes usually consume large amounts of energy; (vi) they necessitate routine maintenance and are; (vii) expensive (Mishra and Sundaram 2023) (Refer to Table 2-3). Consequentially, the need for highly efficient

remediation techniques and materials is essential to reduce the long-lasting harmful impact of these pollutants on the environment and humans and to meet the required standards for water quality (Kakavandi and Ahmadi 2019; Mishra and Sundaram 2023). Hence, exploring advanced oxidation technology is crucial as the development of effective removal technology for OMPs has drawn interest from all around the world.

1.2 Photocatalysis

Photocatalysis (advanced oxidation process) has been explored in wastewater treatment settings with great potential for the remediation of wastewater by the degradation of recalcitrant organic pollutants (Ren et al. 2021). Photocatalysis involves the acceleration of the rate of chemical reactions in the presence of semiconductor catalysts, radiation (UV/Solar), and pollutants. Photocatalysis is responsible for the complete degradation of many bio-recalcitrant organic pollutants contained in wastewater, into harmless substances such as CO_2 and H_2O or other small molecules (Ram *et al.* 2021). The photocatalytic process can be operated at ambient room temperature and pressure with reduced operating costs and usually does not require additional processes or secondary treatment steps to remove reaction byproducts. These features make the process extremely viable and effective for large wastewater treatment plants (Muscetta, Ganguly and Clarizia 2024).

Numerous factors make it one of the most important and promising methods for treating wastewater, including its low cost, high mineralization efficiency, simplicity, good repeatability, ease of handling, quick oxidation response rate, and lack of secondary pollutants (Yan *et al.* 2024). Moreover, it is a green technology that is nontoxic, energy-efficient, and environmentally beneficial for the complete mineralization of contaminants (Zhang *et al.* 2019b; Ma *et al.* 2021).

TiO_2 is an ideal photocatalyst as it is characterized by its great oxidation ability, low production cost, good stability, and non-toxicity. Its excellent hydrolysis activity under ultraviolet (UV) light and its vast applicability in the photolysis of aquatic hydrogen and the degradation of pollutants have garnered a lot of interest. However, due to its large energy band energy (3.2 eV for the anatase phase and 3.0 eV for the rutile phase) and high electron-hole recombination rate, it can only be utilized under ultraviolet light irradiation (Vaiano *et al.* 2017; Sun *et al.* 2024). Since the majority of photocatalysts are activated by UV light, a constant source of UV light is necessary to maintain the

reaction, which is not a financially feasible option and entails high maintenance expenses (Mishra and Sundaram 2023). Hence, conventional TiO_2 photocatalytic technology possesses several disadvantages that limit its large-scale industrial applications, such as being energy-intensive, utilizing less visible sunlight, having poor separation potential, and having low photocatalyst recyclability and recovery (Saravanan, Gracia and Arumainathan 2017; Koe *et al.* 2020; Sun *et al.* 2024).

Consequently, more efforts to acquire ideal and alternative photocatalysts and promote the industrial application of photocatalytic technology have become significant for the reclamation of wastewater (Opoku et al. 2017).

1.2.1 Limitations of TiO_2-based photocatalysts on organic compounds in wastewater

Figure 1-1 highlights and describes the limitations of TiO_2-based photocatalysts on organic molecules in wastewater (Chen et al. 2020b).

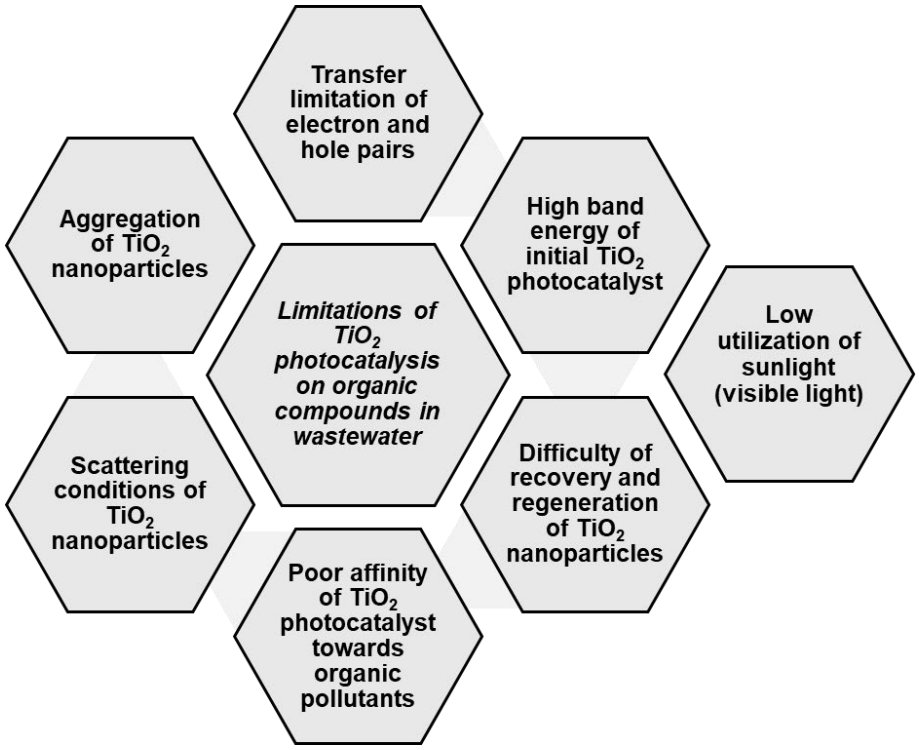

Figure 1-1: Restrictions of TiO_2-based photocatalysts on organic substances in wastewater (Chen et al. 2020b)

I. High electron-hole recombination rate (poor separation potential)

TiO_2 is mostly degraded by photocatalysis on its surface, and TiO_2 photocatalytic efficacy is reduced by transfer limitations of electron and hole pairs. Therefore, inhibition of photocatalytic activity in TiO_2 is likely caused by the recombination of electron and hole charge carriers (Kusiak-Nejman and Morawski 2019). Therefore, TiO_2 must be modified. Modification can alter TiO_2's broadband gap, improve light absorption, and impact key photocatalytic efficiency indicators. Some modification strategies of TiO_2, include doping modification, construction of heterojunctions, crystal plane engineering, and defect engineering (Yang et al. 2024).

II. Energy-intensive (Large band gap energy)

TiO_2 photocatalyst is considered less energy-efficient than a standard heterostructure photocatalyst (composite material made from two or more components with different or similar chemical properties that can create charge carriers when exposed to light) as its decomposition processes are driven by sunlight (Raza et al. 2020). To enable the development of visible/solar light to activate TiO_2-based photocatalysts, more research must be done on improving the photocatalyst's physical and chemical properties. To boost affinity for organic molecules and promote visible light wavelength, the TiO_2 particle size, dopant type, and concentration must be adjusted to get around these restrictions. Secondly, suitable substrates with a high TiO_2 nanoparticle separation capacity must be efficiently recovered and regenerated. Thirdly, for photocatalysis optimization, the photocatalysis environments or other elements like light intensity, calcination temperature, pH, and significant additions need to be assessed.

III. Low utilization of sunlight (visible light)

The photocatalytic efficiency and performance of TiO_2 under visible-light irradiation are critically restricted by rapid electron-hole (e^-/h^+) recombination and the absorption edge in the UV range. Low photocatalytic activity under sunlight is caused by TiO_2's intrinsic large bandgap and inadequate separation of photoinduced charges, which limits its absorption toward visible light, which is the core portion of the solar spectrum (Mohadesi, Sanavi Fard and Shokri 2022). To boost efficiency at the industrial levels, visible light-sensitive photocatalysts with the lowest recombination of photocarriers are required. TiO_2-based S-scheme heterosystems have emerged as the most promising

candidates due to their low charge recombination loss, strong redox ability, and high performance (Ahmad et al. 2024).

IV. Aggregation of TiO_2 nanoparticles

During photocatalytic degradation, TiO_2 nanoparticles may combine due to the instability of the nanosized particles. This could impede the photocatalytic activities of TiO_2 by obstructing the light radiation reaching the active centers. TiO_2 aggregates as a result of organic ionizable molecules bridging the particles (Chen et al. 2020a).

V. Scattering conditions of TiO_2 nanoparticles

TiO_2 photocatalytic activity reduction may be caused by higher scattering circumstances brought on by TiO_2 nanoparticles. To increase the photocatalytic activity, the right UV wavelengths and TiO_2 concentration are essential (Chen et al. 2020a).

VI. Poor affinity of TiO_2 photocatalysts

Low adsorption of organic pollutants on the TiO_2 surface resulted in slow photocatalytic breakdown rates. This is due to photocatalysts' poor affinity for organic pollutants. Immobilization of photocatalysts can offer a specific affinity for the pollutants of interest (Lee et al. 2018).

VII. Difficulty of recovery and regeneration of TiO_2 nanoparticles

Efficient and safe recovery of nanosized TiO_2 particles from treated wastewater is a significant practical barrier for organic compound treatment. TiO_2 nanopowder is said to be more effective than fixed support and to be well distributed in suspension. However, retrieving the dissolved particles from the treated effluent is a practical difficulty pertinent to its applications (Chen et al. 2020a).

1.2.2 Potential for Oxide/Non-oxide semiconductors

A significant type of advanced oxidation processes (AOPs) for addressing energy scarcity and environmental pollution are semiconductor-based photocatalytic reactions. Semiconductor-based photocatalysis emerges as a profoundly promising avenue (Morshedy *et al.* 2024). This technique has many benefits, such as high efficiency, environmental friendliness, and cheap cost, since it uses solar energy, which is a clean, plentiful, and a renewable source (Goodarzi et al. 2023). Semiconductors are a broad class of materials with multiple applications. Many

semiconductors have light absorption capabilities, electrical structures, and charge transport characteristics that make them very useful photocatalysts. Several evaluations conducted in the last few decades have emphasized their application in air purification, hydrogen production, photocatalytic disinfection, wastewater treatment, and CO_2 reduction (Khodabandeloo et al. 2023).

The most notable characteristics of semiconductor materials are their processability, high chemical stability, electron-hole pair separation, narrow and intense emission spectra, continuous absorption bands, bandgap, large surface area, and functionality and reusability (Ahmad *et al.* 2023). These unique properties of semiconductor nanoparticles, like WO_3, CuO, ZnO, ZrO_2, TiO_2, NiO, and ZnO, have been identified as significant photocatalysts, especially for the degradation of organic pollutants (Kannan et al. 2020).

1.3 Problem statement

The duo of water and energy crises are challenges that have spurred the global movement towards sustainable water and wastewater remediation techniques to achieve the increasing demands for clean water and minimize the negative environmental effects (Shehata et al. 2023; Agbajor and Mewomo 2024). Water stress is a major concern as many cities worldwide face a rapidly depleting potable water supply. Herein, South Africa is the epitome of these challenges (Xaba 2023). As population growth, urbanization, and industrialization accelerate, the demand for non-renewable sources increases. Consequentially, organic micropollutants (OMP) and their derivatives such as disinfection byproducts (DBPs), endocrine-disrupting chemicals (EDCs), pharmaceuticals and personal care products (PPCPs), pesticides, E. coli, potentially toxic elements, etc. are discharged as wastewater in colossal amounts (Mishra et al. 2023). Most of these pollutants are bio-recalcitrant and detrimental to human health and aquatic life. Their removal is, therefore, essential for environmental protection and wastewater reclamation (Mecha et al. 2016; Archer, Wolfaardt and Van Wyk 2017; Bio-Sol 2021).

The conventional treatment technologies applied in wastewater decontamination, such as membrane filtration, adsorption, coagulation, flocculation, etc, come with many drawbacks, such as secondary pollution, incomplete removal of organic pollutants, inefficient and non-destructive to some or most persistent organic pollutants

and cost implications (Mecha et al. 2016). In essence, photocatalysis (advanced oxidation process) has been explored in wastewater treatment settings with great potential for the remediation of recalcitrant pollutants (Ren et al. 2021). However, traditional TiO_2 photocatalytic technology possesses several disadvantages, which limit its industrial applications, as mentioned above in Section 1.2.1 (Saravanan, Gracia and Arumainathan 2017; Koe et al. 2020). Consequently, the greatest challenge to accomplishing adequate wastewater remediation is maximizing the overall efficiency of existing wastewater treatment (WWT) systems (Zhang *et al.* 2019b).

Photocatalysis (AOPs) possesses major prospects in WWT settings if a suitable photocatalyst is considered. Hence, exploring alternative visible light stable photocatalysts that are highly efficient in improving photocatalytic efficiency is crucial to address OMP concerns in South Africa's wastewater streams and for the reclamation of wastewater technology (Opoku et al. 2017).

Therefore, this research evaluated the effects of various semiconductor photocatalysts and the photocatalytic performance using various irradiation sources to maximize contaminant removal from wastewater. The performance of the photocatalysts was investigated by varying influential operating parameters at the respective light source with respective physical wastewater quality characteristics before and after the treatment process. Additionally, to supplement the effectiveness of the photocatalytic degradation process, process parameters were optimized using the design of experiment (DOE) based on response surface methodology (RSM). The RSM, as an effective optimization tool was used to identify and understand the relationship that existed between multivariable responses (water quality) using quantitative data obtained from the experimental design (Rajendran et al. 2022).

Furthermore, inadequate research was done on maximizing various photocatalytic degradation process parameters. Thus, there was limited information on simulating experimental data to establish a relationship between the input parameters as a function of the response water quality depending on the water source. Therefore, an optimization strategy for the wastewater treatment process was required to enhance the quality of the water for reuse. These research findings accelerated the development of innovative photocatalysis novel materials into the forefront of sustainable wastewater treatment and contributed to green and sustainable

technology for wastewater treatment and mitigation of environmental challenges in the South African water sector.

1.4 Aims and objectives

This study involved experimental research that aimed to investigate/optimize the performance of oxide (TiO_2, Fe_2O_3) and non-oxide (CuS, ZnS) transition metal photocatalysts using UV, UV-visible, and natural sunlight for municipal wastewater treatment. The measures for removing COD, turbidity, and colour were used as the key performance indicators. One factor at a time (OFAT) approach and RSM were employed to evaluate the following specific objectives:

Objectives:

1. To investigate the applicability and performance of oxide (TiO_2 and Fe_2O_3) and non-oxide (CuS and ZnS) transition metal photocatalysts for municipal wastewater treatment. The parameters investigated were catalyst load (0.5-2.5 g/L) at increments of 0.5 g/L, mixing speed (30-150 rpm) at increments of 30 rpm, and exposure time (60 minutes) at 10-minute time intervals.
2. To investigate the effect of light sources (UV, UV-visible, and natural sunlight) on the performance of photocatalytic degradation of municipal wastewater.
3. To optimize the operating conditions of the photocatalytic process using the best catalyst and light source with response surface methodology (RSM). The input parameters investigated were catalyst load, mixing rate, and exposure time.

1.5 Approach

In this study, a wastewater sample was obtained from a local South African Municipal wastewater treatment plant based in Durban, Kwazulu-Natal province, where the following five water quality parameters were analyzed and utilized as a performance criterion which included pH, turbidity (NTU), colour (Pt. Co), and COD (mg/L). A six-place jar testing apparatus was used for the photocatalytic degradation wastewater treatment using a constant UV light source (PDWT-CUV) experiment. The performance of the photocatalysts was investigated using an OFAT approach by varying catalyst load (g/L), mixing speed (rpm), and exposure time at a constant light source for each proposed catalyst. The optimal catalyst load and mixing speed determined at this stage were used to investigate Objective 2.

A laboratory-scale photochemical reactor (L-SPR) was used for the experiment (Objective 2). The effect of light sources (UV, UV-visible, and natural sunlight) on the above-mentioned photocatalysts was evaluated for an exposure time of 45 minutes using the optimal catalyst load and mixing speed as mentioned above. To establish the degradation trend for each light source, samples were taken every 10 minutes for analysis.

The third objective was carried out using the experimental Box-Behnken design (BBD) matrix adapted from the response surface methodology (RSM) obtained from the Design Expert Software (version 13.0.5.0). The experiments were conducted according to the generated BBD matrix with the most effective photocatalyst, which was efficient and economically viable. Using three input factors, catalyst load (g/L), exposure time (minutes), and mixing rate (rpm), the RSM generated 15 runs. The experimental matrix had duplicates and centre points with response outputs (COD, turbidity, and colour). This was statistically analyzed to develop an empirical model to establish the relationship between the input variables and the response water qualities on the photocatalytic system. Finally, the photocatalytic system's operating parameters were optimized via the numerical optimization technique. The optimized conditions were then validated experimentally with the best photocatalyst and compared with the TiO_2 for the treatment of raw and synthetic wastewater.

1.6 Structure of dissertation

This dissertation consists of five chapters as follows:

Chapter 1: The first chapter provides a brief background and examines the problem statement that motivated this study; it describes the conventional technology and potential for the optimization of Photocatalytic Degradation of Wastewater using Oxide and Non-oxide Photocatalysts emerging technology. It highlights the study's problem statement, aims, objectives, and approaches.

Chapter 2: This chapter describes the need for wastewater treatment on a national and global scale and highlights the impact of water pollution on humans, animals, and the environment. It reviews the literature related to the study where the available and emerging photocatalytic treatment technologies for wastewater are reviewed. It also introduces types of photocatalysts, their shortcomings, the need for improvement concerning municipal wastewater characteristics, and the required key water quality.

It also provides knowledge on the design of experiments, a tool for process optimization.

Chapter 3: This chapter provides the research methodology, including the materials, methods, and descriptions of equipment and processes utilized for the characterization and treatment of the effluent. It also describes the analytical and data simulation approaches for process optimization.

Chapter 4: This chapter imparts the experimental results in a graphical representation for each respective objective. It describes the main findings of the research which are supported by the relevant literature.

Chapter 5: The chapter provides recommendations and a conclusion. It provides a summary of the study's important findings and suggests additional research and factors to be considered when making decisions.

The references section provides full-text references, and the Appendix presents additional information about the study.

CHAPTER TWO
LITERATURE REVIEW

2.1 Introduction

This chapter presents the literature review of photocatalytic degradation of wastewater using oxide and non-oxide photocatalysts related to organic micropollutants (OMP) found in wastewater. It discusses the effects of wastewater pollution on a global scale, the water crisis concerns in South Africa, and the challenges experienced by its municipalities. The effects on the environment, animals, and human health are also emphasized. The review highlights some common organic micropollutants in wastewater. It provides insight into the conventional wastewater treatment techniques used. It describes the mechanisms of TiO_2 photocatalysts for OMPs and the factors affecting photocatalytic degradation. It discusses the fundamental principles of various advanced oxidation processes (AOPs). The review also covers the common classification of various photocatalysts, common preparation methods, and applications of semiconductor photocatalysis for water treatment purposes. The electromagnetic spectrum is also shown to provide a comprehensive understanding of the study by highlighting key concepts using diagrammatical representation. Finally, the response surface methodology and the design of experiments of multiple factor interactions on the response of water quality are provided. The chapter concludes with a summary of the literature review, and the gap in knowledge of this study that forms the basis for optimizing the photocatalytic degradation of wastewater is identified.

2.2 Global water pollution concern

Global water pollution and scarcity issues have harmed people's ability to live a healthy lifestyle in various ways (Mittal, Brajpuriya and Gupta 2023). 80% of all diseases, according to the World Health Organization, are linked to inadequate water quality. Concerns include the devastation of natural habitats, deterioration of water, soil, and air quality, and an increase in illness and animal mortality as well as the destruction of biodiversity. Uncontrolled water body contamination and a delay in reducing the amount of harmful wastewater could have detrimental impacts on people, animals, and the ecosystem. When the maximum allowable limit for the concentration of hazardous pollutants is exceeded in a body of water, it poses a threat to both the ecology and the health of those who use the water for domestic and drinking purposes.

Water contamination incidents are becoming more common and serious in several countries, including China, the United States, and Canada (Forest 2012; Qu, Meng and You 2016; Tang et al. 2016; Pulido-Velazquez and Ward 2017; Issakhov, Alimbek and Abylkassymova 2023).

Approximately 2.4 billion people practice poor hygiene, which directly contributes to water pollution, and nearly 12% of the world's population drinks untreated or contaminated water. In 2015, the annual intake of contaminated water by about 1 billion people resulted in 1.8 million deaths due to water pollution (Landrigan et al. 2018). Additionally, as per the United Nations World Water Development Report, there is currently a risk to water security and the ability of a population to maintain sustainable access to sufficient amounts of water that meet acceptable quality standards, and things could get worse in the coming years (Boretti and Rosa 2019). There is a direct relationship between population density and economic expansion and the contamination of water and water resources. In most impoverished nations, almost 90% of sewage waste is dumped directly into untreated water (Connor 2015). About 730 mega tonnes of sewage waste and other runoff are released into the water each year, and between 300 and 400 megatons of waste effluent are released into the water system each year by industrial operations (Connor 2015; Barasarathi, Abdullah and Uche 2022). In India, about 70% of manufacturing effluent is dumped untreated into bodies of water (oceans, rivers, lakes, and reservoirs), impacting groundwater as well.

2.3 Global fate of water pollution

The presence of persistent micropollutants in surface and groundwater has a major negative impact on the environment and human health (Chen et al. 2023). As is well known, there is a worldwide issue with emerging OMPs in WWTP effluents. Nonetheless, the types and quantities of OMPs vary from location to location and are influenced by the population's yearly patterns of OMP use (Murtaza et al. 2023). The most frequent source of OMPs in potable water, according to a review study in fourteen (14) countries in Europe, North America, and Far East Asia, reported that treated sewage water is discharged into surface water by WWTPs (Jiang, Zhou and Sharma 2013). Additionally, a study conducted on the Yangtze River Estuary in China found that the area where a sewage treatment plant discharged treated water had significant quantities of pharmaceutical chemicals, indicating that the plant was ineffective at

eliminating pharmaceuticals (Murtaza et al. 2023). An additional investigation into the existence of EDCs in Iran's Anzali Wetland discovered elevated levels of 4-nonylphenol, octylphenol, and bisphenol A (BPA) in the vicinity. Investigations linked WWTP effluents and industrial waste discharge to the prevalence of these EDCs (Mortazavi et al. 2012). Similarly, an Ontario Ministry of the Environment survey conducted over sixteen (16) months in Canada found that several of the OMPs considered, including pharmaceuticals and EDCs, were found in drinking water. The most commonly detected OMPs in the water were BPA, carbamazepine, gemfibrozil, and ibuprofen (Kleywegt et al. 2011). Moreover, exceedingly high pharmaceutical concentrations in wastewater were found in a thorough analysis of newly emergent OMPs in India. There were observations of 236,950 µg/L for the fungicide fluconazole and 31,000 µg/L for the antibiotic ciprofloxacin. Furthermore, antibiotic-resistant genes were found in drinking water samples from Indian rivers. As per the previously cited study, a primary cause of the elevated levels of pharmaceuticals in drinking water was the ineffectiveness of sewage treatment plants in handling pharmaceutical waste (Philip, Aravind and Aravindakumar 2018). Research that examined the levels of OMPs in WWTP influents and effluents in two distinct Spanish locations found that while there was a little variation in MP concentrations inside and outside of WWTPs, the removal of OMPs from these resources was inefficient (Fernández-López et al. 2016).

In a different investigation, pharmaceuticals, PCPs, and EDs were detected in surface waters close to agricultural areas in northeastern Denmark at amounts of up to 1476 ng/L (Matamoros et al. 2012). Similar to the previously cited study, the ineffectiveness of WWTPs in removing OMPs resulted in high concentrations of OMPs in Berlin, Germany, and Central Greece (Pal et al. 2014; Papageorgiou, Kosma and Lambropoulou 2016). On the other hand, minimal but noteworthy (ng/L) levels of OMPs (pharmaceuticals and PCPs) were found in Milan's drinking water. According to the study, the reason for the low quantities is that groundwater from deep inside the earth is used to supply drinking water (Riva et al. 2018). Similar to Milan, Singapore's drinking water is mainly shielded from OMPs by the fact that WWTP effluents are not released into surface water. Nevertheless, OMPs have been found in Singapore's metropolitan surface waters, although in trace amounts (Murtaza et al. 2023).

2.4 South Africa’s water security crisis

In South Africa, the water treatment landscape is riddled with hurdles. Municipalities need innovative water treatment solutions, from the strain of aging infrastructure to the challenge of load shedding. Amongst rising urbanization rates and stricter environmental regulations, traditional water treatment technologies are struggling to keep up (NuWater 2023). According to Maluleke (2023), President Cyril Ramaphosa addressed the United Nations General Assembly on 19 September 2023 on the unlikeliness of many developing countries not meeting sustainable development goals. He noted this “requires targeted investment, technology transfer, and capacity building support to address development challenges, especially in key areas such as industrialization, infrastructure, agriculture, water energy, education, and health”. Although our country's energy security issues are being addressed, the public frequently pays less attention to water security, a serious concern that is expected to rise over the next 10 years. The recent cholera outbreak in Tshwane and the ongoing water shortages in the Greater Giyani local municipality serve as stark reminders of the devastating results that can occur when the nation's water infrastructure is not sufficiently addressed. Some communities do not receive water or have suffered water outages lasting days or even weeks (Kretzmann 2022). According to the World Bank, in 2022, the proportion of the population utilizing basic drinking water services climbed from 84.58% to 94.49%. According to calculations, the death rate (per 100,000 persons) were attributable to unclean water, poor sanitation, and inadequate hygiene was 27.6 in 2019 (du Plessis 2023a; Smarte Anekwe et al. 2024).

Drought and water cycle disruptions brought on by climate change are expected to worsen throughout Southern Africa in the foreseeable future, according to the International Panel on Climate Change (IPCC). Among the world's driest nations is South Africa. With an annual rainfall average of almost 50% of the global average, it is ranked 29th out of 193 nations by the IPCC. Furthermore, South Africa has been dealing with record-low annual rainfall levels and rising temperatures since 2015. According to IPCC projections, South Africa's range of climate variability will triple by 2050. Furthermore, the nation's reduced chance of precipitation is three to four times greater than its increased risk. In this situation, mitigating the risks to our water security is essential to averting catastrophe (Edokpayi et al. 2020; Leonard 2023; Muyambo et al. 2023).

Wastewater pollution poses a serious risk to human health and is one of the main causes of biodiversity loss, especially for the most vulnerable individuals and ecosystems. However, if adequately treated it can become a valuable resource in addition to providing water security, the safe and effective management of wastewater for resource recovery and reuse may also enhance people's health and well-being, while simultaneously lowering the reliance on synthetic fertilizers. Regretfully, 15% of South Africa's water supply systems were in poor and/or critical condition according to the 2023 Blue Drop Watch report, which assesses water quality compliance and water chemical quality. In addition, 13 water supply systems had no reported data on water quality, which indicates a glaring lack of monitoring, according to the Blue Drop Watch report. This severely violates citizen's constitutional right to clean water and exposes the extreme carelessness and incompetence of national and local governments in maintaining water, sanitation, and hygiene standards and in achieving sustainable development goal six, which strives for universal access to clean water and sanitation (Adom, Simatele and Reid 2023; Anekwe et al. 2024).

These are flaws with the nation's water infrastructure and the lack of progress made in developing climate-resilient water systems through the use of current science and technology. Therefore, to balance the water needs of people, industry, agriculture, and ecosystems, the government must work together across national boundaries (du Plessis 2023b; Maluleke 2023; Steenkamp 2023).

2.5 Challenges of wastewater treatment by South African municipalities

Wastewater treatment is pivotal to avoiding its potential deleterious impact on animals, humans, and the environment. According to Kassegn Weldegebrieal and Kassegn Sibhatu (2022), the expansion of population growth, urbanization, and industrialization have primarily given rise to the contamination of water sources via direct or indirect routes. The contamination of water sources with bio-recalcitrant organic micropollutants that are endocrine-disrupting is detrimental to human health and aquatic life (Mecha et al. 2016). As reported by Toxopeüs (2019), one of the main concerns at the moment is how effectively wastewater treatment facilities are operating. Nearly half (49.6%) of South Africa's 824 wastewater treatment facilities were in critical or poor condition and needed immediate attention, according to the 2013 Green Drop Report. SA’s 144 municipalities are responsible for treating and

supplying drinking water to at least 22 million people. When matched against Stats SA's 2016 Community Survey, 94 failed as of 11 October 2022. Nearly two-thirds of the municipalities in South Africa that are in charge of providing citizens with drinking water either neglect to test the water they distribute or fail to supply water that satisfies the minimal consumption standards. Making matters worse, drinking water quality was seriously compromised in 112 out of 144 (77%) of these municipalities that supply drinking water by overflowing and contaminating primary strategic water resources, such as streams, rivers, dams, and oceans, with untreated or partially treated sewage. In 81 municipalities, there were clear indications of these combined drinking water and sewage treatment issues. Numerous towns have experienced days or weeks without water or have had water outages (Kretzmann 2022). Wastewater treatment is pivotal to avoid its potential deleterious impact on animals, humans, and the environment. Table 2-1 presents the maximum discharge limits in South Africa (SA) for the parameters considered in this study, i.e. pH, COD, turbidity, and colour.

Table 2-1: Maximum limits of permitted discharges in South Africa

Parameter	South Africa		Ref.
	Not less than	Not to exceed	
pH (value at 25°C)	5.5	12	(City of Cape Town 2014)
COD	-	5 000 mg/L	(City of Cape Town 2014)
Turbidity	-	5 NTU	(South Africa Bureau of Standards 2015)
Colour	-	15 Pt.Co	(South Africa Bureau of Standards 2015)

2.6 Impact of wastewater pollution on human health and the environment

Categories of pollutants and how they can affect the environment or human health are detailed in Table 2-2 (Ramalingam et al. 2022). Additionally, in 2017, more than 220 million people were diagnosed with schistosomiasis, an acute and chronic parasitic worm illness, as a result of drinking contaminated water (Ramalingam et al. 2022). According to a UN report, diarrheal illnesses and water-related diseases claim the lives of approximately a thousand children every day, and 1.5 million children under the age of five pass away annually (Murty and Kumar 2011). To compensate for the losses

and stop additional strain on water bodies, dyes found in wastewater must be treated before being released into water resources (Ramalingam et al. 2022).

Table 2-2: Categories of pollutants and their impact on human health and the environment

(Ramalingam et al. 2022)

Type of water pollutants	Specific pollutant	Causes
Organic contaminants	Excess algae	Produces poisons that are harmful to animals, pets, wildlife, and people's health.
	Phosphorus & nitrogen	Harmful algae growth results in low oxygen levels.
	Fecal	Diarrhea, stomach pain, and fever.
Inorganic contaminants	Arsenic	Harm to the kidney, liver, heart, lungs, bladder, central nervous system, and cancer.
	Fluoride	Brown-stained teeth.
	Lead	Children and expectant mothers are in danger from lead poisoning.
	Nitrate/Nitrite, copper, cyanide & cadmium	Toxic to humans and aquatic creatures when exposure levels are high enough.
	Mercury	Damages the brain, heart, kidneys, lungs, immunological system, and human neurological system.
	Ammonia	It is toxic to fish and results in low oxygen levels, bad odors, and excessive plant growth.
Disinfectants	Chloramines & chlorine	Unpleasant effects on the nose, eyes, and stomach.
	Chlorine dioxide	Causes anemia and affects the neurological system.
Disinfection by-products	Total trihalomethanes	Causes issues with the central nervous system, liver, and kidneys.
	Halo acetic acids	Raises the probability of developing cancer.
	Chlorite	Causes anemia and affects the neurological system.
Grease & oil	Animal fats, gasoline, vegetable oil & fuel oil	Harmful to both plants and animals even in trace quantiles.
Pathogens	Protozoa & viruses	Impacts human health.
Pesticides	Insecticides & herbicides	Impacts the health of fish, plants, animals, and aquatic insects.
Radiation	Certain radioactive metals, such as uranium & radium, raise the risk of cancer.	Increases the probability of developing cancer.

2.7 Conventional wastewater treatment methods

Organic contaminants that are becoming more prevalent include organic dyes, pesticides, phenolic chemicals, potentially toxic elements, and wastewater pollutants from petroleum refineries. These contaminants are hazardous, persistent, and non-biodegradable (Gogoi et al. 2018).

The toxicity of organic pollutants cannot be removed using conventional procedures. For this reason, modern innovations remain essential to reduce this pollution significantly (Rani and Shanker 2017). The various pollution-control strategies are listed in Table 2-3 together with their benefits and drawbacks. The photocatalysis approach demonstrates the contrast between conventional methods (Al-Nuaim, Alwasiti and Shnain 2023).

Table 2-3: The pros and cons of pollution control techniques

No	Physical methods	Pros	Cons	Ref.
1	Filtration	• Autoclaving is possible in some cases.	• Time consuming process. • Filters could block up.	(Medeiros et al. 2020)
2	Sedimentation	• Energy usage is not necessary. • Elevated degree of repeatability.	• The process is selective. • Lack of precision.	(Gottfried et al. 2008)
3	Degasification	• Minimizes the quantity of chemicals required for the process's subsequent stage.	• The capacity to remove pollutants is finite.	(Saravanan et al. 2021)
No	**Chemical methods**	**Pros**	**Cons**	**Ref.**
1	Chemical Precipitation	• Process control is simple • Low-cost operations. • It functions in a broad range of temperatures. • Adjustable pH.	• Large-scale production of sludge. • Sludge disposal issues.	(Son et al. 2020)
2	Flocculation and Coagulation	• It's employed to remove minute particles. • Metals, colour, and turbidity removal.	• The process consists of several steps. • Toxic if misused. • Large-scale production of sludge. • High operational costs.	(Sun et al. 2020)
3	Adsorption	• Low operating expenses. • Relatively high efficiencies. • Simplistic design. • Non-toxic technique. • The process of regeneration.	• Low adsorbent selectivity. • Sludge disposal issues.	(Manikandan, Senthil Kumar and Saravanan 2018)

4	Ion exchange	• Resin regeneration is possible. • Zero hardness is achievable. • Process of rapid separation.	• Pre-treatment may be required in most effluents. • Ionic competition is number two. • Matrix contamination.	(Liu and Qiu 2020)
5	Ozonation	• Chemicals are not required. • Removal of a variety of organic and inorganic substances as well as microbes. • Neither the pH nor the temperature needs to be adjusted. • Increased germicidal efficacy.	• Although ozone is poorly soluble, special mixing methods are required. • The cost of ozone generation is higher than that of techniques. • Ozone generation could be hazardous and cause fires.	(Guo et al. 2019)
No	**Biological methods**	**Pros**	**Cons**	**Ref.**
1	Activated sludge	• Providing a reasonable profit for a new endeavor. • Doesn't take up a lot of room • Easy to operate. • Moderately efficacious.	• Excessive running expenses. • Sludge disposal issues.	(Bayan, Pustovaya and Volkova 2021**)**
2	Aerobic Treatment	• Simplicity of the activity. • Reduces the generation of odors. • Reduces the body's lipid and pathogen levels. • More types of microbes can be employed in processing.	• Expensive capital. • Upkeep issues.	(Pejman et al. 2009)

3	Anaerobic Treatment	• Renewable energy can be generated by it. • Environmental contaminants are reduced. • A symbiotic interaction exists. • It generates renewable energy.	• Expensive capital. • Unpleasant odour.	(Kong et al. 2019)
4	Oxidation ponds	• A high level of concentration. • There is a symbiotic relationship.	• Unpleasant odour. • Requires more room.	(Haq and Kalamdhad 2021)
5	Bioremediation	• A natural occurrence. • Treatment on-site. • A cost-effective process.	• Potentially toxic elements ejection is prohibited. • The soil at the bioremediation site must be highly permeable. • Notable deficiencies in the comprehension of microbial ecology exist.	(GracePavithra et al. 2019)
No	**Photocatalysis**	**Pros**	**Cons**	**Ref.**
1	Photocatalytic degradation	• Environmentally friendly and sustainable technology. • Non-energy intensive. • Low cost. • It can be used to treat all industrial and sewage pollutants.	• UV radiation is used for activation. • If sunlight is utilized in place of UV, it cannot be used on cloudy days. • The photocatalyst needs to be extracted from the slurry and prepared for reuse following a cleaning cycle.	(Aziz et al. 2016)

2.8 Advanced oxidation processes (AOPs)

Currently, reverse osmosis, sand filters, microfiltration, ultrafiltration, and activated carbon adsorption are employed as tertiary treatment methods in wastewater treatment facilities (Escobar, Nieto and García 2005). However, none of these treatment techniques is strong enough to remove the most persistent contaminants from water at acceptable levels (e.g., pesticides, solvents, household chemicals, and pharmaceuticals, etc.) (Ates, Kaplan-Bekaroglu and Dadaser-Celik 2024). Advanced oxidation processes (AOPs) may be used to achieve this goal, which is advised when the components of the wastewater have limited biodegradability and/or high chemical stability.

By employing AOPs in a chemical wastewater treatment process, contaminants can be fully mineralized into CO_2, water, and inorganic compounds, or can be transformed into more benign products [Equation (2-1)]. Moreover, biodegradable intermediates may result from the partial breakdown of organic contaminants that are not biodegradable. This is the reason that coupled AOPs as pre-treatments, followed by biological processes, are very economical and cost-effective (Canizares et al. 2009).

$$\mathrm{AOPs} + \mathrm{OH}^{\blacksquare} \xrightarrow{\text{pollutant}} \mathrm{CO_2} + \mathrm{H_2O} + \text{inorganic ions} \qquad (2\text{-}1)$$

AOPs generate $\mathrm{OH}^{\blacksquare}$ radicals although they utilize various reagent systems, such as chemical oxidation processes (O_3, O_3/H_2O_2, H_2O_2/Fe^{2+}), photocatalysis (TiO_2/UV, photo-Fenton reactive), and photochemical degradation processes (UV/O_3, UV/H_2O_2). These radicals are not particularly selective, very reactive, and target the majority of organic compounds (Rosenfeldt et al. 2007).

Numerous cutting-edge advanced oxidation systems that are presently being investigated for potential application in wastewater treatment are described in the following sections. These sophisticated advanced oxidation processes fall into one of two categories: heterogeneous or homogeneous. It is possible to further categorize homogeneous processes into energy-using and non-energy-using processes (Figure 2-1).

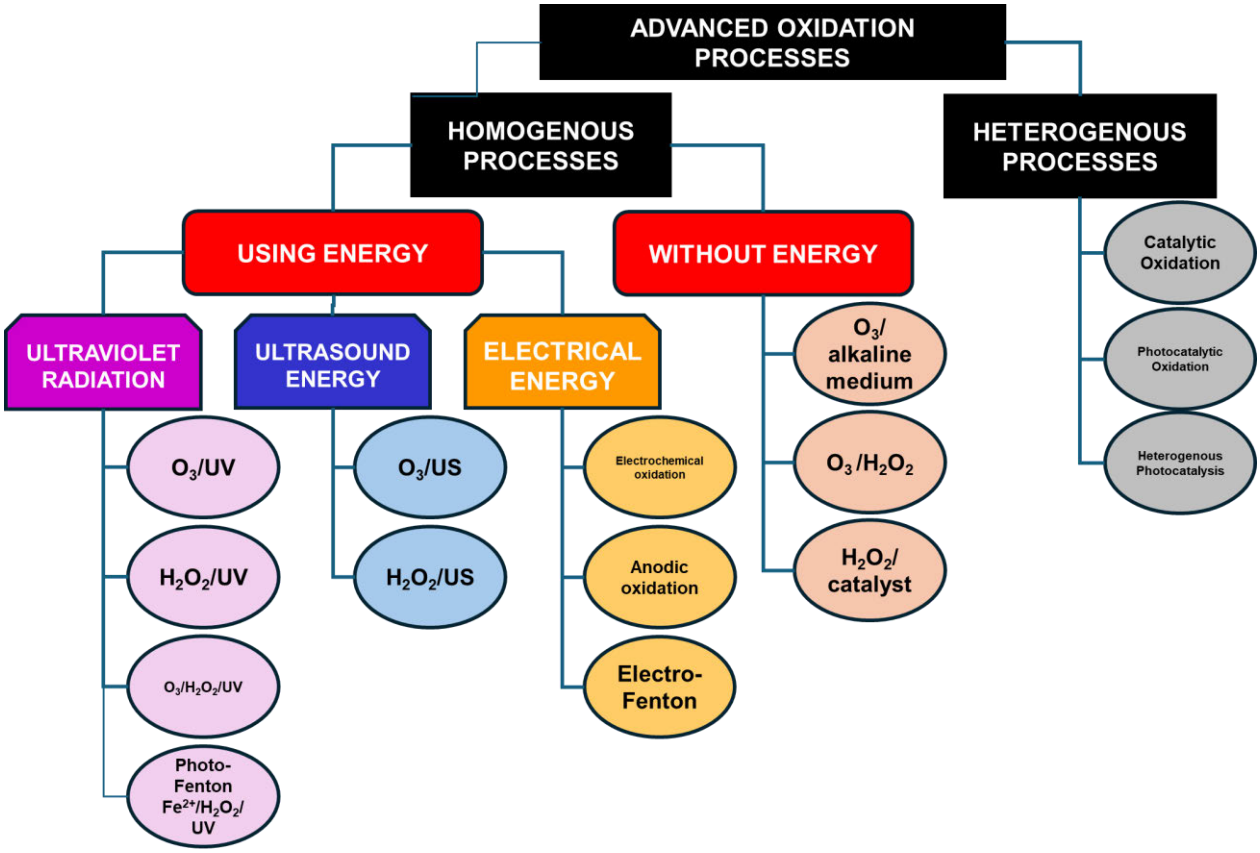

Figure 2-1: Advanced Oxidation Processes (AOPs) classification for Wastewater Treatment; Ozone (O_3), hydrogen peroxide (H_2O_2), ultraviolet radiation (UV radiation), ultrasound (US), and ferrous ions (Fe^{2+})

(Poyatoes et al. 2010b)

The operational costs of ozone-based processes with at least 90% COD removal are compared in Table 2-4 (Yonar et al. 2005). When the process is applied to decontaminate wastewater and the compounds that need to be eliminated merely absorb UV light, adding hydrogen peroxide externally at a lower UV flow rate is more economical. This technique enables the TOC (total organic carbon) to be significantly reduced. In all three of these processes, the oxidation velocity can typically be extremely high. However producing the required UV light in each scenario comes at a very high cost, and the chemical or compounds must absorb that wavelength. Shu and Chang (2005) employed this technique to decolourize a textile industry dye (C.I. Acid Black 22). The H_2O_2/UV method was more time-consuming than ozonation to remove the colour, according to these author's findings.

Table 2-4: Advanced oxidation process operating costs

(Yonar et al. 2005)

Process	Cost of Treatment ($/m^3)
Ozone	5.35
Ozone/UV[b]	8.68
H_2O_2/UV[b]	4.56
Ozone/H_2O_2/UV[b]	11.25

Where *b represents the optimum lamp life at 2 000 h.

2.9 Types of photocatalysts

2.9.1 Oxide photocatalyst

2.9.1.1 Titanium dioxide (TiO_2)-based photocatalysts

Three crystal forms of TiO_2 exist rutile, brookite, and anatase. Anatase and rutile-type TiO_2 are the two most often utilized crystal forms among these three for photocatalysis (Huang et al. 2015). Due to their high activity, stable features, low cost, and non-toxic environment, TiO_2-based photocatalysts have been widely used in many applications such as air purification, water pollutant degradation, deodorant, and antifog.

TiO_2's large band gap is around 3.2 eV. Consequently, TiO_2 can only function as a photocatalyst when it is exposed to ultraviolet light. Even so, just 5% of sunlight is UV, severely restricting the use of TiO_2 in the visible spectrum. Typically, TiO_2 undergoes a sequence of alterations that enhance its ability to utilize visible light while decreasing the rate at which photogenerated electron-hole recombination occurs on its surface. Enhancing photocatalytic efficiency is possible. Semiconductor surface photosensitization, semiconductor surface noble metal deposition, metal/nonmetal doping, and complicated semiconductor modification are commonly used techniques to increase photocatalytic efficiency.

2.9.1.2 Bismuth (III) oxide (Bi_2O_3)-based photocatalyst

Bi-based oxides are a significant family of functional materials with broad applications (Gao et al. 2015). They are employed as materials for photoelectric conversion, high-temperature superconducting materials, electrolyte materials, and electronic ceramic materials. Among these, (Bi_2O_3) has special qualities such as a low bandgap (approximately 2.8 eV), low energy band structure, and strong electrical conductivity,

which allow it to absorb visible light in the solar spectrum. Bi_2O_3 hence has a lot of promise for use in photocatalysis (Cabot et al. 2004).

The four primary crystal forms of the semiconductor Bi_2O_3 are α, β, γ, and δ. At 2.58 eV and 2.85 eV, respectively, the band gaps of β-Bi_2O_3 and α-Bi_2O_3 allow them to absorb visible light with wavelengths longer than 400 nm (Cabot et al. 2004). Since α-Bi_2O_3 has the best thermodynamic stability among all four crystal forms, it is the most often utilized Bi_2O_3 semiconductor in photocatalytic reactions (Hameed et al. 2008).

The development of Bi-based semiconductor materials solves the problem of the visible light absorption of TiO_2. However, Bi-based photocatalysts's low quantum efficiency and photogenerated carrier recombination remain critical issues that must be resolved immediately. Enhancing the photocatalyst's photocatalytic performance can be achieved through a successful doping modification. Semiconductor surface photosensitization, semiconductor surface noble metal deposition, metal/nonmetal doping, and complex semiconductor modification are frequently employed modification techniques. Bi-based photocatalysts have produced several significant research findings thus far in the areas of heavy metal ion removal, organic wastewater treatment, sterilization, and atmospheric purification (Dong et al. 2016; Huang et al. 2016; Qian et al. 2016; Wu et al. 2016; Xiong et al. 2016; Feng et al. 2017).

2.9.1.3 Photocatalysts with various oxides

The IV cycle's transition metal components, including titanium, chromium, manganese, iron, cobalt, nickel, copper, and zinc, along with their respective oxides, have exceptional physical and chemical properties. High redox potential, multivalence, chemical resistance, and high-temperature tolerance are some of these exceptional physicochemical properties (Kim, Hwang and Lee 2004; Amano et al. 2008). Transition metal oxides offer promising future applications in photocatalysis because transition metal components are inexpensive and relatively abundant to store.

The three types of transition metal oxides that are often used such as ZnO, WO_3, and Fe_2O_3 are then introduced.

I. Zinc oxide (ZnO)

One of the few oxide semiconductor materials with good piezoelectric and UV absorption qualities is zinc oxide (ZnO). It can also produce a quantum-size effect. ZnO has a bandwidth of 3.2 eV, or 387 nm, which corresponds to the UV wavelength. Research on ZnO has revealed a correlation between the photocatalytic capabilities of ZnO nanoparticles and their surface composition and structure. On the ZnO surface, oxygen vacancies tend to absorb photogenerated electrons and exhibit a robust interaction with adsorbed oxygen, both of which are advantageous for oxidation processes (Zhang *et al.* 2019b).

II. Tungsten trioxide (WO_3)

WO_3 describes several advantages, including a large specific surface area, excellent absorbing capability, and its potential to be used as an invisible material. The band gap of WO_3 is 2.8 eV, and it is stable. WO_3 can be used both as a main catalyst and as a co-catalyst (Zhang *et al.* 2019b).

III. Iron oxide (Fe_2O_3)

Research on iron as a crucial meta-element in the redox process has been ongoing for a while. Fe_2O_3 has been the subject of extensive research due to its high photocatalysis activity among iron oxides. Having a 2.2 eV bandwidth, Fe_2O_3 is an n-type semiconductor that can absorb some sunlight and has significant visible light absorption capabilities. Reactive dyes can be broken down by Fe_2O_3, which can also be utilized as a reducing agent for the photocatalytic reduction of silver ions (Ercan et al. 2015; Jablonski et al. 2016; Sun et al. 2016).

2.9.2 Non-oxide photocatalyst

Several non-oxides also exhibit strong photocatalytic qualities (Chang et al. 2017). Among these, semiconductor metal sulphides have garnered significant interest due to their unique structure and superior chemical and physical characteristics. Molybdenum sulphide (MoS_2), tungsten sulphide (WS), copper sulphide (CuS), zinc sulphide (ZnS), and cadmium sulphide (CdS) are a few examples of these non-oxides. Nitrides, such as C_3N_4, exhibit superior photocatalytic capabilities in addition to sulphides (Cheng et al. 2014; Chang et al. 2017).

2.9.2.1 Cadmium sulphide (CdS) series photocatalyst

CdS is a semiconductor material with a maximum absorption peak of 514 nm and a bandgap of approximately 2.42 eV. For visible light photocatalysis, CdS is therefore more effective since it can absorb visible light or ultraviolet light with a wavelength of less than 514 nm (Zheng et al. 2019). CdS semiconductors' bandgap position is also advantageous for a variety of photocatalytic processes, including CO_2 reduction and water degradation (Kudo and Miseki 2009; Li et al. 2014). More significantly, the photoelectrons of CdS have a larger reducing power in the photocatalytic reaction because their position in the conduction band edge is lower than that of other common semiconductors (such as TiO_2, $SrTiO_3$, and ZnO). As a result, extensive research has been done on CdS as a photocatalyst. Nevertheless, the CdS material is vulnerable to light damage, which severely restricts the quantity of recovered photocatalysts. Researchers have put up several suggestions to increase the CdS utilization ratio to address this underlying issue. Preparing CdS composite materials with various materials or ion doping techniques is the most popular approach. Additionally, the CdS composite promotes long-wavelength light absorption, allowing for the complete usage of natural light's visible portion (Zhang *et al.* 2019b).

2.9.2.2 Copper sulphide (CuS) series photocatalyst

Copper sulphide (CuS) is a highly significant metal sulphide semiconductor material with exceptional optoelectronic capabilities. CuS has a good ability to absorb visible light, with a bandwidth of 2.2 eV. Electron-hole pairs are produced when the appropriate photons are absorbed by the CuS surface. Electrons and holes move to the surface of the material and react with water molecules or oxygen molecules on the surface of the material to produce several substances. These compounds can break down the organic matter that has been adsorbed on the material's surface due to its strong catalytic activity. Due to CuS's superior qualities, it has been used in solar cells, lithium battery electrodes, photothermal conversion, and photocatalysis, among other optical, electrical, mechanical, and sensor applications (Córdova et al. 2002; Lim et al. 2006); (Bessekhouad, Robert and Weber 2004). CuS nanoparticle’s suitable energy band and absorption wavelength make them highly promising for photocatalysis (Gorai, Ganguli and Chaudhuri 2005; Zhang *et al.* 2019b).

2.9.2.3 Zinc sulphide (ZnS) series photocatalyst

Zinc sulphide (ZnS) has a band gap between 3.6 and 3.8 eV. ZnS has two different crystal structures such as zinc blend and wurtzite. Zinc blende, or β-ZnS, is one of them that can exist steadily at low temperatures, but wurtzite, or α- ZnS, may exist steadily at temperatures higher than 1024°C. ZnS is difficult to oxidize and hydrolyze. More significantly, when ZnS is reduced to the nanoscale, these characteristics remain. Thus, ZnS nanomaterials exhibit good photocatalytic activity (Kanemoto et al. 1992). Furthermore, ZnS is easily fabricated, non-toxic, and widely used. ZnS nanoparticles, nanowires, nanotubes, and nanosheets have been successfully synthesized by numerous research groups to date (Wang et al. 2002; Lv et al. 2004; Reddy et al. 2019). The three following techniques are the most widely used for increasing ZnS's photocatalytic activity: (1) ZnS's morphology is altered to increase its specific surface area. ZnS's photocatalytic activity can be enhanced by expanding the active site on its surface and, consequently, the contact area between ZnS and the reactant, corresponding to its high specific surface area. (2) ZnS can be doped with other metals and non-metallic elements to alter its electronic characteristics and band structure, which increases ZnS's absorption rate of visible light and increases its photocatalytic efficiency. (3) ZnS couples with other semiconductors to produce a heterojunction or a composite structure with noble metals, to increase ZnS's photocatalytic activity and decrease the rate of electron-hole recombination (Zhang *et al.* 2011; Zhang *et al.* 2019b).

2.9.2.4 Nitride series photocatalyst

The photocatalyst based on graphitic carbon nitride (g-C_3N_4) has a layered structure similar to graphite and possesses strong electron-hole transport capabilities, high chemical and thermal stability, and a small band gap (2.7 - 2.8 eV). g-C_3N_4 exhibits considerable light absorption in the visible light region (400 - 450 nm) due to its bandwidth. In addition, g-C_3N_4's structure and characteristics are easily controlled, which makes it a popular subject for photocatalyst research (Wang et al. 2009a; Fina et al. 2015). In the areas of photo hydrolysis, hydrogen production, photodegradation of environmental contaminants, CO_2 reduction, sterilization, and the synthesis of composite capacitor materials, g-C_3N_4 has exceptional photocatalytic performance (Maeda et al. 2014; Cui, Tang and Wang 2015; Fina et al. 2015; Lv et al. 2018).

2.10 TiO_2 photocatalysis

A photoinduced process that is accelerated in the presence of a catalyst is referred to as photocatalysis in general. At room temperature and pressure, heterogeneous photocatalysis is the most popular and efficient method for breaking down organic contaminants since it doesn't create any hazardous intermediates (Ensaldo-Rentería et al. 2018). Electrons are excited and move from the valence band (VB) to the vacant conduction band (CB) at the beginning of this process. In the presence of light, the catalyst absorbs adequate energy to become excited from the light which is equal to its energy bandgaps. In the photocatalytic system, photogenerated species, such as the electron-hole pair, are produced as a result of the excited electrons moving into the conduction band via the holes functioning as a positive charge in the valence band. Superoxide anion radicals ($O_2^{\blacksquare -}$) and hydroxyl radicals ($OH^{\blacksquare}$) are examples of reactive oxygen species that are further produced when the created species react with OH^- groups or oxygen molecules. The organic molecules are attacked by these reactive oxygen species, which oxidize and break them down. Finally, the electron-hole pairs are formed on the surface of the photoexcited catalyst (Alijani, Kaleji and Rezaee 2017; Jiang et al. 2021; Bi et al. 2024).

These materials are often N-type semiconductors, which differ from metals in that their band structures are discontinuous and often consist of low-valence bands that are saturated with electrons. Most photocatalysts affect the photocatalytic performance because of the photo corrosion phenomena. Common semiconductor photocatalysts include ZnO, SnO_2, CuS, ZnS, $ZnWO_4$, WO_3, ZnS, Ag_2CO_3, $BiTiO_3$, $Bi_{20}Ti_{20}$, Bi_2WO_6, Nb_2O_5, Fe_2O_3, $SrTiO_3$, and TiO_2, among others. TiO_2 is one of the photocatalysts that has been investigated extensively by scientists because of its stability, high efficiency, and low cost. The drawback of TiO_2 is that only UV radiation can cause it to activate rather than visible light. Its benefits over other semiconductors include being chemically and biologically inert, easy to use and produce, photo-catalytically stable, reasonably priced, and capable of efficiently catalyzing reactions without endangering people or the environment. There are three different polymorphs of TiO_2: rutile, anatase, and brookite. While brookite appears as orthorhombic crystal lattices, rutile, and anatase both contain tetragonal crystal lattices (Otitoju et al. 2020). In these three phases, the rutile form is the most stable polymorph (Sangchay and Kaewjang 2016).

Only UV light shorter than 400 nm can be absorbed by pure nano-TiO_2 powder due to its bandgap of around 3.2 eV. Since there is less than 10% UV light in the natural world, pure nano-TiO_2 cannot act as a photocatalyst. This greatly affects the utilization rate of the catalyst to sunlight. The poor quantum yield of the catalyst and the quicker recombination of electrons and photogenerated holes are two other important limitations on the practical use of photocatalysts. In general, the photocatalyst's quantum quality, which affects carrier recombination, is determined by the recombination efficiency of photogenerated carriers. The catalyst's surface morphology, grain size, crystal phase structure, surface lattice defects, and light radiation intensity are the primary determinants of the surface charge transfer process (Jiang et al. 2021).

It is necessary to modify the TiO_2 photocatalyst to increase its ability to absorb visible and far-infrared light and boost photocatalytic efficiency. Currently, two methods have been suggested by researchers to improve TiO_2's photocatalytic performance: (1) to stop photogenerated electrons from recombining with photogenerated holes to enable their efficient participation in the process of catalytic degradation; (2) the alternative is to add novel compounds to the TiO_2 lattice, which lowers the catalyst's bandgap energy and increases the range of its photoreaction. In most cases, the activated VB holes and CB electrons join again to form a neutral body to generate power lost in light or heat energy. Therefore, the catalyst can capture the photogenerated electrons, or the mobility of the catalyst’s surface charge can be improved. One efficient method to increase photocatalytic efficiency is to modify the TiO_2 lattice with metal ions, which will slow down the recombination of electron-hole pairs (Jiang et al. 2021).

2.10.1 Mechanisms of photocatalysts for organic pollutants

2.10.1.1 Mechanism of Titanium dioxide (TiO_2) photocatalyst

The photocatalytic reaction in the presence of TiO_2 photocatalysts is initiated by a free radical reaction that is triggered by light irradiation, namely photons. The photocatalyst surface becomes excited and the electrons move from the valence band (VB) to the conduction band (CB) when the energy of solar radiation exceeds the bandgap of TiO_2. The photocatalyst surface becomes excited and the electrons move from the valence band (VB) to the conduction band (CB) when the energy of solar radiation

exceeds the bandgap of TiO_2 (i.e., photon energy reaches or exceeds its bandgap energy). Electron-hole pairs (i.e., generating electron (e^-) and hole (h^+) pairs) are formed when equivalent electron holes from the CB are simultaneously produced in the VB. Since VB holes lose electrons and function as reducing agents, they have a high oxidation reaction activity (1.0~3.5 V). Good reducibility of 0.5~1.5 V is exhibited by electrons in the conduction band when reduced. Equation (2-2) shows that positive holes and electrons are generated in the $\mathrm{VB}(\mathrm{hv}_{\mathrm{vb}}^{+})$ and $\mathrm{CB}(\mathrm{e}_{\mathrm{cb}}^{-})$ of TiO_2 under light irradiation, respectively. These holes can react directly with organic molecules (Equation 2-6), oxidizing them in the process, or they can form hydroxyl radicals (Equation 2-4). Reduced products Equations (2-2)-(2-8) can also be produced by the electrons reacting with organic molecules. When oxygen interacts with photogenerated electrons, it plays a crucial role. When organic compounds combine with hydroxyl and peroxide radicals, VB holes, or electrons, they can then undergo oxidative degradation or reductive breakdown, which produces a variety of byproducts and, in the end, mineral end products (Jiang et al. 2021).

$$\mathrm{TiO_2} + \mathrm{hv} \rightarrow \mathrm{h_{VB}^{+}} + \mathrm{e_{CB}^{-}} \quad (2\text{-}2)$$

$$\mathrm{OH_{surface}^{-}} + \mathrm{h_{VB}^{+}} \rightarrow \mathrm{OH^{\blacksquare}} \quad (2\text{-}3)$$

$$\mathrm{H_2O_{absorbed}} + \mathrm{h_{VB}^{+}} \rightarrow \mathrm{h^{+}} + \mathrm{OH^{\blacksquare}} \quad (2\text{-}4)$$

$$\mathrm{O_{absorbed}} + \mathrm{e_{CB}^{-}} \rightarrow \mathrm{OH_2^{\blacksquare -}} \quad (2\text{-}5)$$

$$\mathrm{Organic} + \mathrm{h_{VB}^{+}} \rightarrow \mathrm{Oxidation\ Products} \quad (2\text{-}6)$$

$$\mathrm{Organic} + \mathrm{OH^{\blacksquare}} \rightarrow \mathrm{Degradation\ Products} \quad (2\text{-}7)$$

$$\mathrm{Organic} + \mathrm{e_{CB}^{-}} \rightarrow \mathrm{Reduction\ Products} \quad (2\text{-}8)$$

Furthermore, electrons $(\mathrm{e}_{\mathrm{cb}}^{-})$ react with adsorbed oxygen molecules (O_2), reducing them to superoxide radical anions $(\mathrm{O_2^{\blacksquare -}})$, which react with protons (H^+) to form peroxide radicals $(\mathrm{HO_2^{\blacksquare}})$, and VB holes $(\mathrm{h}_{\mathrm{vb}}^{+})$ react with water (H_2O) and the hydroxyl ion (OH-) to form hydroxyl radicals $(\mathrm{OH^{\blacksquare}})$ as presented in Equations (2-9)-(2-12) (Shinde et al. 2011).

$$h_{VB}^{+} + H_2O \rightarrow HO^{\blacksquare} + H^{+} \quad (2\text{-}9)$$

$$h_{VB}^{+} + OH^{-} \rightarrow HO^{\blacksquare} \quad (2\text{-}10)$$

$$e_{CB}^{-} + O_2 \rightarrow O_2^{\blacksquare -} \quad (2\text{-}11)$$

$$O_2^{\blacksquare -} + H^{+} \rightarrow HO_2^{\blacksquare} \quad (2\text{-}12)$$

The intermediate state surface electrons become excited when exposed to light irradiation through metal ion-modified TiO_2 and therefore have sufficient energy to access more light absorption and transfer electrons to the TiO_2 surface. Consequently, increasing the number of electrons exposed to light accelerates the redox reactions (Inturi et al. 2014). These properties being displayed by the metal ions help to improve the photocatalytic reactions. The properties being displayed by the metal ions facilitate better photocatalytic reactions. The transfer of electrons takes place at the VB to the CB via the creation of holes in the former and these holes subsequently react with the H_2O molecules present in the pollutant as well as helping to form the $OH^{\blacksquare}$ radicals (Kim et al. 2013). When exposed to light, the supporting $OH^{\blacksquare}$ radicals that are produced are highly effective in breaking down a variety of dyes (Saravanan et al. 2016; Jiang et al. 2021). Figure 2-2 shows the photocatalytic mechanism of metal-ion-modified TiO_2 for organic pollutants.

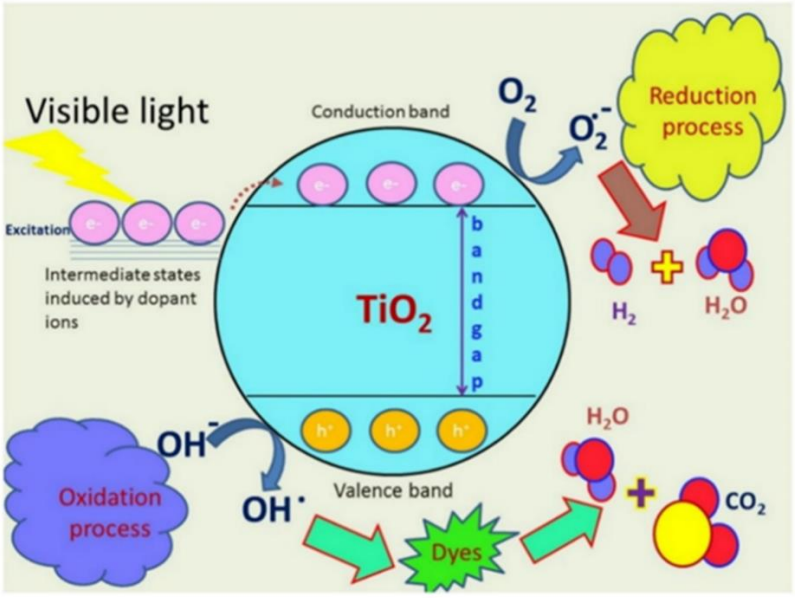

Figure 2-2: The photocatalytic mechanism of metal-ion modified TiO_2 in the presence of visible light

(Jiang et al. 2021)

2.10.1.2 Iron oxide (Fe_2O_3) photocatalyst mechanism

The photoexcited electrons of γ-Fe_2O_3 [Equation (2-13)] are migrated from the conduction band (CB) and holes at the valence band (VB) (Wang et al. 2019; Hitam and Jalil 2020). Subsequently, the Fe(Ⅲ) is reduced to Fe(Ⅱ) by the electrons [Equation (2-14)], which furthermore react with H_2O_2 to form $OH^{\blacksquare}$ and Fe(Ⅲ) [Equation (2-15)].

$$\gamma - Fe_2O_3/GO + hv \rightarrow h^+ + e^- \quad (2\text{-}13)$$

$$Fe(III) + e^- \rightarrow Fe(II) \quad (2\text{-}14)$$

$$Fe(II) + H_2O_2 \rightarrow Fe(III) + OH^{\blacksquare} \quad (2\text{-}15)$$

2.10.1.3 Zinc sulphide (ZnS) photocatalyst mechanism

The photoexcitation of the ZnS [Equation (2-16)] results in the formation of an electron-hole pair on the surface, which allows the direct oxidation of organic matter into reactive intermediates.

$$ZnO + hv \rightarrow (e^-_{CB} + h^+_{VB}) \quad (2\text{-}16)$$

2.10.1.4 Copper sulphide (CuS) photocatalyst mechanism

Furthermore, for the CuS irradiated under UV light, the excited electrons (e^-) move from the valence band (VB) to the conduction band (CB) [Equation (2-17)]. Once the absorption of photon energy becomes greater, a hole (h^+) is then created by the excited electrons (e^-). This photogenerated e^- and h^+ then moved to the surface of the CuS and reacted with oxidants and reductants, respectively (Soni et al. 2008; Zhang et al. 2014).

$$CuS + hv \rightarrow h^+ (Cu) + e^- (S) \quad (2\text{-}17)$$

2.10.2 Band gaps of common photocatalysts

Table 2-5 summarizes the bandwidths of various commonly used photocatalysts as semiconductor bandwidth is a significant factor restricting the wide application of photocatalysts.

Table 2-5: Common photocatalysts band gaps

Semiconductor	Crystal Structure	Band Gap Structure = 7			Ref.
		CB	VB	Eg/eV	
TiO_2	Anatase	−0.50	2.70	3.20	(Liu et al. 2018)
ZnO		−0.31	2.89	3.20	(Zhang *et al.* 2019a)
CuO		−1.16	0.85	2.00	(de Jongh, Vanmaekelbergh and Kelly 1999)
CdS		−0.90	1.50	2.40	(Finlayson et al. 1985)
ZnS		−1.04	2.56	3.60	(Zheng et al. 2019)
g-C_3N_4		−1.30	1.40	2.70	(Wang et al. 2009b; Zhang et al. 2010)
g-C_3N_4		−1.53	1.16	2.70	(Yan et al. 2010)
Ta3N_5		−0.75	1.35	2.10	(Chun et al. 2003)
TaON		−0.75	1.75	2.50	(Memar, Phan and Tade 2012)
Fe_2O_3		0.28	2.48	2.20	(Li, Chen and Xue 2013)
Bi_2O_3		0.33	3.13	2.80	(Cai and Kisch 2008)
$BiVO_4$		−0.30	2.10	2.40	(Hardee and Bard 1977)
WO_3		−0.10	2.70	2.80	(Yi et al. 2010)
Ag_3PO_4	Cubic	0.04	2.49	2.45	(Doshi and Reneker 1995)

2.10.3 Electromagnetic spectrum

The electromagnetic spectrum is the collection of all possible frequencies of electromagnetic waves, which we commonly refer to as light. The energy reaching Earth from the sun is a form of electromagnetic radiation, which is represented by the electromagnetic spectrum (Figure 2-3). Approximately 52-55% of the sunlight reaching the Earth's surface is Infrared (IR), 42-43% is visible, and 3-5% is UV light. Most of the solar energy reaching the Earth's surface falls within the visible light region, with wavelengths between about 400-700 nm (Shahid et al. 2024). The colours of the visible spectrum comprise the familiar "ROYGBIV"; red, orange, yellow, green, blue, indigo, and violet.

The wavelength range of ultraviolet (UV) light is separated into three fractions: UVA (315-400 nm; 3.94-3.10 eV), UVB (280-315 nm; 4.43-3.94 eV), and UVC (100-280 nm; 12.4-4.43 eV) (Zou et al. 2018; Kneissl et al. 2019). The photons associated with UV radiation carry substantially more energy (3.10-12.4 eV) than those associated with visible light (1.6-3.10 eV), while the wavelength of UV radiation is slightly shorter than that of visible light (400-780 nm) (Silva et al. 2023). The various wave types that comprise the electromagnetic spectrum are shown in Table 2-6 along with the corresponding frequency and wavelength ranges (AoPs Online 2023).

Table 2-6: The Electromagnetic Spectrum

(AoPs Online 2023)

Wave type	Frequency range	Wavelength range
Radio waves	300 GHz - 3 kHz	1 mm - 100 km
Microwaves	0.3-300 GHz	1 mm - 1 m
Infrared	300 GHz - 430 THz	
Visible light	430-790 THz	390-700 nm
UV	750-30,000 THz	10-400 nm
Xray	30,000-300,000 THz	0.001-10 nm
Gamma	300,000-30,000,000,000 THz	0.000000001-0.001 nm

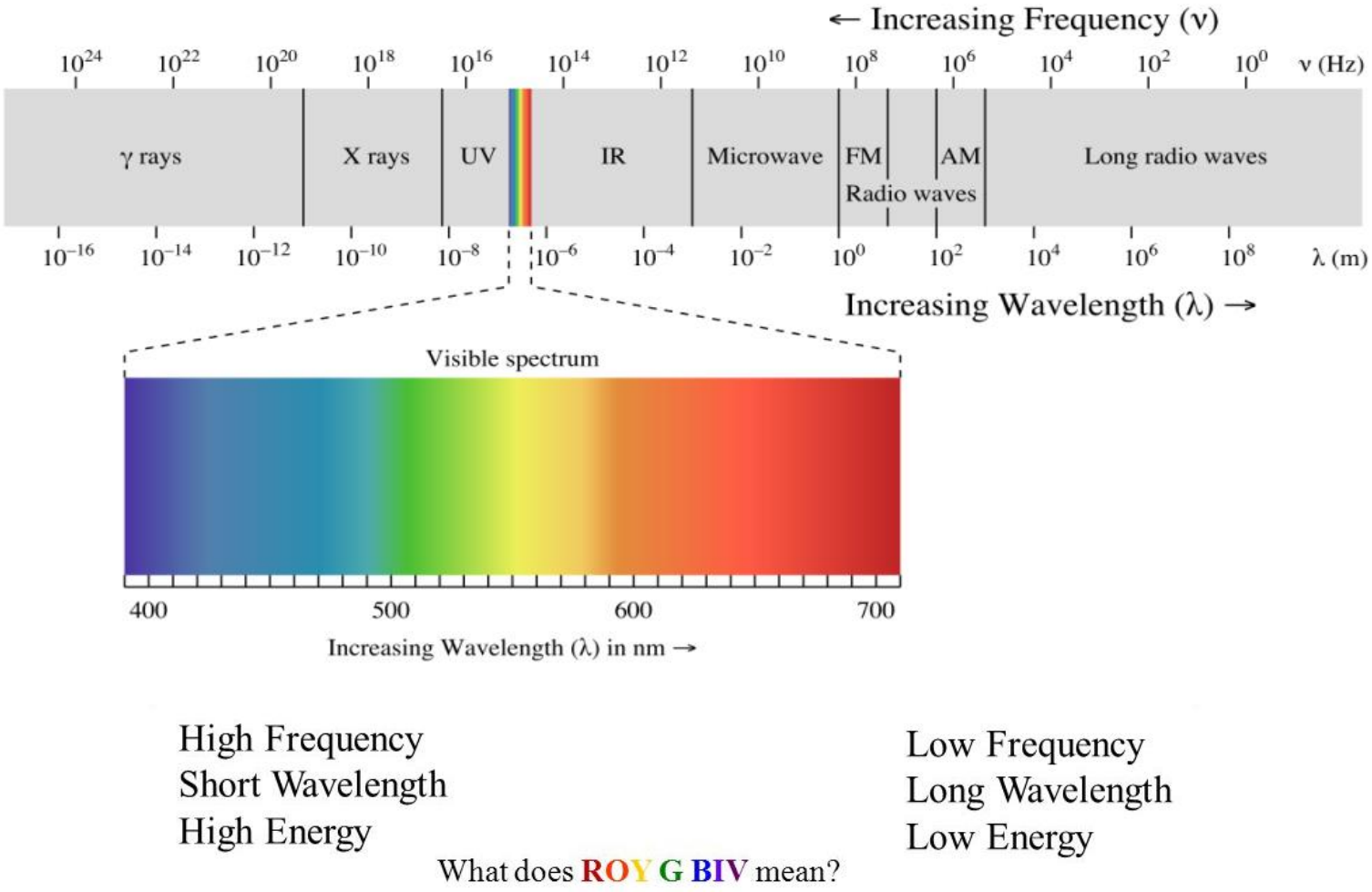

Figure 2-3: The electromagnetic spectrum. Frequency is expressed in Hertz (Hz), or waves per second, while wavelengths are expressed in meters (Roger Williams University n.d.)

2.11 Factors influencing the photocatalytic degradation performance

This section discusses a few important variables that influence the performance of photocatalytic degradation, including photocatalyst loading, exposure time, direct photolysis, particle size, and morphology.

2.11.1 Effect of photocatalyst loading

The most significant factor influencing photocatalytic activity is considered to be the concentration of the photocatalyst. To prevent the need for extra dosage, it's critical to maximize the amount of photocatalyst used throughout the photocatalytic process. For photoreaction to be economically viable, it must be as efficient as possible while requiring the least amount of photocatalyst possible (Zare et al. 2021). The photocatalytic activity rises with an increase in photocatalyst concentration. This was due to the increase in active sites on the photocatalyst surface. As a result, a large number of hydroxyl radicals and other ROS will be produced, which is what enables organic contaminants to be destroyed (Ammar, Elaibi and Mohammed 2020). On the other hand, overuse of photocatalysts will limit the activity of photocatalytic degradation, creating a hazy environment inside the reactor that decreases light penetration through the solution (Coleman et al. 2007). Sun et al. (2008) stated that by enhancing the aggregation effect of nanoparticles and decreasing the photoactive surface area, a higher dose of the photocatalyst can result in a lower degradation efficiency.

Riga et al. (2007) stated that when the pace at which the photocatalyst load (TiO_2) increases, the amount of dye adsorbed usually increases as well. The impact of several heterogeneous nanocomposite photocatalysts on the photocatalytic degradation performance is shown in Figure 2-4. Using varying concentrations (0.5 to 1.5 g/L) of Fe_3O_4@SiO_2@PT\$SiMo_{12}$ photocatalyst in the core/shell structure, Figure 2-4a depicts the photocatalytic oxidative desulfurization (ODS) in gasoline fuel (Shafi, Ammar and Rashed 2021). Adeel et al. (2021) examined how the percentage of Co-ZnO composites affected the MO dye's photocatalytic degradation. Considering a degradation efficiency of 93%, 10% Co-ZnO was the ideal photocatalyst, according to the experimental data shown in Figure 2-4b. Jabbar and Ebrahim (2021) studied the photocatalytic degradation effectiveness against MB dye, which rose from 75% to 88% upon 45 minutes of illumination by increasing the dose of SiO_2/Fe_3O_4/Ag_2WO_4 from

0.5 to 1 g/L. This was explained by an increase in photogenerated electron-hole pair production (Figure 2-4c).

Nadeem et al. (2021) investigated CFA/$ZnFe_2O_4$ photocatalyst (coal fly ash-based zinc ferrite) at composite concentrations (20-200 mg/L) for Methyl blue dye. It was discovered that due to the aggregation of the photocatalyst and the release of Fe (II) ions, which scavenge the hydroxyl radicals produced. Therefore, removal activity was reduced when the concentration of photocatalyst was increased above 110 mg/L (Figure 2-4d). Table 2-7 provides a summary of additional research that explains how photocatalyst dose affects the breakdown of organic contaminants by photocatalysis.

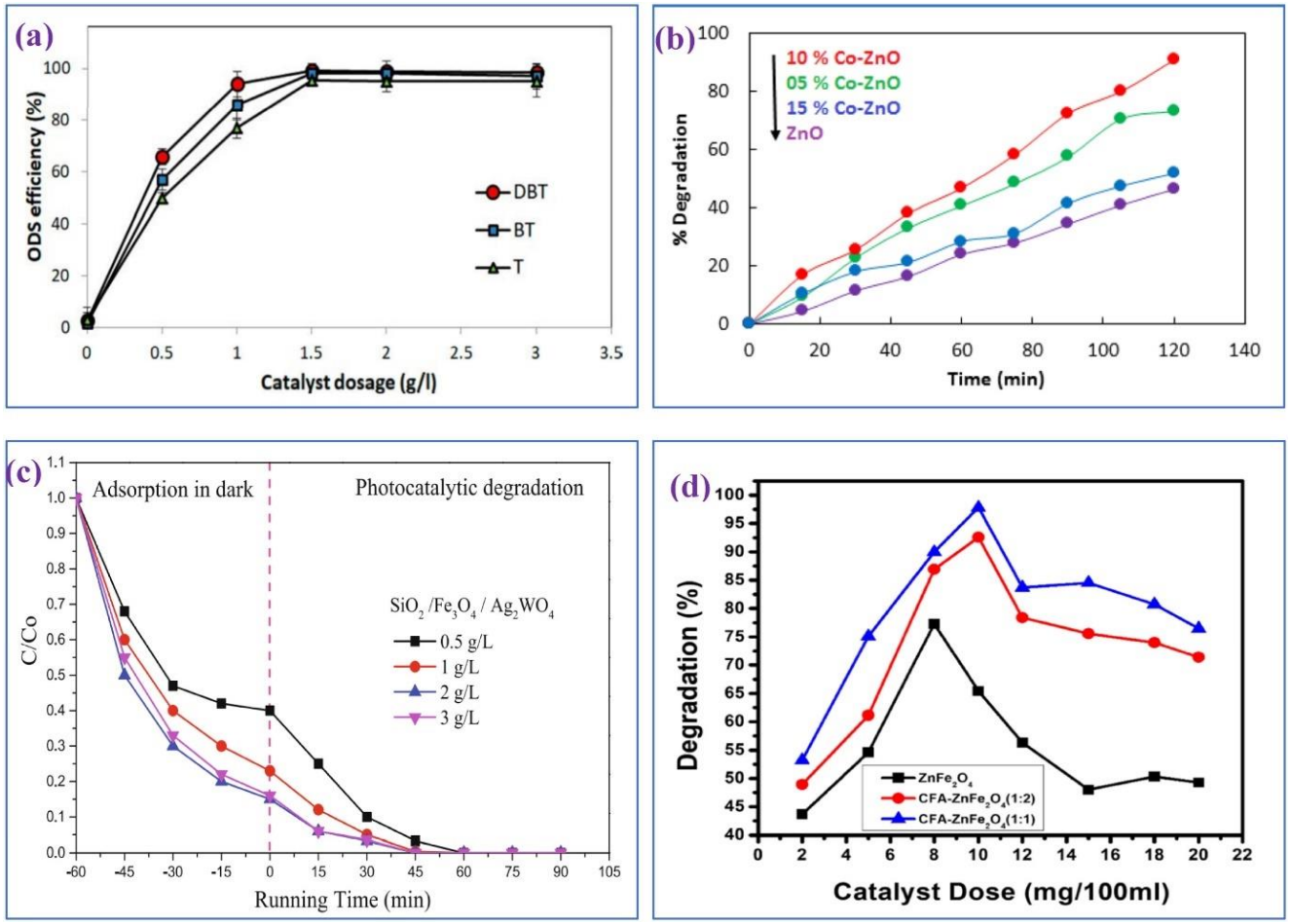

Figure 2-4: (a) Fe_3O_4@SiO_2@PT\$SiMo_{12}$ dosage's effect on the photocatalytic degradation of ODS in gasoline fuel at 250 mg/L sulphur concentration initially, 1:1 H_2O_2:S molar ratio, 60 minutes of irradiation, and 40°C reaction temperature, (b) The photodegradation efficiency for MO at 15%, 10%, and 5% Co-ZnO, (c) The photodegradation of MB dye at pH = 11, H_2O_2 = 0.1 M, and MB dye concentration of 30 ppm using varying SiO_2/Fe_3O_4/Ag_2WO_4 concentrations, (d) The photodegradation efficiency of MB dye at various CFA/$ZnFe_2O_4$ photocatalyst concentrations (20-200 mg/L) (Jabbar and Graimed 2022)

Table 2-7: Summary of research utilizing semiconductor heterojunction photocatalysis at photocatalyst load (0.25-6 g/L) for the photocatalytic degradation of several organic compounds

Photocatalyst	Photocatalyst load	Irradiation source	Contaminant	Exposure time (minutes)	Photodegradation efficiency (%)	Ref.
$Fe_3O_4@Al_2O_3$-PMo	0. 5-3 g/L	UV (360 nm)	Cibacron brilliant yellow 3G-P	300	>90	(Ammar and Abdulnabi 2020)
Pt-TiO_2	0.5-6.0 g/L	UV	Methyl orange	Not given	90.5	(Huang et al. 2008)
Sn/TiO_2/AC	5.0-15.0 g/L	UV	Orange G	60	99.1	(Sun et al. 2006)
Cu-doped ZnO	0.1-1 g/L	125 W medium-pressure UVC lamp	Diazinon	120	96.97	(Shirzad-Siboni et al. 2017)
Fe_3O_4@ZnO/PMOs	0.25-1.5 g/L	40 W white LED lamps	Methyl orange	180	98.2	(Ammar and Abdulnabi 2020)
$Fe_3O_4@SiO_2@Ag_2WO_4@Ag_2S$	0.5-3 g/L	Xenon + LED lamps (95 W)	Methyl blue	60	99.9	(Jabbar and Ebrahim 2021)
Bi_2O_3/SnO_2	(20-60) mg/50 mL	350 W Xenon lamp	Bisphenol A	60	93.42	(Chen et al. 2020a)
P-ZnO1.8%	0.5-3 g/L	300 W halogen lamp	Rhodamine B	180	99	(Saffari, Shariatinia and Jourshabani 2020)
Fe^0@PEDOT\PW_{12}	0.5-3 g/L	Visible light	Oxidative desulfurization	60	98.4	(Ammar, Salman and Shafi 2021)

2.11.2 Effect of mixing speed

Xu and Ma (2021) investigated the effect of varying revolutions per minute (rpm) (mixing speeds) on rhodamine B degradation at the initial reaction concentration of 20 mg/L. The mixing speed of the ultrasonic (US) cleaner was set to 300 rpm, 400 rpm, 500 rpm, 600 rpm, and 700 rpm, respectively. The mixed solution was sampled from the reaction system every 10 minutes. The effect of mixing speed on degradation rate is illustrated in Figure 2-5. As shown, at different mixing speeds, the degradation efficiency increased with the increase of US treatment time. The degradation rate at the various mixing speeds was 38.08% (300 rpm), 85.41% (400 rpm), 98.60% (500 rpm), 71.33% (600 rpm), and 55.80% (700 rpm) respectively when the US catalysis reached 40 minutes. It was found that the degrading efficiency first increased with the increase of revolutions per minute, then reached a maximum degradation effect at 500 rpm. Thereafter, the degradation effect began to decrease with the increase in mixing speed. It was seen that the mixing speed had a significant effect on the degradation rate. In the solid nanoparticle reaction system, the cavitation bubbles failed to expand to a specific size and burst at high revolutions per minute, resulting in a decrease in the efficiency of hydroxyl radical production and consequently the degradation efficiency. The cavitation bubbles also failed to collapse completely and quickly at low revolutions per minute. Thus, in the nanoparticle reaction system, either too low or too high mixing speed leads to less efficient production of hydroxyl radicals, and thus the degradation efficiency was reduced (Xu and Ma 2021; Fallahizadeh et al. 2023).

Another study was investigated by Zakaria et al. (2014) for the removal of organic pollutants (methyl blue, methyl red, molasses, and lactic acid) from wastewater using an agitated batch photocatalytic reactor. It was found that as the mixing speed was increased from 350 to 450 rpm, the rate of adsorption decreased significantly. Thus, increasing the mixing speed significantly reduced the percentage removal. Concerning methylene blue, methyl red, molasses, and lactic acid, the percentage removal was reduced from 28.4 to 4.7 (~83.5%), 23.4 to 4.3 (~81.6%), and 29.5 to 4.1 (~85.1%). When the mixing speed was increased, the reversible process known as the desorption reaction began. The mixing then promoted the desorption of waste molecules from the surface of the TiO_2 particles before the oxidation reaction took place. Since adsorption is a physical phenomenon in nature, it can be assumed that with increasing the mixing speed, the weakly adsorbed waste compounds were easily

desorbed back from the surface of the TiO_2 particles to the solution. Consequently, it was shown that the mixing speed had an adverse effect on the waste removal percentage which could be attributed to its role in promoting the reversible process. Increasing the mixing speed therefore resulted in the desorption of the adsorbed waste molecules back into solution. This may explain the significant reduction in the percentage removal observed when the mixing speed was increased.

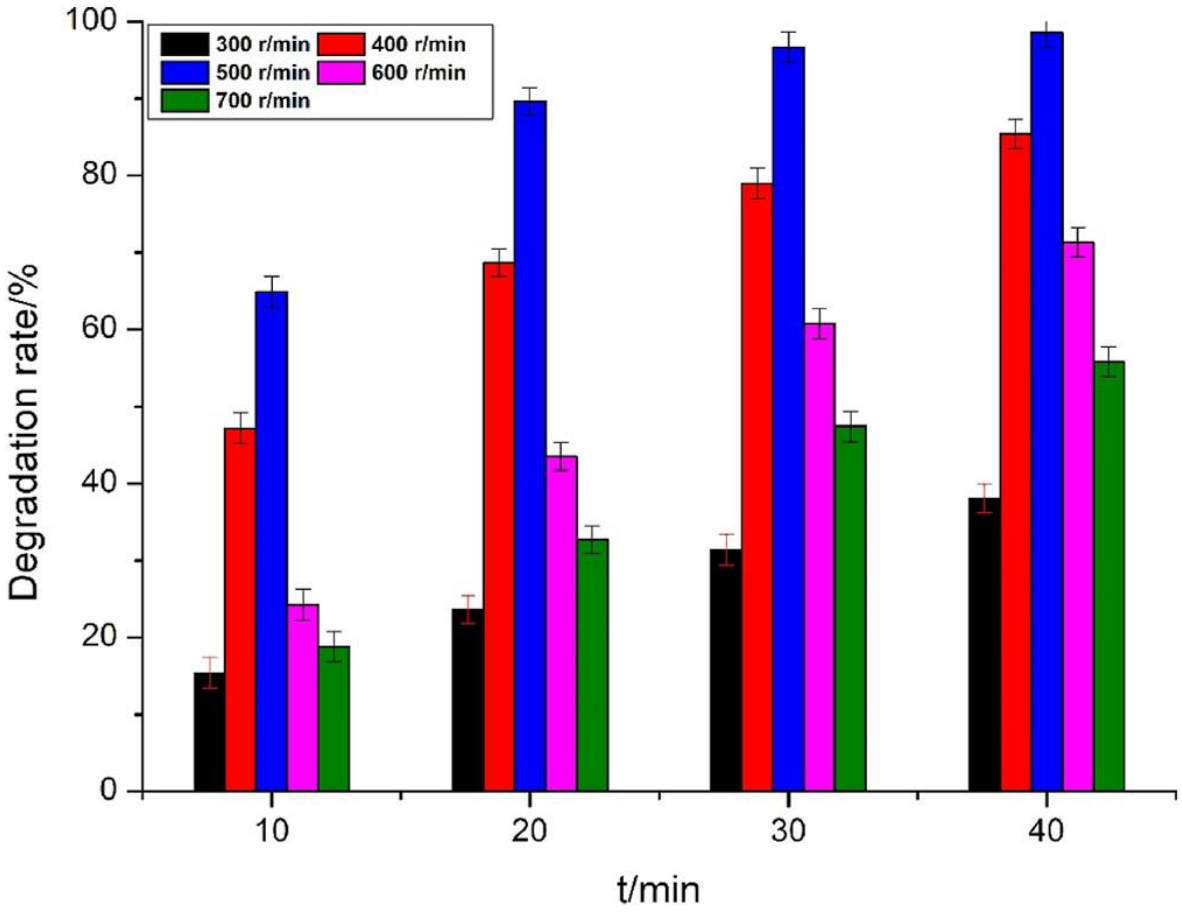

Figure 2-5: Effect of mixing speed on degradation rate

(Xu and Ma 2021)

2.11.3 Effect of exposure time

Kumar et al. (2023), studied the removal efficiency for MO (methyl orange) and TC (tetracycline) degradation over time with the optimized photocatalyst amounts. The degradation profile of MO was found to be linear, resulting in total removal within 120 minutes, while the profile of TC was found to be rapid initially, showing around 70% removal after 30 minutes, and subsequently exponential to reach an equilibrium removal efficiency of 97% after 180 minutes. The reactive oxygen species (ROS)

destruction of both targets was an explanation for the observed reduction in concentration over time. It was found that the ideal times for zinc hydroxystannate/zinc-tin oxide (ZHS/ZTO-1) to completely remove MO and TC are 120 and 180 minutes, respectively. In the range of 30 to 150 minutes at neutral pH. Azmoon et al. (2023) examined the impact of exposure time on the adsorption and photodegradation of synthetic oilfield-produced water (SOPW). The trend revealed changes in the removal percentage with contact time for all types of synthesized nanoparticles were similar. The removal rate was rapid at the initial period of contact time and then reached equilibrium. After this time, the change in the removal percentage was insignificant. The results revealed that increasing the exposure time enhanced the possibility of the pollutant interacting with the active sites, hence boosting the removal effectiveness. Additionally, in the photocatalytic area, longer contact times result in increased exposure to light, which increases the generation of active radicals and enhances the efficiency of photocatalytic degradation (Azmoon et al. 2023). Shivaraju (2011), studied the relationship between exposure time and the effectiveness of organic pollutant degradation and discovered that an increase in exposure time increased the degradation efficiency, as the highest degradation efficiency was correlated to the longest exposure time. Kumar and Pandey (2017a) investigated how the exposure time affected the photodegradation of methyl green and came to the same conclusion as Shivaraju (2011). This resulted from a longer period of interaction time between the pollutant and the photocatalyst surface.

2.11.4 Effect of direct photolysis

Direct photolysis uses light irradiation from a particular source to achieve the photo-degradation of organic contaminants without the use of a photocatalyst. The photolysis process can be aided by a variety of light sources, including solar light, LED lights, xenon lamps, and UV lamps. When compared to the photocatalysis process, the photolysis method of photo-degradation of organic contaminants showed less degradation activity. Numerous operational factors, including light intensity, reaction temperature, organic pollutant content, and solution pH, influence the photolysis process (Truppi et al. 2019). Furthermore, UV lamps with a wavelength of 254 nm, often known as low-pressure mercury lamps, can generate excellent photoelectric conversion efficiency. Thus, exposure to UV lamps can result in the formation of mercury resonance lines at 185 and 254 nm. The photolysis elimination efficacy of

these lamps ranges from 8% to 25%, contingent upon the UV lamp manufacturer and intensity (Bozzi, Yuranova and Kiwi 2005; Zoschke, Börnick and Worch 2014).

Shemer and Linden (2007), reported on the direct photolysis of dibenzothiophene (DBT), fluorene (FLU), and dibenzofuran (DBF) by UV (LP or MP) and UV/H_2O_2. These PAHs are polycyclic aromatic hydrocarbons. A high removal efficiency could not be achieved following the photolysis irradiation using UV fluence of 1000 mJ/cm2; only 15% of FLU and 6% of each DBT and DBF were destroyed (Figure 2-6a). Following UV/H_2O_2 irradiation, a notable improvement in the photolysis breakdown performance was observed. Consequently, when compared to the UV-LP lamp alone, the degradation rate rose 36-fold (Figure 2-6b). Equation (2-18) explains this finding by stating that more hydroxyl radicals are produced in the solution as a result of photolysis of the H_2O_2 molecules.

$$H_2O_2 + \text{UV light} \rightarrow 2OH^{\blacksquare} \qquad (2\text{-}18)$$

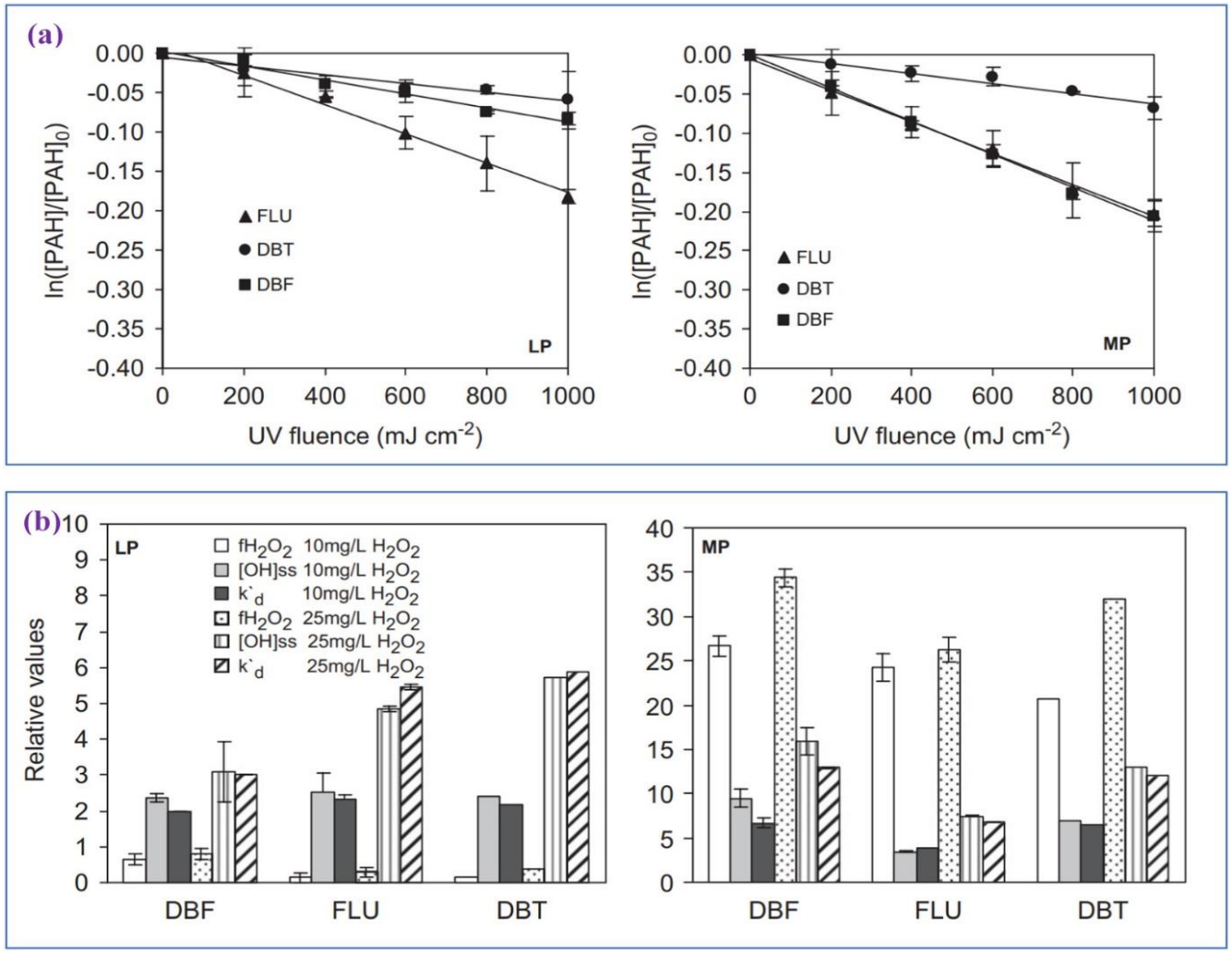

Figure 2-6: (a) FLU, DBT, and DBF degradation through direct photolysis under MP and LP UV lamps, (b) DBF, FLU, and DBT photolysis degradation rates by UV (MP and LP)/H_2O_2, and the percentage of light absorbed via H_2O_2 (10 and 25 mg/L)

(Jabbar and Graimed 2022)

Table 2-8 shows additional research that has been compiled to understand how light affects the photocatalytic degradation of organic contaminants.

Table 2-8: Summary of research utilizing various irradiation sources for the photocatalytic degradation of several organic compounds

Photocatalyst	Targeted pollutant	Irradiation source	Performance of photocatalysis	Ref.
TiO_2 powder	Rhodamine B	UV	• In 90 minutes, the removal efficiency was 42.1% at a light intensity of 23 W/m^2. • In 90 minutes, the removal effectiveness was 87.8% at 114 W/m2.	(Chanathaworn et al. 2012)
TiO_2	Coke water	UV	• In 60 minutes, the removal efficiency was 15% at 400 mW/cm^2 of light intensity. • In 60 minutes, the removal efficiency was 30% at a light intensity of 1300 mW/cm^2.	(Ba-Abbad et al. 2012)
TiO_2	Acid Yellow 17	UV	• Degradation activity was considerably enhanced when light intensity was increased from 1.24 mW/cm^2 to 3.15 mW/m^2.	(Liu et al. 2006)
TiO_2 nanorod arrays	COD in cooking wastewater	300 W UV light (250-380 nm)	• In ~60 minutes, 85% of COD was eliminated at 400 mW/cm^2. • In under 60 minutes, 92% of COD was eliminated at a light intensity of 1300 mW/cm^2.	(Gao et al. 2011)
TiO_2 (organic fibers)	Acid Orange 7	UV Solar	• Solar light deteriorates at a pace 1.5 times faster than artificial UV light.	(Rao, Subrahmanyam and Boule 2004)
TiO_2 (Degussa P25)	Reactive Yellow 17	UV Sunlight	• In 360 minutes, 100% of reactive yellow 17 was deteriorated under UV radiation. • In 720 minutes, 100% of reactive yellow 17 was broken down in the sun.	(Neppolian et al. 2002)
9 AC-ZnO	4-Acetyl phenol	UV Sunlight	• In 150 minutes, 100% of 4-acetylphenol was broken down by UV radiation. • In 120 minutes, 100% of 4-acetylphenol was broken down in the sun.	(Sobana, Muruganandam and Swaminathan 2008)
Nitrogen-doped TiO_2	Benzene	Visible light	• At 36×10^{-4} Lux light intensity, the photoreaction coefficient (kpm) is 3.992×10^{-6} mol·kg^{-1}·s^{-1}, while at 75×10^{-4} Lux illumination intensity, it is 11.55×10^{-6} mol·kg^{-1}·s^{-1}.	(Sun et al. 2018)

2.11.5 Effect of particle size

Modifying the particle size of the catalyst has been seen as an inexpensive improvement that improves surface area and photo-degradation. After a great deal of research, it was discovered that the photochemical reactions and degrading activities of bulk and nanoscale TiO_2 systems differ significantly (Zhou et al. 2018). High pollutant adsorption has been shown in recent research to be caused by larger surface areas between pollutants and TiO_2. It appears that increasing the surface area can be achieved by using small particle sizes. Reduction in particle size has two primary benefits: There will be a rise in (1) internal electron and hole recombination and (2) surface active sites. However, when the TiO_2 photocatalyst's particle size was reduced, two significant adverse consequences could happen: (1) There will be more electron and hole surface recombination; or (2) decreased photon usage (Liu, Jaffrezic and Guillard 2008). The optimal particle size for methylene blue was 35 nm after examining TiO_2 particle size from 15 to 60 nm. As a result, an optimum particle size may have arisen where an equilibrium between these two opposing effects was reached (Toyoda et al. 2004). Among a range of particle sizes from 4.5 to 12.8 nm, ~10 nm was probably the most optimal for TiO_2 on phenol degradation (Liu, Jaffrezic and Guillard 2008; Chen et al. 2020b).

2.11.6 Effect of morphology

Surface morphology (surface area, structure, and size of the photocatalyst) such as particle size and agglomerate size, are important factors to be considered in the photocatalytic degradation process. The number of photons striking the photocatalyst controls the rate of reaction which signifies that the reaction takes place only in the absorbed phase of the photocatalyst (Hoque and Guzman 2018).

The surface morphology of TiO_2 is a crucial factor in its use as a photocatalyst, as all the chemical events take place at the surface of the particle. Surface area can be substantially increased by using very fine particles, either suspended in solvents or made into a porous film. Nanostructured materials with a crystallite/grain size below 20 nm are of great research interest mainly since they may differ significantly from their bulk counterparts in terms of their physical attributes. Additionally, this had created opportunities for their use as photocatalysts in a variety of fields.

Kumar and Pandey (2017c) investigated the effect of surface area on the photodegradation of rose bengal dye in the presence of PAni/Graphene nanocomposites. The photodegradation of rose bengal was enhanced by an increase in the photocatalyst's surface area. This was attributed to the fact that materials with high surface area have more active sites than those with low surface area.

Kumar and Pandey (2017b) synthesized TiO_2 in several different forms to obtain the desired characteristics for the photocatalyst. The photodegradation of methyl red dyes using Cu-TiO_2 and TiO_2 nanocomposites revealed that less photodegradation happened with TiO_2 and more occurred with modified Cu-TiO_2. This was due to modified Cu-TiO_2 having a different surface to that of the pure TiO_2. The rough, zigzag surface of the modified Cu-TiO_2 aids in the adsorption of organic molecules on the catalyst surface. Thus, compared to pure TiO_2, modified Cu-TiO_2 demonstrated superior photocatalytic activity.

Li et al. (2020) acknowledged that the size and shape of the catalyst play a major role in determining its surface structure and adsorption capacity, which in turn affects photocatalytic effectiveness. Additionally, a catalyst's crystallite size also matters a lot in the photocatalytic process since increasing crystallinity might boost photoreactivity. Given that the adsorption of pollutants is a crucial step, photocatalytic activity was also greatly influenced by the surface area of the materials used as photocatalysts. As a result, a large surface area exhibited enhanced photocatalytic activity and had more active sites (Tian et al. 2014; Rani et al. 2018).

All the above factors mentioned affect the performance of the photocatalytic process. To improve treatability efficiency, the operating parameters were optimized. The next section will discuss the process by which the photocatalytic process will be optimized using the response surface methodology (RSM).

2.12 Process parameter optimization

Process parameter optimization involves selecting the best operational parameters to optimize the yield and efficiency of the intended product while lowering total costs (Sakkas et al. 2010; Okolie et al. 2021).

2.12.1 Merit of RSM over OFAT approach

The application of photocatalytic procedures for remediation has been mostly studied in terms of the determination of reaction kinetics, the reaction mechanism involved in the process as well as the identification of major transient intermediates. Most of the studies dealing with kinetics make use of the traditional one-factor-at-a-time (OFAT) approach, examining the effect of parameters such as initial concentration of target compounds, degradation time, catalyst load and characteristics, pH, temperature, UV light source, and intensity. If the process factors involved in the process are independent, the most common practice is OFAT while holding all others constant. Moreover, the OFAT approach is costly in the sense of time and reagents, and not that efficient. Therefore, chemometric methods such as response surface methodology (RSM) based on statistical design of experiments (DOEs) are becoming increasingly popular. These statistical studies are more effective because they take into consideration the interaction effects between the variables under study and precisely identify the set of levels that result in the process's optimal outcome. Thus, it is evident that the capacity to achieve the catalytic reaction's optimal state in photocatalytic processes greatly depends on the chemometric experimental design.

2.12.2 Design of experiments (DOE)

In a range of experimental scenarios, the link between process parameters (factors) and their output (response) can be assessed using the DOE, a useful tool for data collecting and analysis. It is possible to examine the impact of multiple factors on the reaction as well as their interactions by utilizing DOE. Additionally, after doing a minimal number of structured experiments, DOE makes it possible to represent the process factors mathematically (Rakić et al. 2014).

Selecting an appropriate design of experiment (DOE) is crucial before implementing the RSM methodology since it greatly affects how the response surface is constructed and, consequently, how accurate the prediction is. Simply, the purpose of DOE is the selection of the experimental points at which the response should be evaluated (Sakkas et al. 2010). Table 2-9 compiles several optimization techniques for analyzing how process factors affect photocatalysts (Sakkas et al. 2010; Okolie et al. 2021).

Table 2-9: Summary of various optimization techniques investigating the influence of process parameters

(Sakkas et al. 2010; Okolie et al. 2021)

Approach	Description	Key features	Merits	Limitations
Response surface methodology (RSM)	The response surface methodology (RSM) is a very popular statistical technique employed to model and optimize a process where the output (i.e. response) is sensitive to various parameters. The RSM technique aids in assessing how various parameters affect the response and how they interact with one another. It models the relationship between process variables and the response using empirical statistical techniques. The response, or output, is referred to as the dependent variable, while the variables that affect the process are referred to as the independent variables.	• It depends on the surface placement method for identifying the optimal region, ridgelines, and local minimum and maximum of the response surface. • The Box Behnken design (BBD) and the Central composite design (CCD) are the two primary experimental designs utilized in the response surface.	• It is possible to investigate parameter interactions. • In comparison to the univariate technique, which could necessitate more experiments, it requires fewer experiments and does not examine the relationships between parameters that could impact the process.	• Mostly, a second-order polynomial model fits the experimental data. A second-order polynomial, however, is incompatible with some curved systems. • For regions outside of the investigated range of components, the developed model is typically invalid (considered as a local analysis). • It can be difficult to assess the RSM approximation's accuracy at times (black-box technique).
Central composite design (CCD)	The two commonly utilized RSM techniques for optimization studies are Central Composite Design (CCD) and Box-Behnken (BBD). The CCD approach is a factorial or fractional factorial design that contains a centre point augmented with a group of star points or axial points. These points enable the estimation of curvature in the model. Experiments with multiple factors can be screened to identify the most important ones, and the CCD approach works well for these kinds of sequential experiment designs. As seen in Figure 2-7, the embedded factorial design of the CCD approach allows for the modification of its results to incorporate axial and center points.	• With two n factorial runs, two × n axial designs, and m number of centre runs, it is a five-level fractional factorial design. • The sum of the factorial runs, axial design, and centre run is the total number of runs.	• It can investigate how different parameters interact. • It can operate up to five levels per factor. • It provides precise estimates for both first- and second-order terms.	• Compared to the BBD design, it requires more experimental runs • It contains exceptionally high or low values.

Box-Behnken design (BBD)	The BBD approach does not include an embedded fractional or full factorial design. Instead, the design points fall at a combination of the high and low factor levels and their centre (mid) points. Axial points are absent from the BBD approach in contrast to the CCD method. Thus, the BBD method is useful for performing experiments that are feasible to operate beyond the safe operating limits. The axial points in the CCD design may drift outside the cube (Figure 2-7), causing the design points to expand above the initial levels.	• It uses a spherical design and is three-leveled. • Its foundation is a combination of incomplete block designs and the two-level factorial.	• Compared to CCD and FFD, it takes fewer experimental runs when the number of factors is the same. • It offers a very good estimate inside the design space. • It avoids all the corners and star points. • Both the first- and second-order coefficients can be estimated with efficiency.	• Runs from the factorial experiment cannot be used in the designs. • There can only be three levels for each factor. • Runs in which every factor is at its extreme are not included. • All of the designs are rotatable or almost rotatable, regardless of how many parameters are examined.
Factorial design (FD)	The influence of multiple factors and levels can be simultaneously studied using factorial designs. Different combinations of factors and levels are frequently included in factorial designs, allowing for the screening and identification of the factors that have the greatest impact on the response. These techniques help conduct initial optimization steps or for conducting preliminary investigations. There are two types of factorial design: fractional factorial design and full factorial design. Every potential combination of each factor level is fully tested within the full factorial design.	• It investigates how several factors, which are measured at every possible combination of the factorial levels, affect the response.	• The quantity of factors determines the quantity of experiments.	• Since these designs are rotatable, not all of the space equidistant from the centre can be predicted with accuracy. • It could take a lot of trial runs and be laborious.

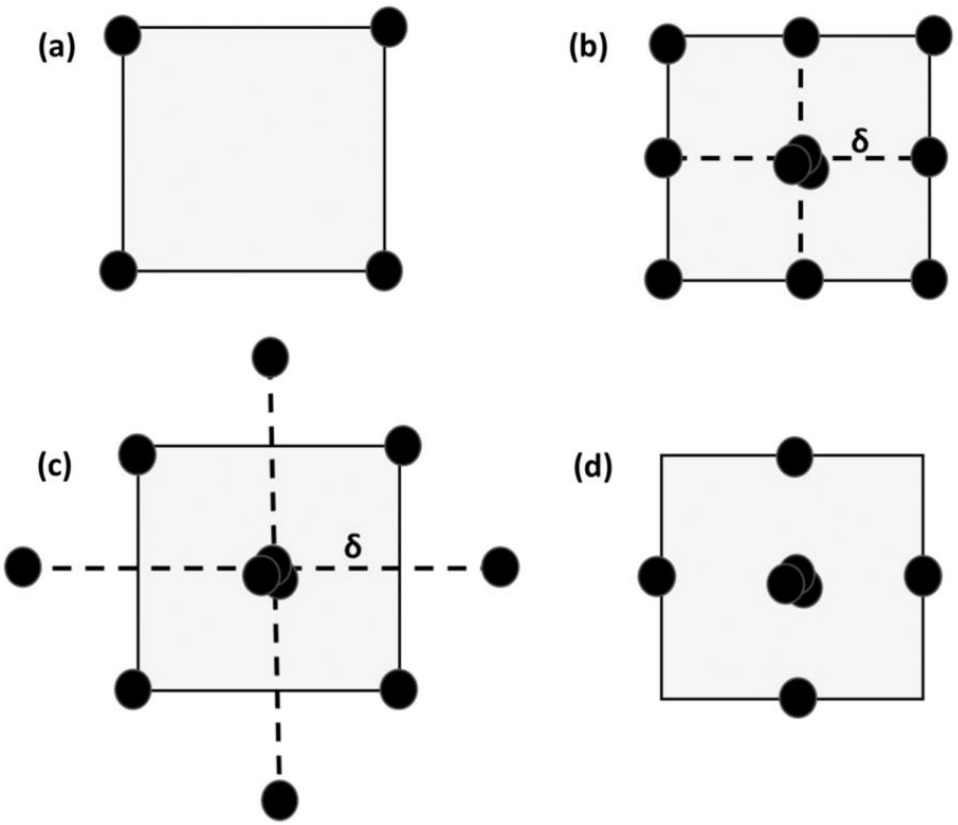

Figure 2-7: 2D representation of different experimental designs: (a) factorial design, (b) central composite design with δ = 1, (c) central composite design with δ > 1, and (d) Box-Behnken design. δ represents the coded axial-point distance

(Okolie et al. 2021)

2.12.3 Application of DOE in the photocatalytic process

Few studies addressing the use of the statistical design of experiments towards the photocatalytic degradation process have been investigated for the last three decades, even though the photocatalytic oxidation process is a newly developed technique employed for the destruction of dangerous substances. The optimal photocatalytic degradation efficiency is incorrectly predicted by the univariate or OFAT approach, which also neglects the interaction effect of certain photocatalytic variables. Some relative studies are summarized in Table 2-10 (Sakkas et al. 2010).

Table 2-10: RSM models for photocatalytic processes

Catalyst	Contaminant	Inputs	Outputs	Method	No of points	R^2	Ref.
ZnO@g-C_3N_4	Sulfamethoxazole	pH Catalyst load Air flow rate	Sulfamethoxazole degradation	CCD	20	0.98	(Mirzaei et al. 2018)
Nano carbon dots	Phenol	Irradiation time Catalyst load H_2O_2 amount	Phenol degradation	CCD	18	0.96-0.98	(Pirsaheb et al. 2018)
Bi4Ti3O12	Tetracycline	pH Temperature Irradiation time	Tetracycline degradation	BBD	14	0.99	(Khodadoost et al. 2017)
ZnO	Palm oil mill effluent	Initial COD Catalyst load O_2 flow rate Catalyst load	COD removal	CCD	24	0.93	(Ng et al. 2016)
Fe_3O_4 zeolite 13×	Biebrich scarlet	pH Catalyst load Concentration	Biebrich Scarlet degradation	CCD	20	0.98	(Khatri et al. 2016)
TiO_2	Direct red 16	pH Catalyst load Concentration	Direct red 16 degradation	CCD	20	Not given	(Soleymani et al. 2015)
$BiVO_4$	Methylene blue	pH Catalyst load Concentration	Methylene Blue degradation	CCD	17	0.98	(Abdullah, Moey and Yusof 2012)
Ag-TiO_2	Methyl blue	pH Catalyst load Concentration	COD removal Colour removal	BBD	15	0.99-0.99	(Sahoo and Gupta 2012)
TiO_2	Chloramphenicol	pH Catalyst loading Concentration	Chloramphenicol degradation	CCD	20	0.95	(Chong, Zhu and Jin 2010)

2.13 Summary

Real-time and relevant literature reveals that South Africa is the epitome of water and wastewater challenges. Water outages lasting several days, inadequate wastewater treatment facilities, and pollution of primary water resources (rivers, dams, and oceans) with untreated or partially treated sewage from which drinking water is extracted, severely compromises the quality of water. This wastewater contains several bio-recalcitrant pollutants and contaminants such as potentially toxic elements, pathogens, organic micropollutants, etc. that are detrimental to human health and aquatic life. The removal of these pollutants and contaminants is consequently given the highest priority considering its detrimental effects on people, animals, and the environment.

Wastewater generated from industrial applications is characterized by a high content of COD, turbidity, and organic pollutants. Physical, biological, and chemical treatment methods are ineffective and inefficient and are either slow or non-destructive to some or most persistent organic pollutants. Photocatalysis (advanced oxidation process) is a promising eco-friendly, cost-effective technology for degrading organic pollutants and contaminants from water and wastewater into harmless compounds (CO_2 and H_2O). Photocatalysis involves the acceleration of the rate of chemical reactions in the presence of semiconductor catalysts, radiation (UV/Solar), and pollutants. However, the current photocatalytic technology cannot meet industrial requirements. The photocatalyst prepared at this stage possesses several disadvantages. Therefore, exploring alternative semiconductor photocatalysts to mitigate the organic micropollutants (OMP) concerns and treating South Africa's wastewater streams with an optimized performance is significant to adhere to the stringent regulations for water quality requirements (SDG goals) and essential for wastewater reclamation and reuse.

CHAPTER THREE
METHODOLOGY

3.1 Introduction

This chapter presents the methodology utilized in this study, such as materials and methods, including the effluent sample and characterization, chemicals and reagents, test work solution preparation, and analytical methods used. The experimental setup, description of equipment, and operational procedures were described. Two experimental equipment configurations were used for Objective One and Two respectively in treating the OMPs from a local South African municipal wastewater treatment plant. A photocatalytic degradation wastewater treatment system using a constant UV light source (PDWT-CUV) and a laboratory-scale photochemical reactor (L-SPR) were used for Objective One and Two respectively. The one-factor-at-a-time OFAT approach was used to evaluate the key factors that affect the municipal wastewater treatability performance using the PDWT-CUV and L-SPR, followed by the optimization of the operating conditions for the photocatalytic process using the best catalyst, where the response surface methodology (RSM) was employed. The Box-Behnken design (BBD) adapted from the RSM was employed to design the experimental runs, analyze the results, and optimize the key interactive factors. Finally, the optimum conditions (catalyst load, mixing speed, and exposure time), the best photocatalyst (CuS) obtained from Objective One, and the best light source determined from Objective Two were applied to raw and synthetic wastewater, where a comparison of the best photocatalyst (CuS) and TiO_2 was illustrated.

3.2 Materials and methods

3.2.1 Effluent sample and characterization

The raw municipal wastewater effluent samples were obtained from a local eThekwini municipality WWTP located in Durban, Kwa-Zulu Natal, South Africa, which was sampled in 25L drums and utilized to conduct this study. Before every experiment, the samples were carefully agitated to guarantee a homogenous feed combination.

Characterization of the samples was done to suit each objective at hand and the performance criteria were well defined. This was carried out for both objectives; Firstly, to investigate the applicability and performance of oxide (TiO_2 and Fe_2O_3) and non-

oxide (CuS and ZnS) transition metal photocatalysts. Secondly, to investigate the effect of light sources (UV, UV-visible, and natural sunlight) on the performance of photocatalytic degradation. The results for each case study's findings are tabulated in Appendices B and C, respectively.

The critical performance criteria were assessed based on the OMP's removal efficiency concerning the water quality characteristics: pH, turbidity (NTU); COD (mg/L); and colour (Pt. Co). This wastewater was characterized below, which was used as the basis for analyzing the experimental results obtained (Tables 3-1, 3-2, and 3-3).

Table 3-1: Properties of raw and synthetic wastewater before treatment for Objective 1

Component	Raw Wastewater	Synthetic Wastewater
	Value	Value
pH	6.95	6.14
Colour (Pt. Co)	104	1812
Turbidity (NTU)	17.23	506.3
COD (mg/L)	1716	1923

Table 3-2: Properties of raw and synthetic wastewater before treatment for Objective 2

Component	Raw Wastewater	Synthetic Wastewater
	Value	Value
pH	8.12	8.63
Colour (Pt. Co)	1949	3950
Turbidity (NTU)	124	519
COD (mg/L)	8950	9150

Table 3-3: Properties of raw and synthetic wastewater before treatment for Objective 3 (RSM)

Component	Raw Wastewater	Synthetic Wastewater
	Value	Value
pH	7.24	6.98
Colour (Pt. Co)	569	2724
Turbidity (NTU)	48.33	307
COD (mg/L)	855,33	8960

Synthetic wastewater was simulated using 15 L of distilled water which contained the synthetic water chemical makeup tabulated in Table 3-4, and 5 L of raw wastewater which was then homogenized into a solution. This synthetic wastewater solution represents the typical composition for the wastewater treatment plant as the organics are increased with the addition of chemicals found within the synthetic water makeup. The composition of the chemicals used was adapted from Munien *et al.* (2023) and is

displayed in Table 3-4. The best-performing photocatalyst was determined using synthetic wastewater.

Table 3-4: Chemical composition of synthetic wastewater

(Munien *et al.* (2023))

Chemical Name	Chemical Formula	Mass Added (g)
Calcium Chloride Monohydrate	$CaCl_2H_2O$	1
Peptone	Peptone	40
Glucose	Glucose	27.52
Bicarbonate of soda	$NaHCO_3$	68.75
Urea	Urea	7.52
Magnesium Sulphate	$MgSO_4$	0.5
Potassium Hydrogen Phosphate	K_2HPO_4	7
Copper (II) Chloride Heptahydrate	$CuCl_2$•7H2O	0.0125
Sodium Chloride	NaCl	2.2

3.2.2 Chemicals and reagents

All the chemicals and reagents used in this study were supplied by local South African suppliers and all photocatalysts used in this study were supplied by Sigma Aldrich, Durban, South Africa which are listed in Table 3-5. Four (4) photocatalysts, two (2) oxide photocatalysts, and two (2) non-oxide photocatalysts were used for the investigation. The physicochemical characteristics of the semiconductor photocatalysts considered are depicted in Table 3-6.

Table 3-5: List of chemicals and reagents used for the study

Chemical Name	Chemical Formula	South African local Suppliers
Photocatalysts		
Titanium (IV) Oxide	TiO_2	Sigma Aldrich
Iron (III) oxide / Ferric Oxide	Fe_2O_3	Sigma Aldrich
Zinc Sulphide	ZnS	Sigma Aldrich
Cupric Sulphide	CuS	Sigma Aldrich
Synthetic Water		
Calcium Chloride Dihydrate	$CaCl_2 \cdot 2H_2O$	Associated Chemical Enterprises (ace)
Peptone	$C_{13}H_{24}O_4$	OXOID
Glucose	$C_6H_{12}O_6$	RADCHEM (PTY) LTD
Sodium Hydrogen Carbonate	$NaHCO_3$	Rochelle Chemicals (RC)
Urea	CH_4N_2O	RADCHEM Laboratory Supplies
Magnesium Sulphate Heptahydrate	$MgSO_4 \cdot 7H_2O$	RADCHEM (PTY) LTD
Di-Potassium Hydrogen Orthophosphate	K_2HPO_4	Associated Chemical Enterprises (ace)
Copper Chloride Dihydrate	$CuCl_2 \cdot 2H_2O$	Associated Chemical Enterprises (ace)
Sodium Chloride	NaCl	Associated Chemical Enterprises (ace)
Analytical Reagents		
Chemical Oxygen Demand (COD)	COD vials high range (0-1500 mg/L)	Universal Water Solutions

Table 3-6: Properties of semiconductor photocatalyst chemicals

Property	Semiconductor Photocatalyst				Ref.
	TiO_2	Fe_2O_3	ZnS	CuS	
Band Gap (eV)	3.2 eV	2.2 eV	3.6 eV	1.6-2.2 eV	(Zhang *et al.* 2019b; Shaikh *et al.* 2022)
Absorbance Wavelength (nm)	275-405 nm	320-420 nm	375-575 nm	380-800 nm	(Parkavan, Viswanathan and Prabakar 2014; Cedeño et al. 2018; Ghamarpoor, Fallah and Jamshidi 2023; Wei and Zheng 2024)
Purity	ReagentPlus®, ≥99%	≥96%	97% (from Zn)	≥99% trace metals basis	(MERCK 2024c, 2024b, 2024d, 2024a)
Phase mixture	ratio anatase to rutile is 75/25	N/A	N/A	N/A	(Munien et al. 2023)
Molecular Weight (g/mol)	79.87 (g/mol)	159.69 (g/mol)	97.46 (g/mol)	95.61 (g/mol)	(MERCK 2024c, 2024b, 2024d, 2024a)
Density (g/cm^3)	4.26 g/mL at 25°C	5.25 (g/cm^3) at 25°C	4.1 g/cm^3 at 25°C	4.6 g/mL at 25°C	(MERCK 2024c, 2024b, 2024d, 2024a)
Water Solubility	N/A	0.001 g/L at 20°C	N/A	N/A	(MERCK 2024c, 2024b, 2024d, 2024a)
Physical Description	Powder	Red to Brown Powder	White to Faint Yellow Crystals	Blue to Black Powder	(MERCK 2024c, 2024b, 2024d, 2024a)

3.2.2.1 Test work solution preparation

The synthetic wastewater solution was prepared for experimental analysis using the chemicals and photocatalysts listed in Table 3-4. The goal was to find the optimal conditions for the photocatalytic degradation of the OMPs. The respective catalyst loading quantities suitable for use in the jar tests were precisely measured in preparation.

i. Synthetic wastewater solution:

A 20 L volumetric bucket was used to conduct the experimental runs.14 L and 5 L of deionized water and raw wastewater, respectively, were transferred into the 20 L volumetric bucket. 1 L of deionized water was then added to a 2000 mL (2 L) beaker. The chemicals and respective quantities presented in Table 3-4 were weighed precisely into weigh boats. These chemicals were then added into the 2 L beaker containing the 1 L of deionized water. Two magnetic stirrers were then placed into the mixture and were allowed to mix for 15-30 minutes until homogenous. This mixture containing the synthetic wastewater chemical constituents where then added to the volumetric bucket containing the wastewater and deionized water, where it was mixed well until adequately homogenized. This combined mixture was used as synthetic wastewater which was utilized to run all experimental runs and test work.

ii. Actual wastewater sample (synthetic wastewater and the photocatalyst):

0.5; 1; 1.5; 2 and 2.5 g of the respective photocatalyst were weighed into weigh boats. Six 2 L beakers were used for six photocatalyst solutions. 1 L of synthetic wastewater was measured into each 2 L beaker. The respective photocatalyst dosage was then added to the respective beakers which is then referred to as the actual sample.

3.2.3 Analytical methods

The essential contaminants in the raw wastewater were used in determining the performance of the photocatalytic degradation for the treatment of the OMPs including pH, turbidity, colour, and COD. These parameters were analyzed by their specific standards using the equipment listed in Table 3-7, and the procedure is vividly explained in Appendix A. The treatability efficiencies were computed using Equation (3-1).

$$R\,(\%) = \frac{Z_A - Z_B}{Z_A} \times 100 \qquad (3\text{-}1)$$

Where R represents the removal efficiency percentage, and Z_A and Z_B are the initial and final values of each pollutant (COD, turbidity, and colour).

Table 3-7: List of instruments and methods utilized to test the water quality.

Water quality test	Instrument
pH	Thermo Scientific Eutech Elite PTCS
Chemical Oxygen Demand (COD) (mg/L)	Hach DRB 3900 Spectrophotometer
Turbidity (NTU)	Turbidity Meter (Hanna HI 98703).
Colour (Pt. Co)	Hach DRB 3900 Spectrophotometer

3.3 Experimental setup

For the first and second objectives, respectively, two experimental setups were used. Firstly, for Objective 1 (Section 3.3.1), the photocatalytic degradation wastewater treatment system experimental setup with a constant UV source (PDWT-CUV) was used. Secondly, Objective 2 (Section 3.3.2) examined the effect of UV and UV-visible light sources on the efficiency of photocatalytic degradation of municipal wastewater using a laboratory-scale photochemical reactor (L-SPR). Section 3.3.3 described and illustrated the experimental setup to for the effect of sunlight irradiation investigation.

3.3.1 Description of the PDWT-CUV [Objective 1]

The primary objective of the use of PDWT-CUV was to determine the effect of the degradation parameters to which the photocatalytic treatment process of the OMP is optimum concerning the water quality using COD as an indicative degradation measure.

The pictorial view of the apparatus for Objective 1 in Figure 3-1 shows the photocatalytic degradation in progress using a constant UV light source. The experiments were carried out in a six-place jar testing apparatus (JLT 6, flocculation

tester, Velp Scientific, New York, NY, USA) shown in Figure 3-1. The setup consists of six identical 2 L beakers, where all wastewater was fed. All beakers were equipped with a stirrer. These beakers allow for evaluating different catalyst dosages simultaneously. Two 1-inch-diameter radiant fluorescent T8 black light blue bulbs (wavelength 400 nm), with a power rating of 18 W were used as the UV light source to excite the catalysts to trigger a reaction. The light intensity (Lux) was noted as 42x100 (4 200) Lux using the MT940 handheld Lux Meter under constant UV irradiation (Refer to Appendix A4). The light was incident on the beakers equally to ensure uniformity of light distribution, as depicted in Figure 3-1. The experimental setup was properly covered to prevent any other light source emissions from penetrating through the system since the constituents are photoreactive.

3.3.1.1 PDWT-CUV operational procedure [Objective 1]

The first experiment varied catalyst load from 0.5-2.5 g/L in increments of 0.5 g/L, whilst exposure time and mixing speed remained constant at 45 minutes and 90 rpm, respectively. The optimal catalyst load was then obtained and applied to the second experiment. The second experiment varied mixing speed from 30-150 rpm in increments of 30 rpm, whilst exposure time and catalytic load remained constant at 45 minutes and 1.5 g/L, respectively. The third experiment varied exposure time from 10-60 minutes in increments of 10 minutes, whilst catalyst load and mixing speed remained constant at 1.5 g/L and 90 rpm, respectively. The volume of effluent used for each beaker was 1 L. After each experimental run, the mixer was turned off, and the contents were allowed to settle for ~30 minutes and filtered using general laboratory filter paper (MACHEREY-NAGEL (MN 615), Pore size (4–12 µm)) and then collected in 50 mL sample bottles. Thereafter each solution was analyzed for pH, colour, turbidity, and COD removal.

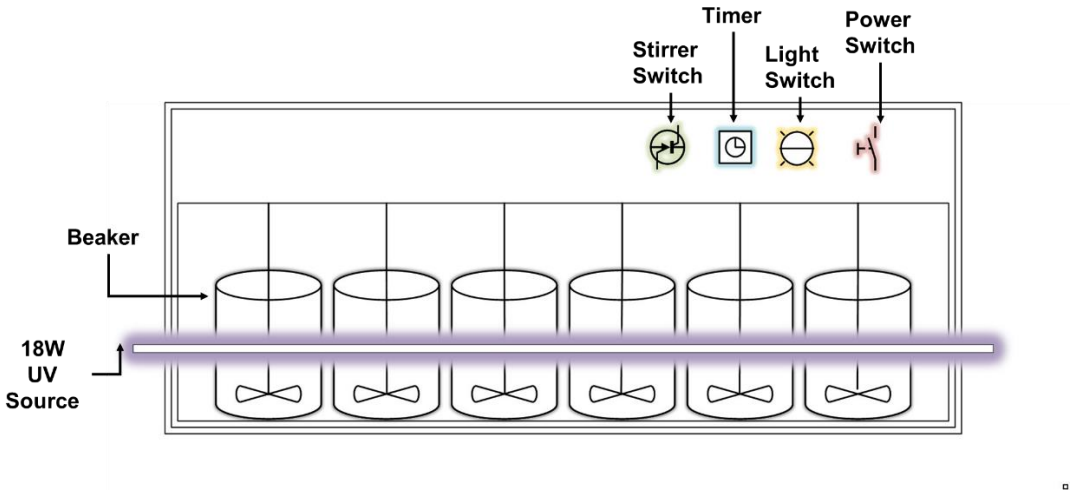

Figure 3-1: Schematic representation of the PDWT-CUV photocatalytic degradation wastewater treatment system experimental set-up using constant UV light irradiation [Objective 1]

3.3.1.2 PDWT-CUV start-up procedure

To start-up the PDWT-CUV in Figure 3-1, the following procedure was followed.

i. The prepared photocatalyst was introduced into the 6 respective until the desired measurement (1 L) was obtained and then inserted into the PDWT-CUV unit.
ii. The two constant UV light sources were then placed incident on the beakers equally to ensure uniformity of light distribution to excite the catalysts to trigger a reaction.
iii. The stirrers were all inserted into the respective beakers containing the photocatalyst.
iv. The power switch was switched on, and the mixing/stirrer speed and timer were set respectively.
v. The PDWT-CUV system was then sheltered to prevent light from compromising the experiment since the constituents are photosensitive.
vi. The start-up was then successfully initiated.
vii. The PDWT-CUV built-in timer then indicated when the experimental run was completed.

3.3.1.3 PDWT-CUV shutdown procedure

To shut down the PDWT-CUV in Figure 3-1, the following procedure was followed.

i. After the experimental run was completed, the power switch was switched off.
ii. The shelter was removed.
iii. The stirrers were all withdrawn, and the two constant light sources were then removed to allow beakers to be extracted for storage and analysis later.

3.3.2 Description of the (L-SPR) [Objective 2]

For Objective 2, the effect of the various light sources (UV and UV-visible) on the performance of photocatalytic degradation was investigated. The experiments were carried out using the optimum conditions achieved in Objective 1, i.e. catalyst load (1.5 g/L) and mixing speed (90 rpm). Figure 3-2 shows the set-up of a laboratory-scale photochemical reactor (Lelesil Innovative Systems). The photochemical reactor consists of a reaction vessel that has a 1.5 L capacity, and an immersion well made of quartz, which houses the UV lamp. A cold-water circulating tank was used to cool down the immersion well that contains the lamp. A 250 W, 365 nm mercury UV and UV-visible lamp was used. The light intensity (Lux) under UV and UV-visible irradiation was noted as 600x100 (60 000) and 1910x100 (191 000) Lux, respectively.

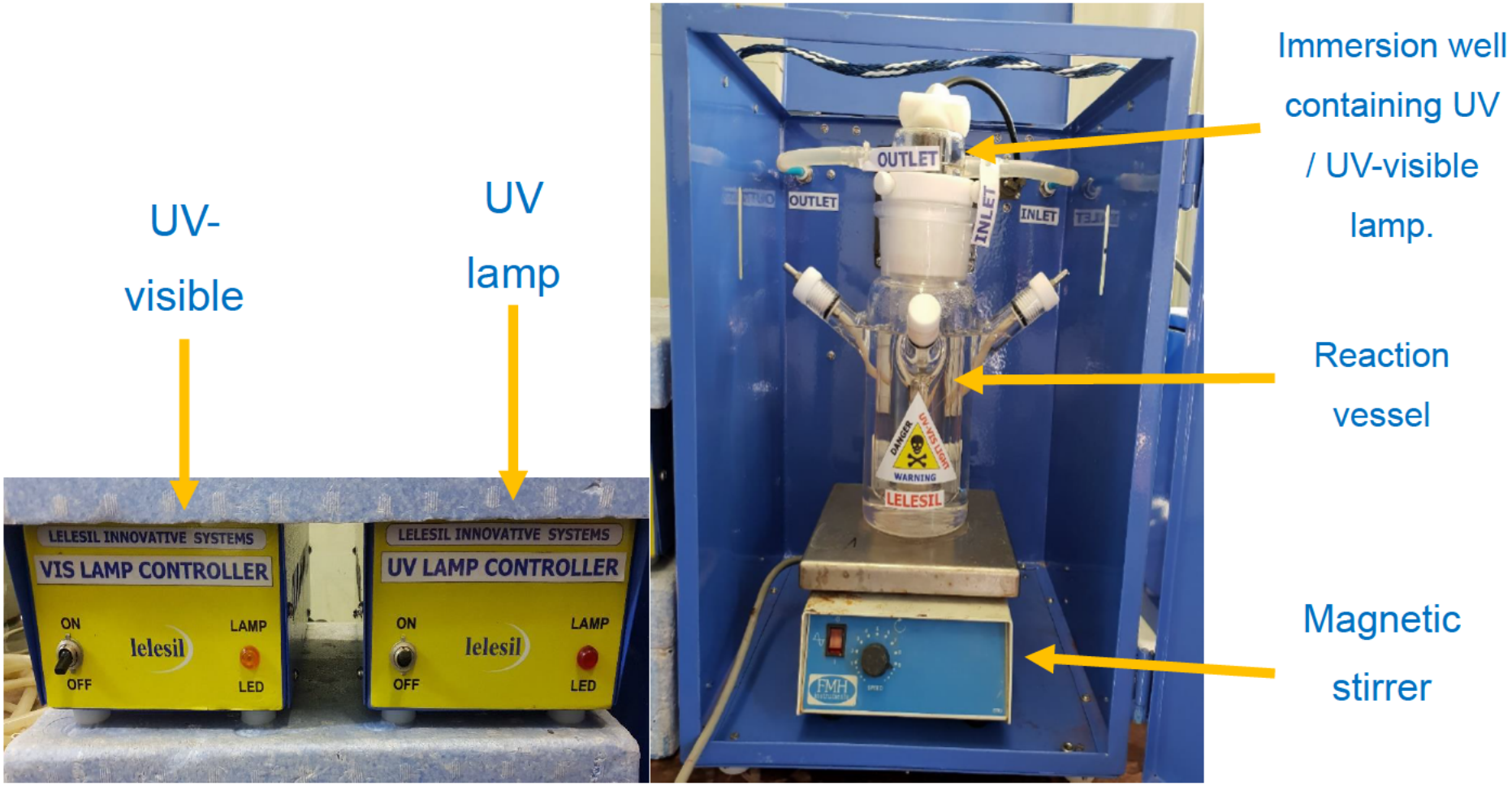

Figure 3-2: (L-SPR) Laboratory-scale photochemical reactor

(Lelesil Innovative Systems)

3.3.2.1 Overview of the (L-SPR) [Objective 2]

Table 3-8 shows the description, functionality, and precautions of the respective components within the photochemical reactor (Lelesil Innovative Systems) (AOP) (Tetteh 2022).

Table 3-8: Component unit and checklist of the Laboratory-scale photochemical reactor (Lelesil Innovative Systems) (AOP)

(Tetteh 2022)

Advanced oxidation process (AOP)		
Components	**Functionality**	**Remarks**
❖ UV/UV-visible photoreactor (LELESIL, Model: 1140 - Alpha, India) • TQR Super 500 ml German Borosilicate Glass Reactor - working volume 100 - 450 ml. • Central double UV jacket with dip tube, for UV & VIS lamp. • Virgin Teflon TQR super taper sealable for sealing quartz to the outer reactor. • Ports: liquid sampling In, liquid sampling Out, Solid Port. • 250 W Visible & 250 W UV lamps with safety resister with 4 pin connector, single-ended 2 P design. • Transformer, 2 pins for 250 W Vis and 250 W UV, 3 pins for 230 AC main power. • Eye-protect TM safety cabinet with LED lamps, • 4” cooling vent fan, PU coating Flexi top lid for inserting lamp. 3 pin for 230 AC main power • Magnetic drive: digital display 100-1500 RPM with LED display for RPM.	• Photocatalytic degradation of organic matter. • Charge with photocatalyst.	✓ Always protect your eyes. ✓ Ensure there is enough water in the cooling tank. ✓ Handle UV/UV-visible lamps with care. ✓ Maintain AOP level at 150-450 mL. ✓ Ensure intermittent mixing. ✓ Switch off and unplug the system after runs.
❖ 3 L cooling tank with submersible pump	• To maintain the temperature of the photoreactor.	✓ Ensure there is enough water before starting the reactor.
❖ UV/UV-visible controller	• Lamp controller with pulsating (4 pulses per second) igniter Switch and electronic ballast.	✓ Use the right controller for the suitable lamp in use.

3.3.2.2 L-SPR start-up procedure

To start-up the L-SPR in Figure 3-2, the following procedure was followed.

i. All electronic cables were connected, and the power switch was switched on.
ii. The cooling tank was fed with adequate water.
iii. The prepared photocatalyst was introduced into the beaker/immersion well until the desired measurement (1 L) was obtained and then inserted into the immersion well unit.
iv. The mixing/stirrer speed on the magnetic stirrer and timer was set and adjusted accordingly.
v. The AOP system was then closed.
vi. The right controller was used for the suitable lamp (UV/UV-visible lamps) in use.
vii. The L-SPR start switch was then initiated.

3.3.2.3 L-SPR shutdown procedure

To shut down the L-SPR in Figure 3-2, the following procedure was followed.

i. After the experimental run was completed, the power switch was switched off.
ii. The stirrer speed was switched off.
iii. The valves were closed after sampling.
iv. The water quality was checked after it was allowed to settle.

3.3.3 Description of sunlight irradiation light source set-up [Objective 2]

In this experimental setup, all wastewater was fed into four identical 2 L beakers which were all fitted with magnetic stirrers and exposed to sunlight to stimulate the catalysts and initiate a reaction. The sunlight was incident on the beakers to ensure uniformity of light distribution, as depicted in Figure 3-3. The light intensity (Lux) under sunlight irradiation was noted as 1337x100 Lux within the allocated experimental location (Chemical Engineering Laboratory Basement) to provide an accurate display of light levels.

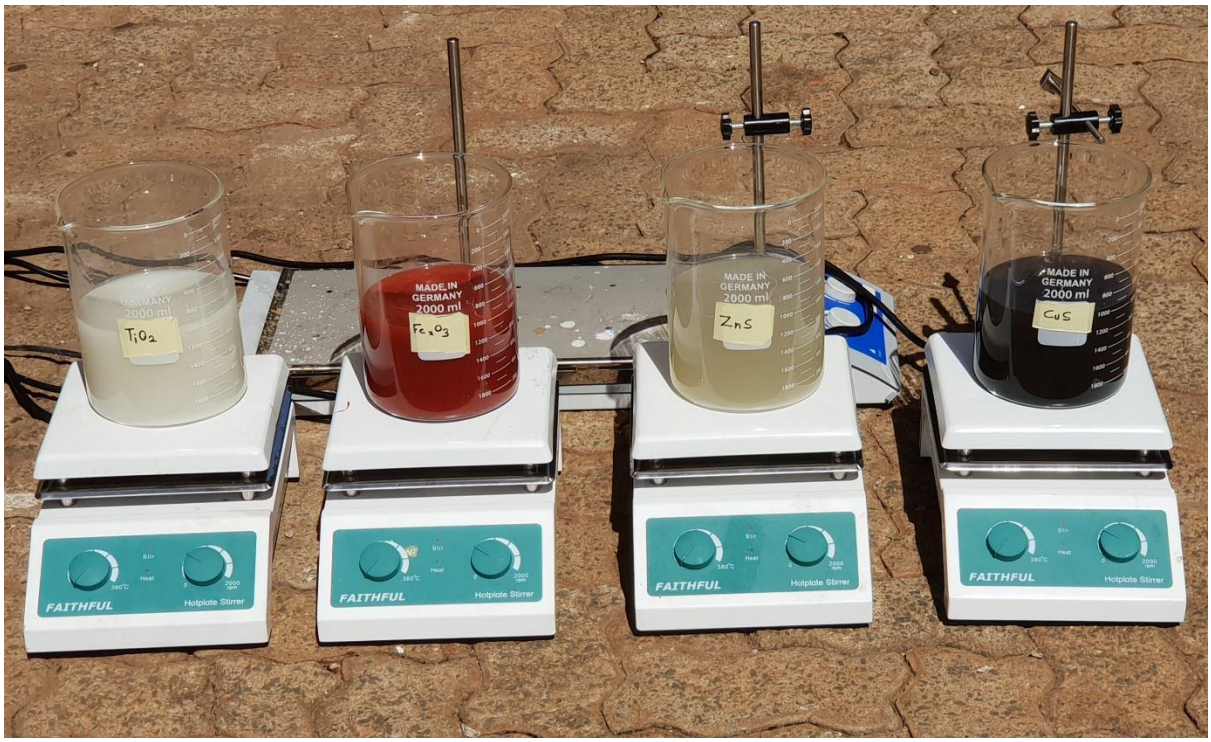

Figure 3-3: Demonstration of the photocatalytic degradation wastewater treatment system experimental set-up using sunlight irradiation

3.3.4 PDWT-CUV and L-SPR investigation conditions

The following experimental procedure was followed to complete the investigation to determine the applicability and performance of oxide transition metal photocatalysts for municipal wastewater treatment using the PDWT-CUV and L-SPR.

i. A mixing speed of 90 rpm and exposure time of 45 minutes was kept constant and was used to evaluate the effect and performance of each of the four photocatalysts (TiO_2, Fe_2O_3, CuS, and ZnS) at a catalyst load between the range of 0.5, 1, 1.5, 2 and 2.5 g/L.
ii. Using the optimal catalyst load (1.5 g/L) determined from (i), catalyst load of 1.5 g/L and exposure time of 45 minutes were kept constant and were used to evaluate the effect and performance of each of the above-mentioned photocatalysts at mixing speeds within the range of 30, 60, 90, 120, and 150 rpm.
iii. Using the optimal catalyst load (1.5 g/L) and mixing speed (90 rpm) determined from (i) and (ii), respectively, the catalyst load of 1.5 g/L and mixing speed at 90 rpm was kept constant and was used to evaluate the effect and performance of each of the above-mentioned photocatalysts at exposure time intervals of 0, 10, 20, 30, 40, 50, 60 minutes.
iv. To investigate the interactional effects and the relationship between the input variables (catalyst load, mixing speed, and exposure time) for the L-SPR using the experimental matrix of the BBD adapted from RSM, as shown in Table 3-9, was used.

3.4 Design of experiments (DOE)

Utilizing Design Expert (11) software, a systematic design of the experiment was developed in this study to obtain sufficient data to optimize the process with the least number of experiments. The motive was to identify the optimum range of the operating parameters and the most significant to control, maximize, and enhance the efficiency of the photocatalytic process for the treatment of municipal wastewater. Furthermore, to obtain a comprehensive grasp of the interactions and correlations that exist between the input variables and the response (water quality), data that could fit and be utilized to develop empirical models for each of the responses (pH, colour, and COD) should be gathered.

The following are a few of the features that the Design Expert offers:

I. **Construction of the design matrix:** This entails creating the subsequent experimental runs based on the input parameters to collect the response (output) data.

II. **Analyzing data and modeling responses:** The response data must first be computed. Thereafter, model graphs illustrating the interactional effects of the input variables in actual vs. predicted contours and 3D surfaces will be provided for modeling and statistical analysis. The polynomial relationship between the factors and the response concerning actual or coded factors (-1, 0, 1) will also be expressed by the analysis of variance (ANOVA) and regression coefficient (R^2).

III. **Process Optimization**: The Design Expert generates a satisfying condition for the desired response which combines levels of each input factor. Numerical and graphical representation could also be used to optimize numerous factors at the same time.

3.4.1 Response Surface Methodology (RSM)

Response Surface Methodology (RSM) is a suitable optimization tool for developing and studying the independent and interactive factors in a process. This includes enhancement, process optimization, and product development (Lamidi et al. 2022). Essentially, RSM establishes the relationship between a variable and its effect (response), with the advantage of producing a mathematical model. The design of the experiment was performed based on the Box-Behnken design (BBD) adopted from RSM using Design Expert (version 11) developed by Stat-Ease, Minneapolis, MN, USA.

3.4.1.1 The Box-Behnken Design (BBD) procedure

The input variables are provided in Table 3-9.

Table 3-9: Experimental design conditions and factor levels using BBD-adapted from RSM

Cases	Process	Input variables		Coded levels (X)		
				-1	0	1
1	L-SPR	X_1	Catalyst Load (g/L)	1	1.5	2
		X_2	Mixing Speed (rpm)	60	90	120
		X_3	Exposure Time (minutes)	10	35	60

The BBD adapted from the RSM, obtained fifteen (15) trial runs, three (3) input factors, three (3) levels, and triplicated (3) centre points. The following procedure was followed:

i. The problem was identified and thereafter optimized with experimental data
ii. The type of input facto levels and ranges were defined with the number of centre points.
iii. The number of response variables was defined as the water quality (COD, turbidity, and colour).
iv. The Box-Behnken design was selected as the suitable response surface experimental design to generate the matrix.
v. The experimental matrix was followed, and the response data was generated.
vi. The response data was entered, and the data was statistically analyzed.
vii. The response models generated were verified by comparing their predicted values with that of the experimental results where necessary with the optimum conditions or the most influential factors.
viii. The conclusion and recommendations were then deduced.

CHAPTER FOUR
RESULTS AND DISCUSSION

4.1 Introduction

This chapter analyses and explains the experimental results obtained to investigate the performance and suitability of oxide and non-oxide transition metal photocatalysts for the treatment of municipal wastewater. Additionally, it evaluates the effect of light sources on the photocatalytic degradation of municipal wastewater. It further reveals the optimization of the operating conditions of the photocatalytic process with RSM utilizing the optimum photocatalyst and light source to determine the relationship that exists between the most significant factors and the water quality metrics. Section 4.2 evaluates the applicability, performance, and effect of oxide and non-oxide transition metal photocatalysts in terms of catalyst load, mixing speed, exposure time, and cost. Section 4.3 evaluates the effect of light sources on performance using COD as a performance indicator. Finally, in section 4.4, RSM is used to optimize the operating conditions (catalyst load, mixing speed, and exposure time) of the photocatalytic process.

4.2 Evaluation of the applicability and performance of oxide and non-oxide transition metal photocatalysts

This section discusses the effect of the significant operational parameters at their respective ranges such as catalyst load (section 4.21), mixing speed (section 4.2.2), and exposure time (section 4.2.3). The parameters investigated were catalyst load (0.5-2.5 g/L) at increments of 0.5 g/L, mixing speed (30-150 rpm) at increments of 30 rpm, and exposure time (60 minutes) at 10-minute time intervals, using the experimental analysis one-factor-at-a-time (OFAT) approach. The photocatalysts considered were TiO_2, Fe_2O_3, ZnS, and CuS, and the MWW characterized in Table 3-1. To ascertain photocatalytic efficiency, water quality parameters, including chemical oxygen demand (COD), turbidity, colour, and pH of the treated effluent, were analyzed to evaluate the effectiveness of the semiconductor photocatalysts at different catalyst loading/dosages. The respective semiconductor photocatalyst costs were then estimated and compared at the optimum catalyst load rate (section 4.2.6).

4.2.1 Effect of catalyst load on photocatalytic treatment

The photochemical impacts of the UV light used with a wavelength emitting span of 400 nm had a significant effect on each photocatalyst examined. Thus, the photocatalysis electron-hole generation was greatly influenced by the light intensity within the reactor, which influenced the pollutant transformation and destruction efficiency. By evaluating the catalyst load (0.5-2.5 g) of TiO_2, Fe_2O_3, ZnS, and CuS in increasing sequence of 0.5g. It was observed that each catalyst load affected the photocatalytic degradation of the wastewater contaminants. As shown in Figure 4-1, the photocatalytic degradation efficiency first improved by the photocatalytic loading but decreased with excessive addition. For TiO_2 and Fe_2O_3, the COD removal rates decreased from 0.5 g/L to 1.5 g/L and increased from 1 g/L to 1.5 g/L, respectively. This could be a result of the photocatalyst's surface becoming saturated due to high pollutant concentrations, which reduced its efficiency. Likewise, a higher pollutant concentration would have resulted in slower degradation since fewer photons would have reached the catalyst surface because the light intensity had remained constant. Additionally, the presence of scavengers in the solution can trap radicals and diminish the rate of degradation (Eniola *et al.* 2021; Groeneveld *et al.* 2023).

Evidently, at the best catalyst load of 1.5 g, the decreasing order of the COD removal (Figure 4-1a) by the catalyst was CuS (73%) > Fe_2O_3 (70%) > TiO_2 (30%) > ZnS (24%). This was due to the CuS with a bandgap of 2.2 eV (absorption wavelength 600-800 nm), having a good visible light absorption capacity, which produced electron-holes to bond with the organic contaminants (COD). On the contrary, TiO_2 and ZnS with bandgaps of 3.2 eV and 3.6-3.8 eV, respectively, were difficult to oxidize or hydrolyze the organics at a high electron-hole recombination rate (Zhang *et al.* 2019b). In terms of turbidity removal (Figure 4-1b), at the same catalyst load of 1.5 g, ZnS showed a good performance of 79% followed by Fe_2O_3 (75%) > TiO_2 (71%) > CuS (61%). Moreso, the decolourization (Figure 4-1c) favoured ZnS (66%) > TiO_2 (64%) > Fe_2O_3 (57%) > CuS (37%). It was deduced from the results that the tendency of agglomeration, such as particle-particle contact increased concerning time, where active sites of the catalysts were ignited by the light source (Wang et al. 2020; Deng et al. 2021). However, at that point where the active particle in the water exceeds that of the catalyst or vice-versa, the light penetration becomes impeded due to the suspended particles. These phenomena adversely affected the optimal photocatalyst

load required for photocatalytic oxidation and, therefore, caused the irregular illumination of the catalyst with a slow reaction rate.

To avoid excess catalyst, the optimal dosage of 1.5 g considered affirms that photocatalyst reactions must consider a dosage lower than the saturation threshold photocatalyst utilized for effective degradation. These results concur with the findings of previous work (Tayade, Natarajan and Bajaj 2009; Jallouli et al. 2018), that state removal efficiencies increase with an increase in catalyst load, up until the optimum catalyst load and then a decrease in removal efficiency is experienced above the optimum catalyst load. According to Fawzi Suleiman Khasawneh and Palaniandy (2021), the photocatalyst concentration in the treatment system plays an important role in the degradation process. It has been reported by authors Kaur and Kansal (2016), that the quantity of photons absorbed on the catalyst's surface increases as the photocatalyst in the treatment system is added. Consequently, there is a rise in the production of electron-hole pairs and hydroxyl radicals ($OH^{\blacksquare}$). Akpan and Hameed (2010) also stated that as the catalyst loading amount is increased during the treatment process, more active sites are created on the photocatalyst surface, which in turn causes more hydroxyl and superoxide radicals to be produced.

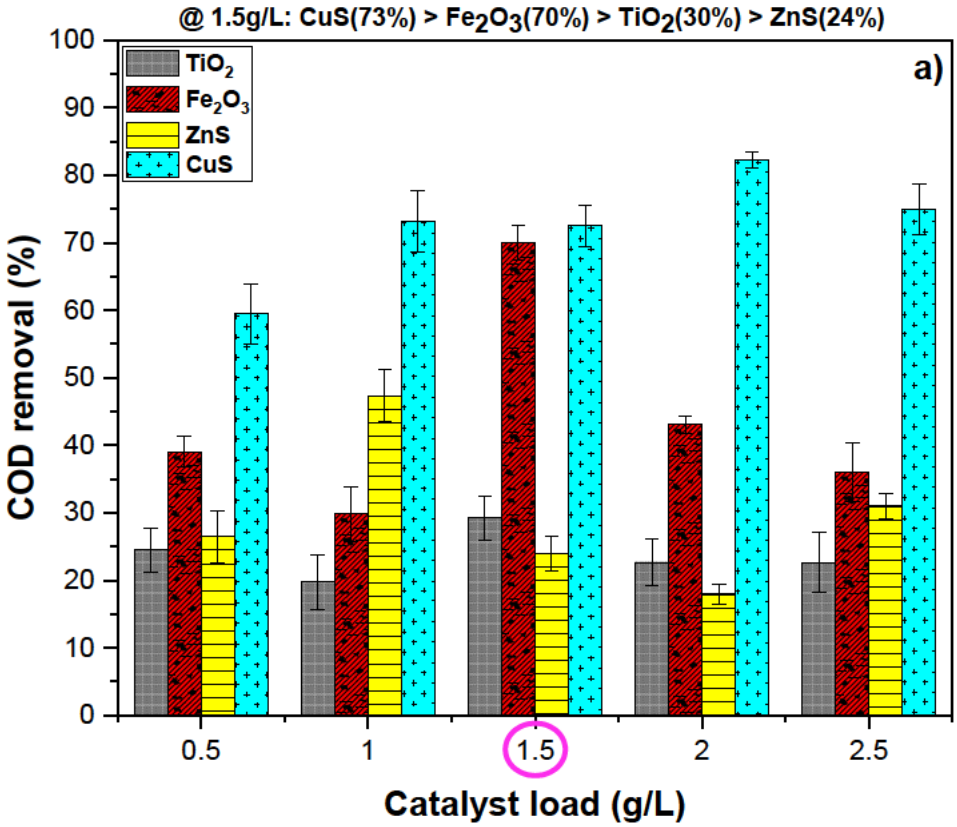

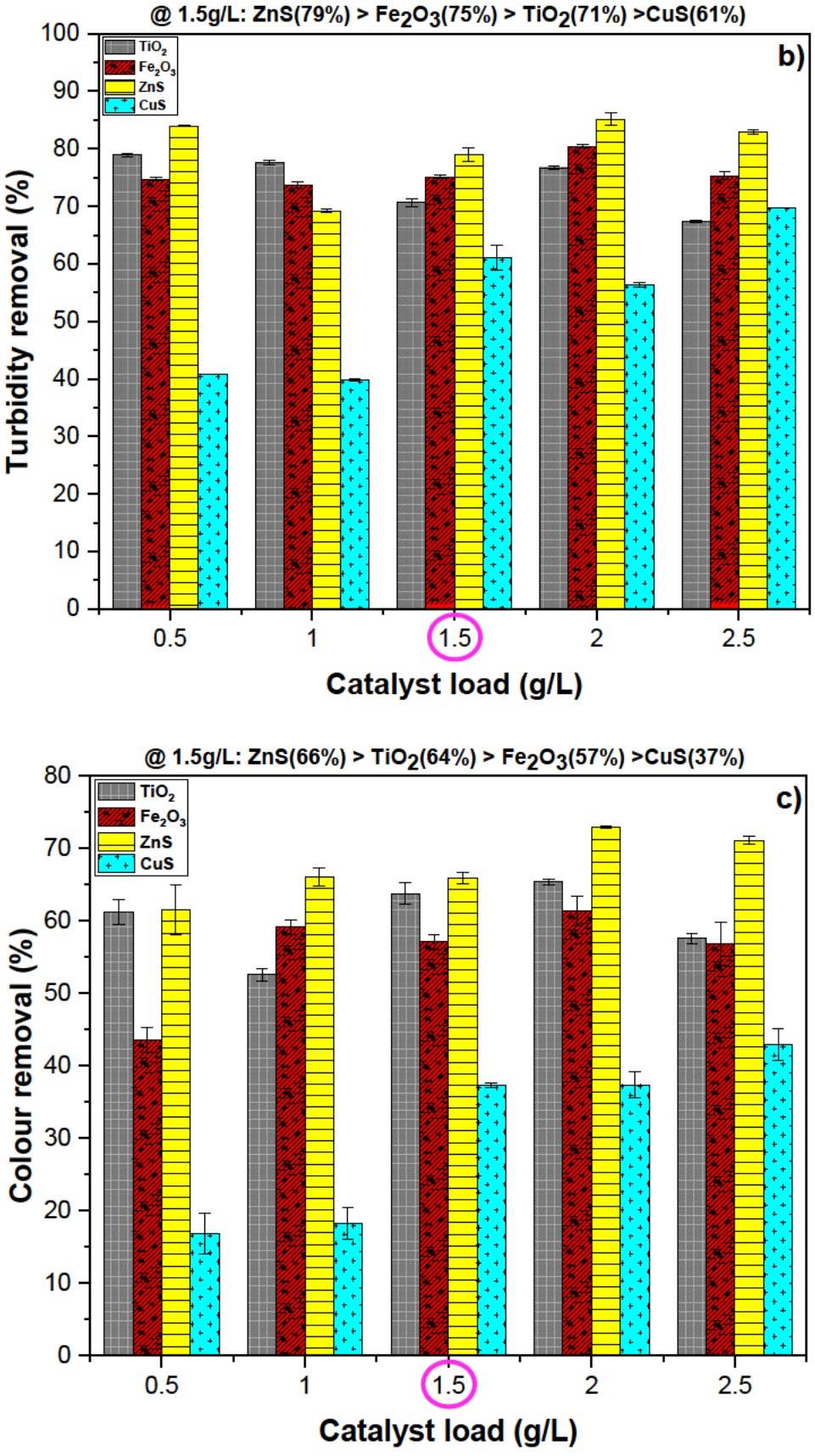

Figure 4-1: Effect of catalyst load (0.5-2.5 g) of TiO_2, Fe_2O_3, ZnS, and CuS for the removal of (a) COD, (b) turbidity, and (c) colour

4.2.2 Effect of mixing speed on photocatalytic treatment

The microstructure and homogeneity of the catalysts and the water molecules were influenced by the mixing speed. As shown in Figure 4-2, an increase in mixing speed (30-150 rpm) affected the catalyst-water molecules inter-particle reactions. The lower mixing speed (30 rpm) favoured Fe_2O_3 > ZnS > CuS > TiO_2 for the removal of COD (Figure 4-2a). Fe_2O_3 semiconductor photocatalyst was the most effective for COD removal with a value of 68.35% at 30 rpm. TiO_2 showed a COD removal efficiency of 65.96% at 60 rpm. ZnS and CuS resulted in COD removal efficiencies of 63.96% and 58.19% at 30 rpm, respectively. This is because higher agitation introduces and increases the oxygenation of the water molecules which affects the amount of COD removed. Due to the high surface-to-volume ratio property for ZnS, more electrons get excited into the conduction band which resides on the surface. Also, sulphur vacancies may reside on the photocatalyst surface, which acts as electron traps for excited electrons. The existence of electron traps present at the ZnS/CuS surface can react with the adsorbates, and there these excited electrons react with molecular O_2 which results in the formation of superoxide ion radicals ($O_2^{\blacksquare -}$), and its further conversion to hydrogen peroxide (H_2O_2). The ($O_2^{\blacksquare -}$) can react with H_2O to generate ($OH^{\blacksquare}$) and ($HOO^{\blacksquare}$) with powerful oxidizing ability which directly oxidizes all dye molecules in the UV-visible light radiation. Pre-existing saturation of Zn^{2+}/Cu^{2+} ions on the surface would have given emission in the range of 375-575 nm. The surface defects also could improve the electron-to-hole ratio on the photocatalysts by preventing electron-hole recombination (Sharma *et al.* 2012). This could explain the relatively minor rise increase in the region between 120 – 150 rpm for ZnS and CuS. There were oscillating trends observed with an increase in the mixing speed for the removal of turbidity (Figure 4-2b) and colour (Figure 4-2c). In Figure 4-2b, CuS and ZnS semiconductor photocatalysts displayed the most efficacy for turbidity removal efficiency of 98.59% and 91.70% at 90 rpm and 120 rpm, respectively.

TiO_2 shows an optimum turbidity removal efficiency of 78.60% at 30 rpm. Fe_2O_3 displays an optimum turbidity removal efficiency of 74.39% at 120 rpm. In Figure 4-2c, Fe_2O_3, CuS, and ZnS semiconductor photocatalysts displayed the most efficacy for colour removal efficiency at 51.31%, 92.17%, and 91.91%, at 90 rpm and 120 rpm, respectively. Likewise, TiO_2 showed a colour removal efficiency of 55.98% at 30 rpm. This could be attributed to CuS and ZnS having higher stability, which require higher

mixing speeds as compared to TiO_2 (powder) which tends to agglomerate in the water system, thereby increasing the turbidity and colour (Wang et al. 2020; Deng et al. 2021).

Moreover, the high agitation develops more surface area contact interactions between particles of the catalyst and the water molecules. However, this affected the homogeneity of the water molecules and agglomeration of the particles (Govindaraj and Pattabhi 2015). This study conforms with the findings of previous work, which state that the degradation rate increases slightly with mixing speed (Wu, Chang and Chern 2006; Aislen and Aislen 2021).

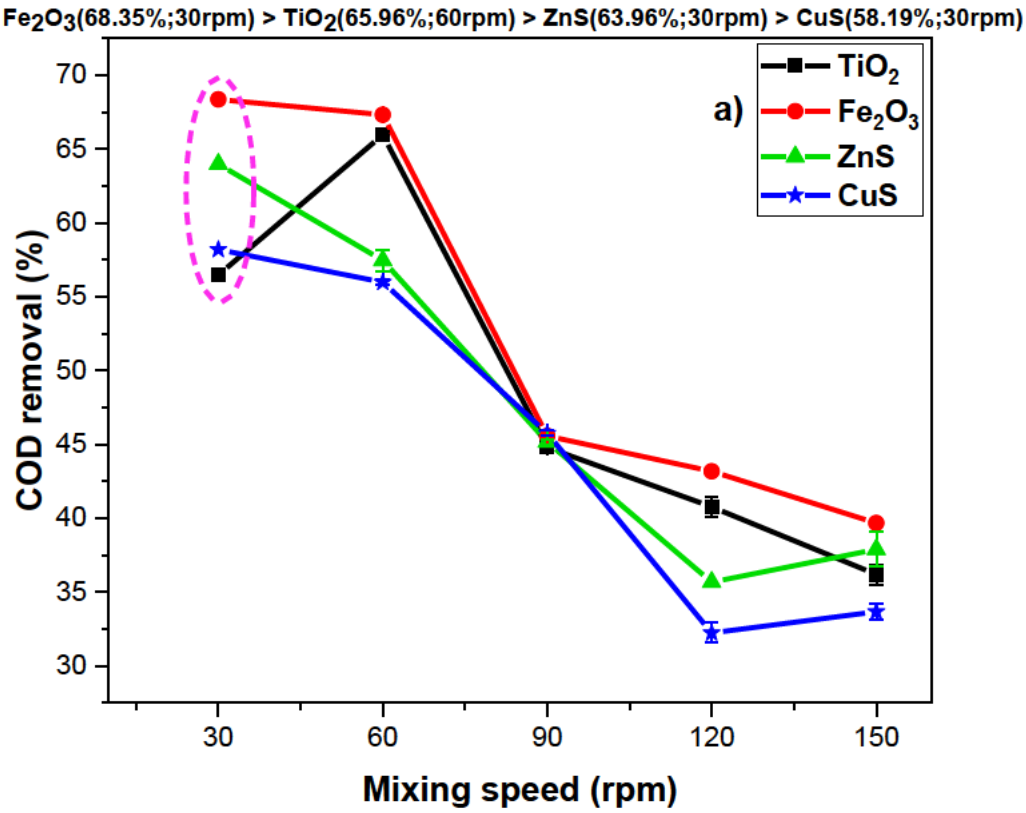

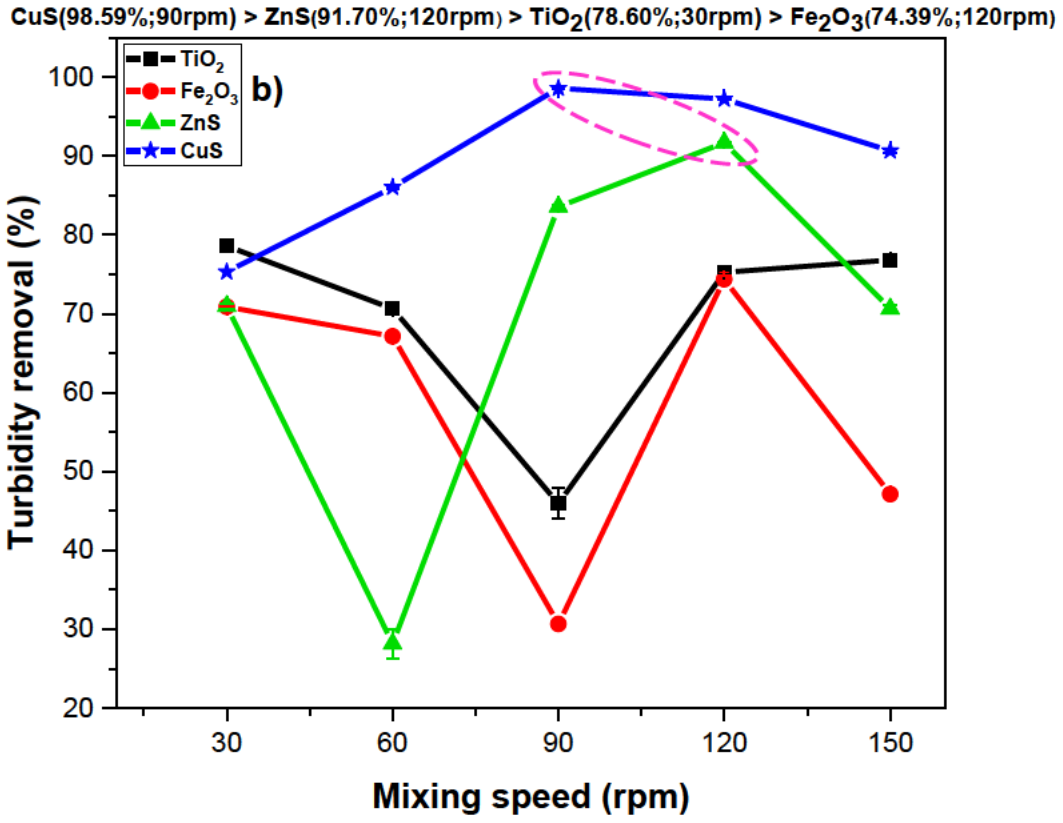

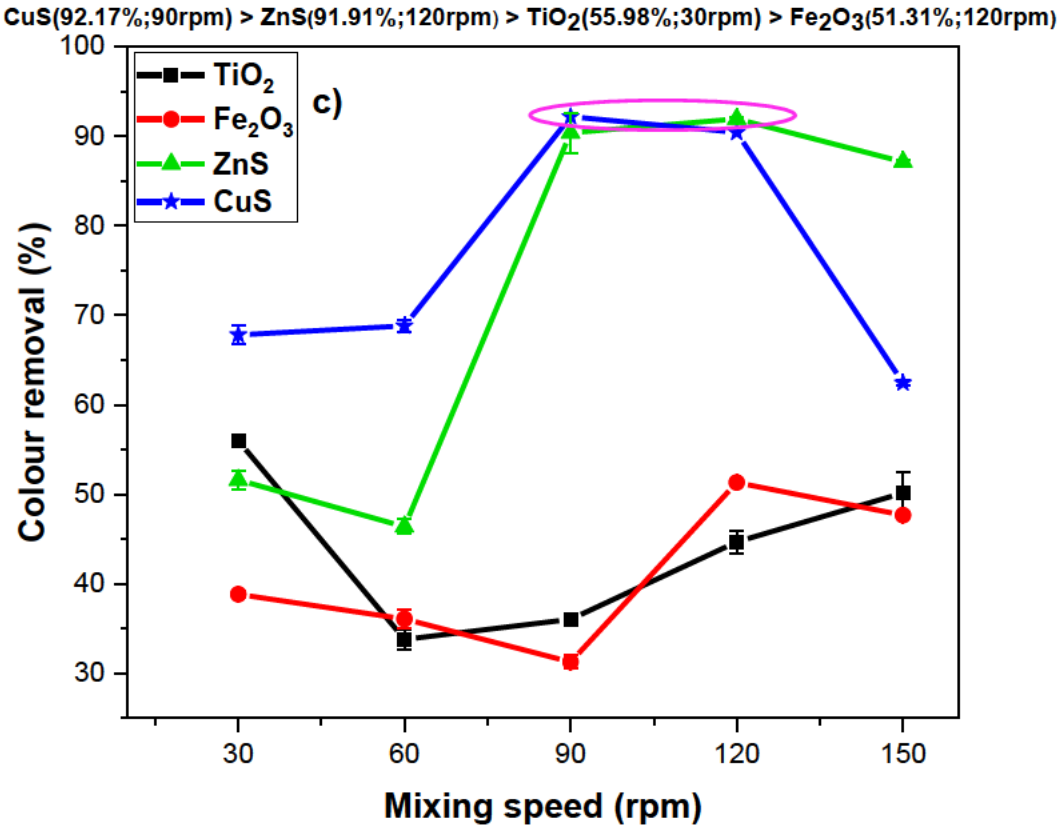

Figure 4-2: Effect of mixing speed (30-150 rpm) on (a) COD, (b) turbidity, and (c) colour removal using TiO_2, Fe_2O_3, ZnS, and CuS

4.2.3 Effect of exposure time on photocatalytic treatment

The exposure time was varied from 10 to 60 minutes, whilst the mixing speed and catalyst load were kept constant at 90 rpm and 1.5 g/L, respectively. As shown in Figure 4-3a, ZnS, TiO_2, and CuS have the best COD removal efficiency at 79.03%, 75.30%, and 74.93% at 20, 10, and 20 minutes, respectively. Fe_2O_3 had the best COD removal efficiency of 77.08% at 50 minutes. The initial increase in COD removal efficiency is such that with an increase in contact time, the availability of hydroxyl radicals for the oxidation of pollutants present in wastewater increases (Syed, Mauriya and Shaik 2022). Kumar and Pandey (2017a) studied the effect of exposure time on the photodegradation of methyl green and also found that an increase in exposure time increased the degradation efficiency, which they attributed to increased interaction time between the pollutant and the surface of the photocatalyst.

The decrease thereafter might be due to the aggregation of photocatalysts with the pollutants, and with time, the interactive surface of the photocatalyst became saturated and dissociated, contributing to secondary complex pollutants (Tayade, Natarajan and Bajaj 2009; Al-Nuaim, Alwasiti and Shnain 2023). The sudden drop in photocatalytic degradation followed by a sudden rise observed with CuS and ZnS at 20, 30, and 40 mins and 40, 50, and 60 mins respectively could be due to several factors, such as: (i) pollutant concentration, i.e., at high concentrations, the surface of the photocatalyst may become saturated, reducing its efficiency; (ii) light intensity, i.e., when the irradiation light intensity remained constant, but the pollutant concentration increased, fewer photons reached the catalyst surface, which can lead to slower degradation and (iii) the presence of scavengers in the solution can trap radicals and decrease the rate of degradation (Eniola *et al.* 2021; Groeneveld *et al.* 2023). There were oscillating patterns observed for all photocatalysts with an increase in the mixing speed for turbidity removal, which could be attributed to a chemical reaction in which the concentrations of the products and reactants change periodically, either with position or time in the reacting medium (Figure 4-3b). CuS semiconductor photocatalysts displayed the most efficacy for turbidity removal efficiency of 95.87% at 40 minutes. ZnS, Fe_2O_3, and TiO_2 show optimum turbidity removal efficiency of 89.65%, 84.38%, and 84.29% at 20, 30 and 40 minutes, respectively. CuS and ZnS semiconductor photocatalysts displayed the most efficacy for colour removal efficiency at 93.62% and 85.79% at 40 and 50 minutes, respectively (Figure 4-3c). Similarly, this could be

attributed to CuS and ZnS having higher stability, which favour more exposure time as compared to TiO_2 and Fe_2O_3 (powder), which tend to agglomerate in the water system, thereby increasing the turbidity and colour. Fe_2O_3 and TiO_2 show optimum colour removal efficiency of 76.48% and 75.06% at 10 minutes.

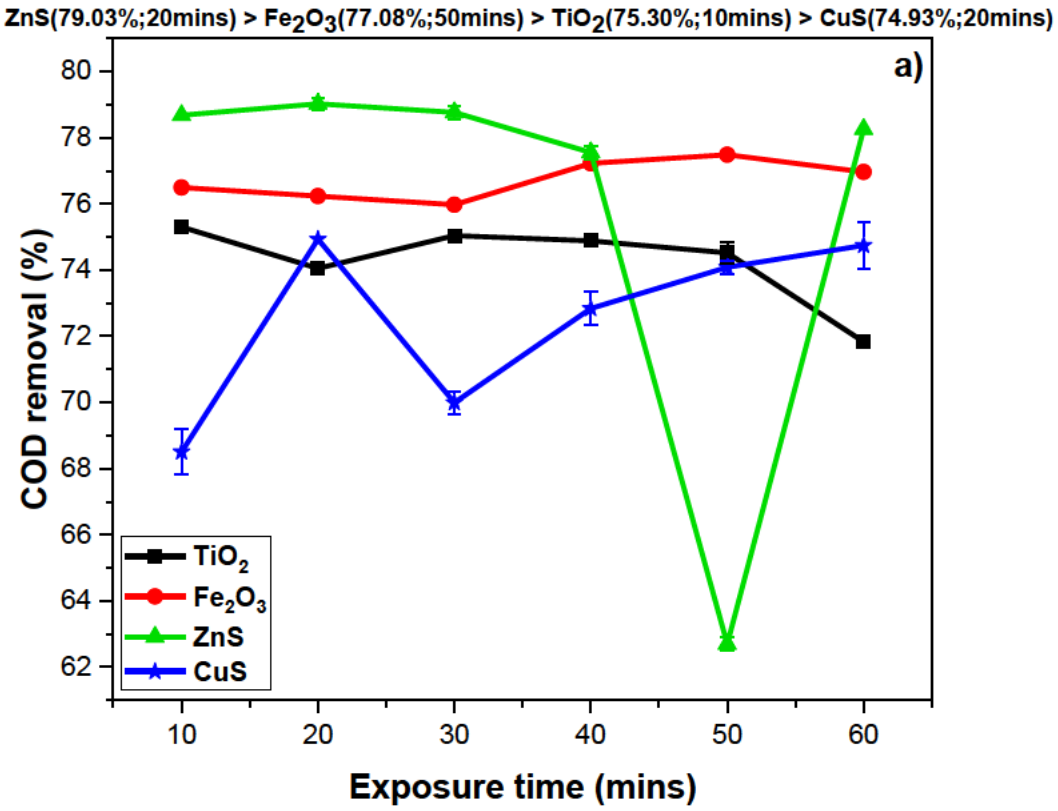

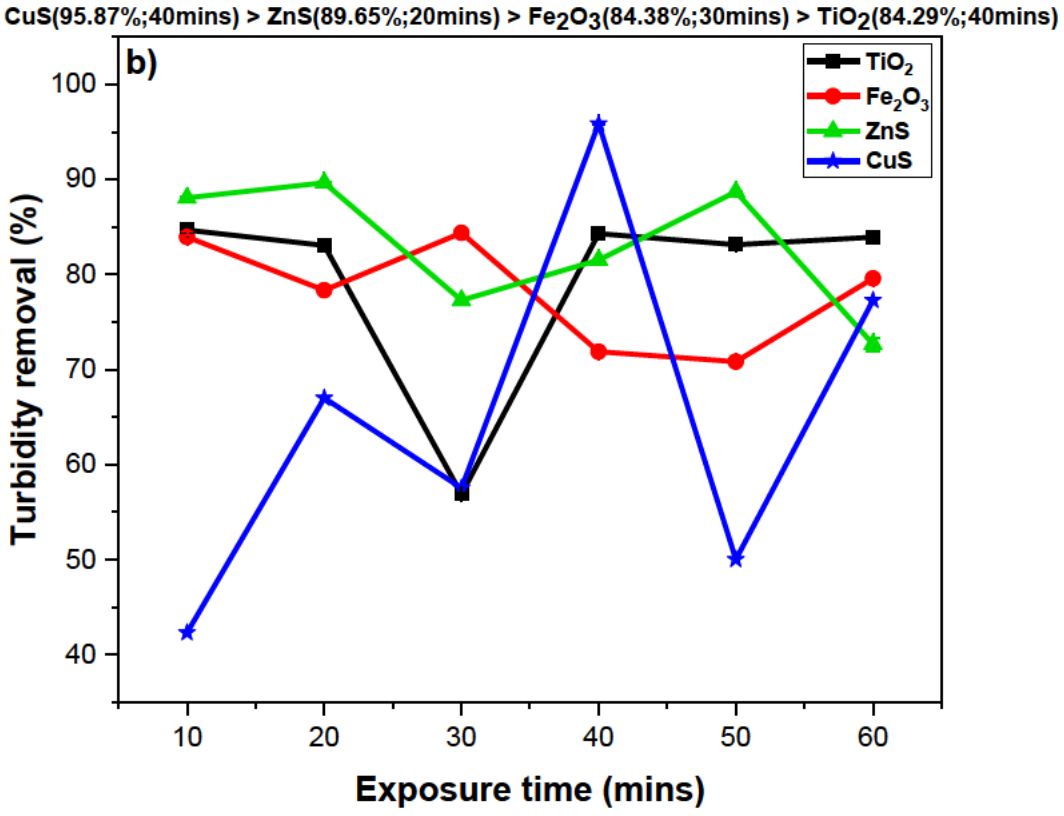

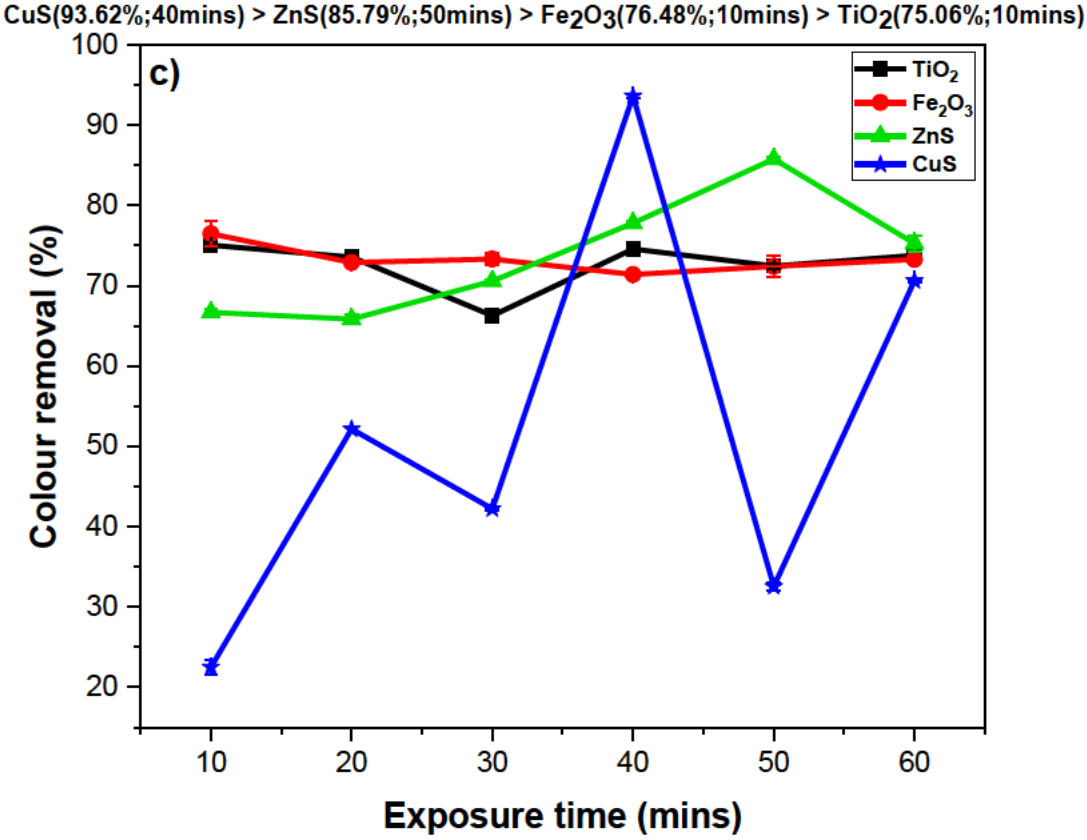

Figure 4-3: Effect of exposure time (10-60 minutes) on (a) COD, (b) turbidity, and (c) colour removal using TiO_2, Fe_2O_3, ZnS, and CuS

4.2.4 Kinetic study - pseudo-second-order model

The objective here was to evaluate the kinetics of the photocatalytic degradation reaction of COD using the four respective semiconductor photocatalysts. Figure 4-4 shows a plot of t/qt versus exposure time. It was hypothesized that this reaction follows pseudo-second-order reaction kinetics. The pseudo-second-order Equation is expressed in its integrated linear form as follows (Das et al. 2021):

$$\frac{t}{C_t} = \frac{1}{k_2 C_e^2} + \frac{1}{C_e} t \qquad (4\text{-}1)$$

Where C_e and C_t represent the amount of organic pollutant adsorbed at equilibrium and at the final exposure time t respectively, k_2 is the second-order rate constant (Das et al. 2021).

This is verified with a line that passes through the origin, with a correlation coefficient (R^2) and adjustment (Adj R^2) equal to 0.999 and 0.999, respectively, for Fe_2O_3, proving that the hypothesis is true. Thus, the specific rate of reaction (k_2) for these conditions is 0.002 g/L.min (de Mello Peters et al. 2018). Degradation of COD in the presence of Fe_2O_3 semiconductor photocatalyst is best fitted with a pseudo-second-order kinetic model. The relatively high R^2 values (close to 1), indicated that the pseudo-second-order model significantly fits the experimental data. This suggests that the model sufficiently explains the kinetics of the photocatalytic degradation process (Aisien, Amenaghawon and Urhobotie 2015; Mecha et al. 2016). The results of the regression analysis are shown in Table 4-1.

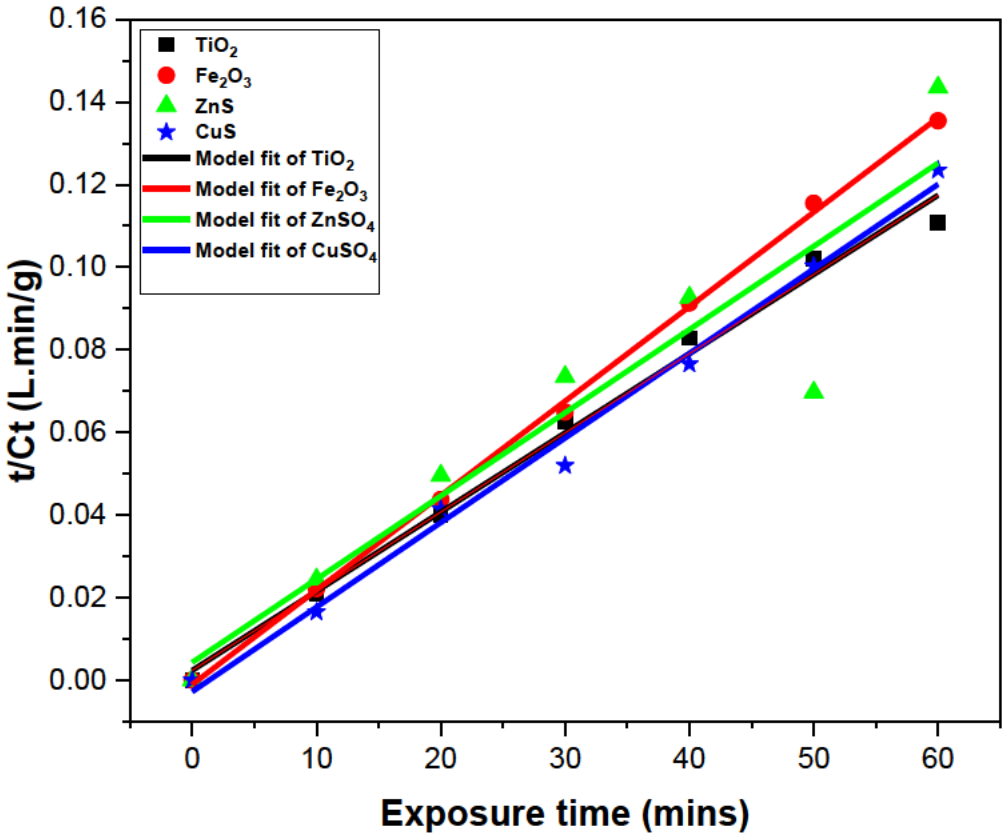

Figure 4-4: Pseudo-second-order kinetic plot for the photocatalytic degradation of COD

Table 4-1: Kinetic constant parameter values for the photocatalytic degradation of COD

Semiconductor photocatalyst	k_2 (g/L.min)	R^2	Adj R^2
TiO_2	0.002	0.992	0.990
Fe_2O_3	0.002	0.999	0.999
ZnS	0.002	0.866	0.839
CuS	0.002	0.993	0.992

Where k_2 is the second-order rate constant, c is the y-intercept, R^2 is the correlation coefficient and Adj R^2 is the adjusted correlation coefficient.

4.2.5 Cost-benefit analysis

The cost-benefit analysis of this study was estimated based on the cost of the catalyst at the desirable performed catalyst load (1.5 g), which influenced the photocatalytic process. Figure 4-5 shows the basic cost analysis of comparing the catalyst load at 1.5 g with the averaged desirability performance of removing the contaminants. CuS, with an estimated cost of R2.01/1.5g, was found as the cheapest with 56,93±1.88% treatability performance. This was followed by ZnS with an estimated cost of R2.03/1.5g with 56,30±1.48% performance. Likewise, Fe_2O_3 had an estimated cost of R5.21/1.5g with a treatment efficiency of 67,37±1.29%. TiO_2 had the highest cost (R32.47/1.5g) with 54,52±1.82 removal efficiency. Therefore, with desirable cost-effective performance at 50%, among the catalysts examined in this study, CuS was considered the best. This affirms that good water quality and maximum efficiency with the least quantity of catalyst load and cheaper cost are highly recommended (Tetteh, Rathilal and Robinson 2017; Al-Nuaim, Alwasiti and Shnain 2023). CuS is superior and preferable due to it being economic viability with an appropriate energy band (band gap of 2.2 eV), which has good visible light absorption capacity (Mills, O'Rourke and Moore 2015).

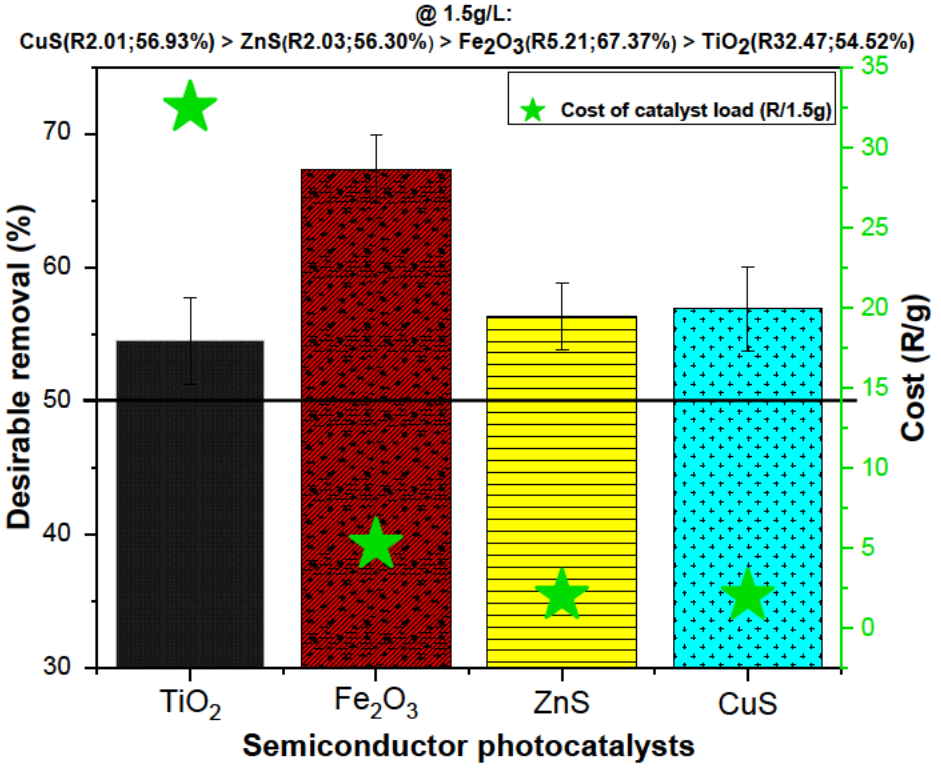

Figure 4-5: Cost-benefit analysis of photocatalyst contaminant removal efficiency (%) at 1.5 g of catalyst load of TiO_2, Fe_2O_3, ZnS and CuS

4.3 Effect of light source on the performance of oxide and non-oxide transition metal photocatalysts

This section investigates the effect of different light sources in three experiments i.e. UV (experiment 1); UV-visible (experiment 2); and sunlight (experiment 3) on photocatalytic degradation using the above-mentioned photocatalysts. The optimum conditions were obtained from Objective 1 (catalyst load = 1.5 g/L) and (mixing speed = 90 rpm) for 60 minutes, using the experimental analysis one-factor-at-a-time (OFAT) approach. MWW was characterized in Table 3-2. The water quality parameter chemical oxygen demand (COD) of the treated effluent was analyzed to evaluate the effectiveness of the various light sources at optimum conditions.

4.3.1 Effect of UV, UV-visible, and Sunlight irradiation on the photocatalytic treatment

The exposure time was varied from 10 to 60 minutes, whilst the mixing speed and catalyst load were kept constant at 90 rpm and 1.5 g/L, respectively for all three experiments. The light intensity (Lux) was noted as 600x100 (60 000) Lux using the MT940 handheld Lux Meter under UV irradiation. As shown in Figure 4-6a, ZnS and CuS optimum values (40.78% and 36.02%) were obtained at 50 minutes due to their visible light (long) absorption wavelength (375-575 nm / 380-800 nm) as compared to TiO_2 with a shorter absorbance wavelength (275-405 nm) and large band gap energy (3.2 Ev) which was achieved sooner at a shorter time of 20 minutes and 36.20% under the UV light irradiation (Table 3-6). Fe_2O_3's shorter absorbance wavelength (320-420 nm) was also favoured sooner under UV light irradiation. It is also apparent that ZnS's large energy band gap of 3.6 eV enhanced optimum contaminant removal under UV irradiation. Additionally, ZnS and CuS possess higher stability (crystal lattice) and have a large absorbance wavelength of (375-575 nm) and (380-800 nm) respectively. Therefore, an increase in contact time (interaction time) between the pollutant and the surface of the photocatalyst aided a higher COD removal percentage as the availability of hydroxyl radicals for the oxidation of pollutants present in wastewater increases with an increase in contact time (Wang et al. 2020; Deng et al. 2021). It is also observed that TiO_2 (275-405 nm) and Fe_2O_3 (320-420 nm) with shorter absorbance wavelengths favoured faster peaks under UV light, and rightfully so, as these wavelengths fall within the UV-visible regions on the electromagnetic spectrum (Roger Williams University

n.d.). It is also known that the larger band gaps and shorter wavelengths absorb UV light. Hence optimum values and UV light response for TiO_2 and Fe_2O_3 were likely to be obtained sooner (Silva et al. 2023). A decrease in COD removal percentage is thereafter observed which could be due to the tendency of TiO_2 and Fe_2O_3 (powder) to agglomerate in the water system and therefore the interactive surface of the photocatalyst became saturated and dissociated concerning time (Tayade, Natarajan and Bajaj 2009; Al-Nuaim, Alwasiti and Shnain 2023).

The light intensity (Lux) under UV-visible irradiation was noted as 1910x100 (191 000) Lux. As shown in Figure 4-6b, the UV-visible light source favoured the UV-visible absorption wavelength for Fe_2O_3 (320-420 nm) and ZnS (375-575 nm), with the optimum COD removal values at 72.25% and 70.87% at 10 and 50 minutes, respectively. CuS's best COD removal efficiency was 70.20% at 20 minutes, which precisely illustrated its compatibility with the UV-visible light source favouring its visible absorption wavelength (380-800 nm) and at a short time interval of 20 minutes as compared to the optimum COD removal efficiency of 36.02% at 50 minutes in experiment 1 (UV light source). TiO_2 showed the best COD removal efficiency at 46.66% at 30 minutes. This could be attributed to the UV-visible light source promoting a longer absorption wavelength incident on the TiO_2 photocatalyst surface, which elevated the removal efficiency as compared to 36.20% at 20 minutes in experiment 1. Compared to experiment 1 (UV light source), experiment 2 (UV-visible) has higher COD removal percentages.

The light intensity (Lux) under sunlight irradiation was noted as 133 700 Lux. Figure 4-6c shows the effect of sunlight on COD removal percentage; sunlight consists of visible light rays, which favoured the Fe_2O_3's visible light absorption wavelength, with the best COD removal efficiency of 57.14% at 20 minutes. The sunlight also favoured CuS's visible light absorption wavelength at a gradual rate, with the optimum COD removal efficiency of 47.16% at 60 minutes. The best COD removal efficiency for TiO_2 and ZnS was 56.56% and 42.50% at 40 and 20 minutes, respectively, and thereafter gradually decreased. This could be due to TiO_2 and ZnS's large energy band gap of 3.2 eV and 3.6 eV, respectively, which makes it difficult to oxidize or hydrolyze the organics at a high electron-hole recombination rate as ideally large band gap energy can absorb UV light (shorter wavelength) and small energy band gap can absorb visible light (longer wavelength) (Zhang *et al.* 2019b; Silva *et al.* 2023).

ZnS(40.78%;50mins) > TiO_2(36.20%;20mins) > CuS(36.02%;50mins) > Fe_2O_3(35.63%;20mins)

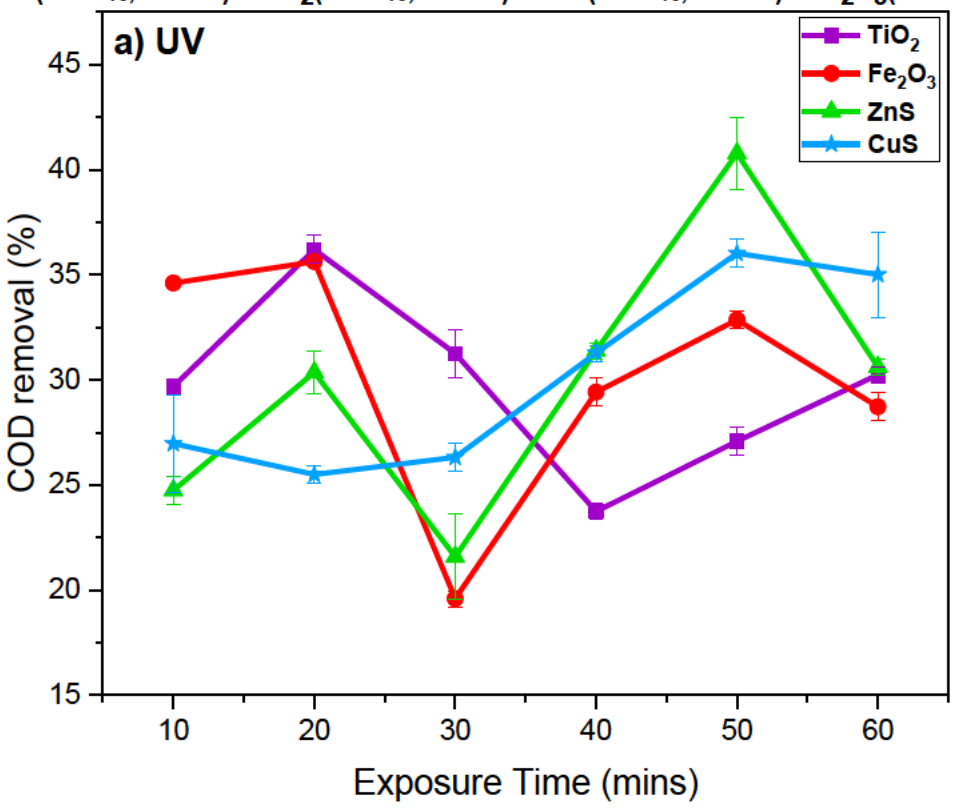

Fe_2O_3(72.25%;10mins) > ZnS(70.87%;50mins) > CuS(70.20%;20mins) > TiO_2(46.66%;30mins)

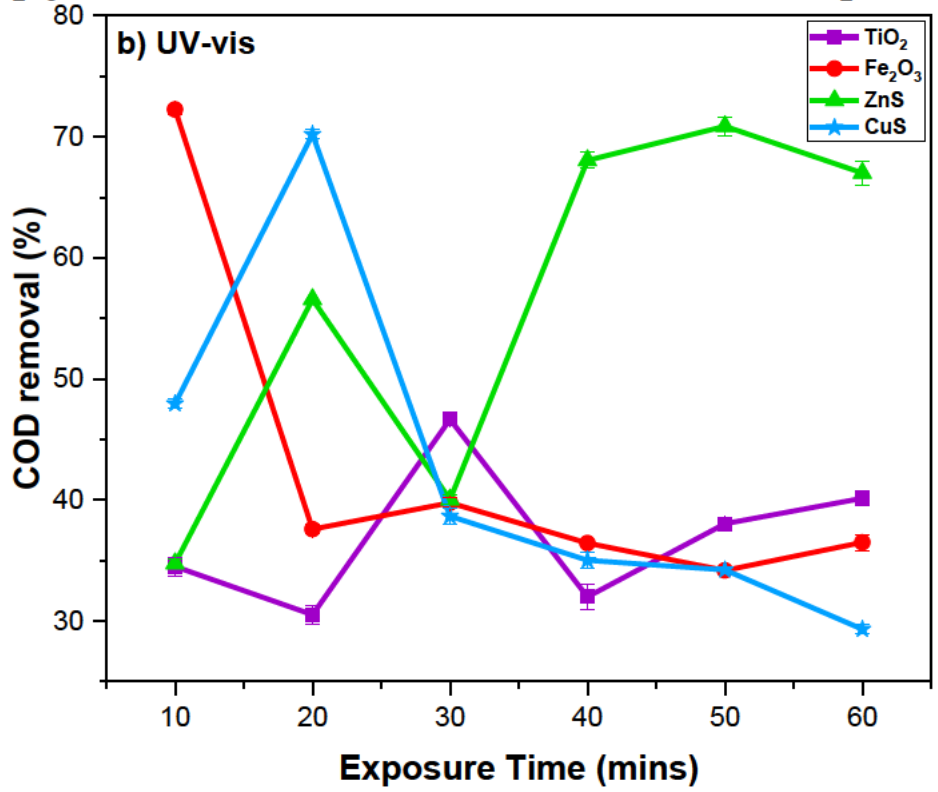

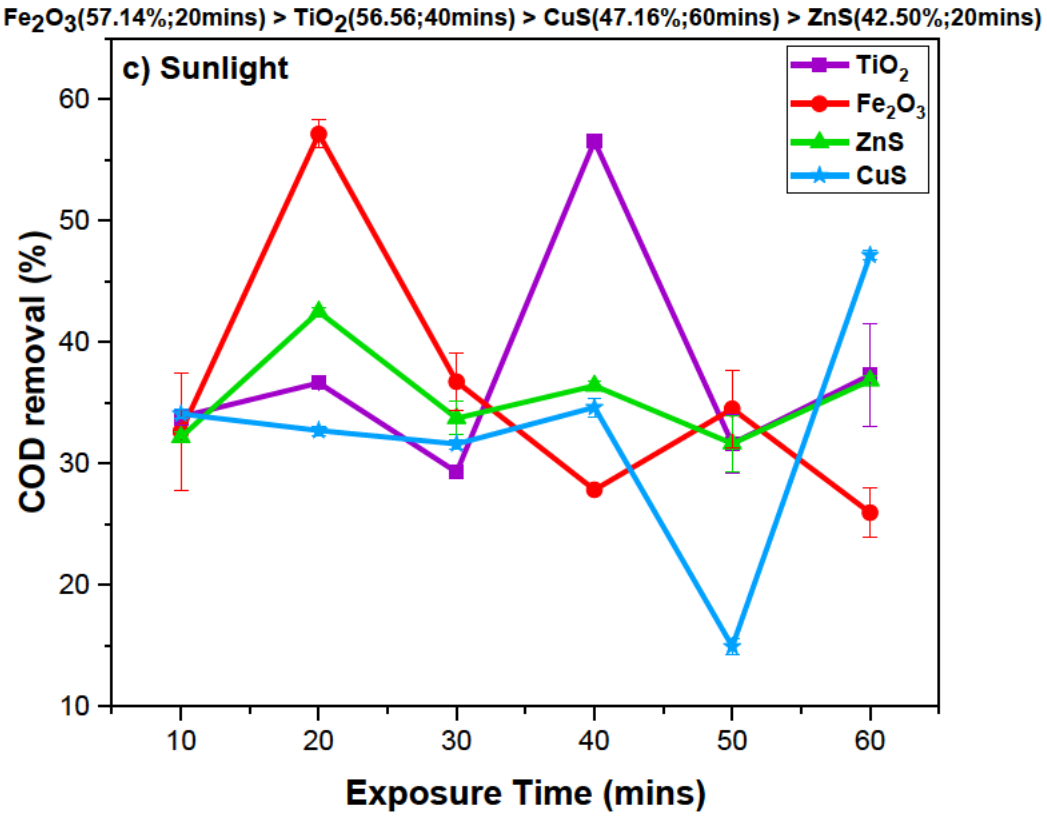

Figure 4-6: Effect of (a) UV (b) UV-visible and (c) Sunlight irradiation on COD removal using TiO_2, Fe_2O_3, ZnS, and CuS

4.3.2 Comparative study for UV, UV-visible, and Sunlight

The comparative study was estimated based on the average COD removal percentage for each respective photocatalyst. Figure 4-7 shows the comparative study for the effect of UV, UV-visible, and Sunlight irradiation on the photocatalytic treatment for all four photocatalysts (TiO_2, Fe_2O_3, ZnS, and CuS) with the averaged COD removal efficiency represented. The desirable COD removal performance is at 35%. UV-visible irradiation was estimated to be the most efficient method for COD removal among all three examined. ZnS had an estimated COD removal efficiency of 56.21% and was found to be the best under the UV-visible irradiation, followed by Fe_2O_3 with 42.79%, CuS with 42.57%, and TiO_2 with 36.98% COD removal efficiency.

Sunlight was shown to be more effective than the UV light irradiation. TiO_2 had an estimated COD removal efficiency of 37.55% and was the best under sunlight, followed by Fe_2O_3 with 35.80%, ZnS with 35.55%, and CuS with 32.53% COD removal efficiency. Concerning the solar spectrum, approximately 52-55% of the sunlight reaching the Earth's surface is Infrared (IR), 42-43% is visible, and 3-5% is UV light.

Almost half of the sunlight on the earth's surface falls within the visible region (400-700 nm) (Shahid et al. 2024). Consequently, this could justify the Sunlight's superiority over UV light in correspondence with the favourable visible absorbance wavelength of photocatalysts and their respective band gaps. The UV light irradiation illustrated the lowest COD removal efficiency compared to UV-visible and Sunlight.

CuS had an estimated COD removal efficiency of 30.18% and was found to be the best under the UV light source, followed by Fe_2O_3 with 30.14%, ZnS with 29.91%, and TiO_2 with 29.70% COD removal efficiency. This could be due to the restriction within the UV region absorbance wavelength therefore limiting the potential COD removal efficiency of the photocatalysts. Also, UV light has a shorter wavelength and relatively higher energy than visible light, thereby leading to phototoxicity or photodamage as well as lower penetrability in the samples (Zhang and Tian 2018). UV light irradiation might cause problems such as photobleaching, material damage, and reduced fatigue resistance (Zhang et al. 2022; Hong et al. 2024). Furthermore, the light intensity (Lux) under UV-visible irradiation was noted as 1910x100 (191 000) Lux, which was found to be the highest amongst the light sources examined. Therefore, a higher COD removal efficiency was achieved by the respective photocatalysts in comparison to sunlight (133 700 Lux) or UV (60 000 Lux) [UV-visible > Sunlight > UV].

Therefore, UV-visible irradiation was the most effective with the desirable COD removal performance at 35%, among the light sources examined in this study. These results obtained are in agreement with the literature that suggests a smaller band gap (longer absorbance wavelength) promotes visible light absorption (Offenloch et al. 2019). One of the major challenges or limitations of TiO_2 photocatalysis on OMPs is the need to efficiently harvest visible light photons as discussed in Section 1.3.1. Almost half of the sunlight on the earth's surface falls within the visible region (400-700 nm). Therefore, efficiently capturing visible light photons is of utmost importance in addressing this challenge (Hisatomi, Kubota and Domen 2014; Wang et al. 2017; Shahid et al. 2024). This study successfully reveals possibilities for utilizing visible light irradiation using alternative photocatalysts, as absorption toward visible light, is the central part of the solar spectrum.

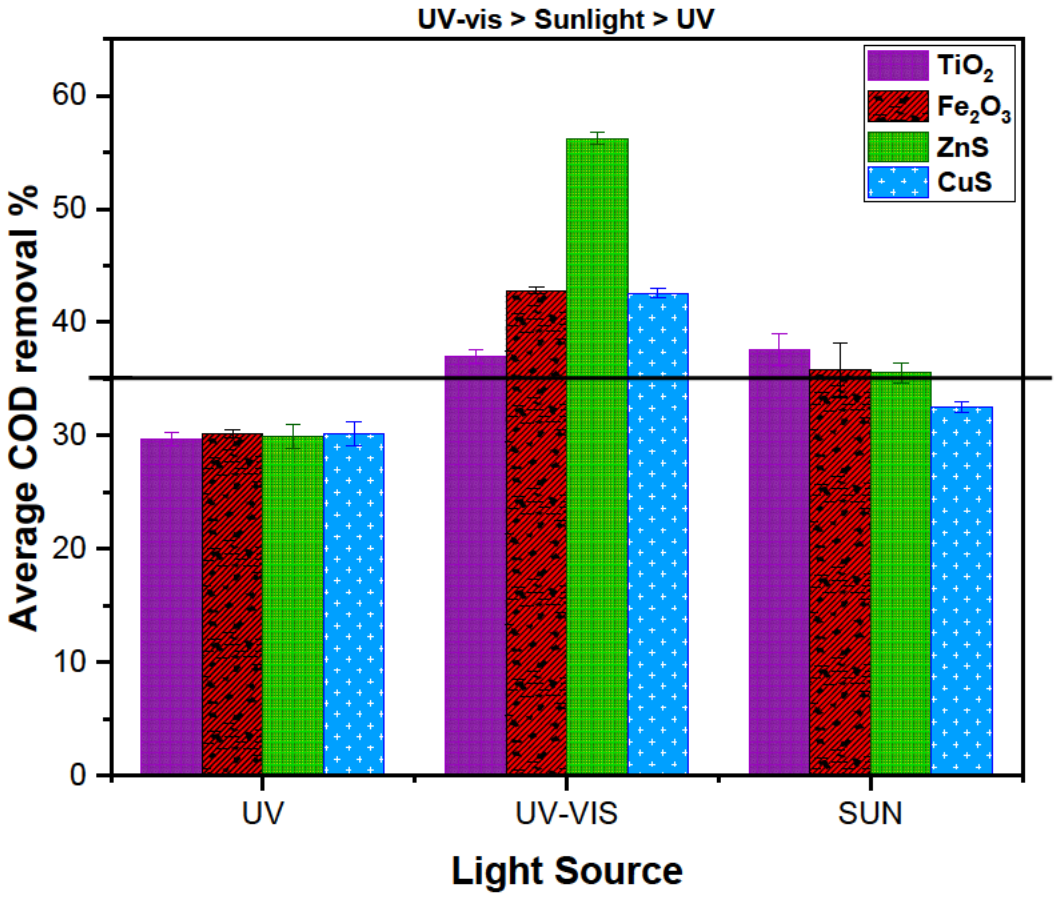

Figure 4-7: Comparative study between UV, UV-visible, and Sunlight irradiation for COD removal efficiency (%) using TiO_2, Fe_2O_3, ZnS, and CuS photocatalysts

4.4 Optimization of photocatalytic process operating conditions using RSM

4.4.1 Design of experiment by RSM

The experimental runs were designed by the RSM via the BBD (Design Expert Software Version: 13.0.5.0 64-bit, Stat-Ease Inc., Minneapolis, MA, USA), to investigate the key operating parameters such as catalyst load (A), mixing speed (B), and exposure time (C). The BBD matrix obtained 15 randomized sets of experimental runs for CuS, along with the response and predicted results obtained, are presented in Table 4-2. These experimental runs were randomized to eliminate bias. The input factors were (A) catalyst load, (B) mixing speed, and (C) exposure time. The responses were COD, Turbidity, and colour. The minimum and maximum values for the input factors were (A) catalyst load (1-2 g/L), (B) mixing speed (60-120 rpm), and (C) exposure time (10-60 minutes).

Surface imperfections and Cu-vacancies on the CuS surface are thought to be responsible for the efficacy of CuS nanoparticles. Due to the high rate of electron-hole recombination on large surfaces, there are fewer free charges available on the surface, which reduces photocatalytic efficiency (Ajibade and Oluwalana 2021). Additionally, because of their greater specific surface energy, CuS nanoparticles (NPs) exhibit aggregation/precipitation in an aqueous media, completely impeding photocatalytic performance (Sudhaik et al. 2022). Therefore, the low COD percentage removal for Response 1 (Actual), obtained in Table 4-2 below could be explained by Equation (4-2), whereby the Sulphur anion (negative charge) trapped the contaminants (positive charge) and the resulting precipitate contributed to high organic pollution.

$$\text{Photocatalyst (CuS)} + \text{hv} \rightarrow \text{h}^{+}\ (\text{Cu}) + \text{e}^{-}\ (\text{S}) \qquad (4\text{-}2)$$

Table 4-2: Actual design matrix and response values for copper sulphide (CuS)

	Factor A	Factor B	Factor C	Response (COD) %		Response (Turbidity) (%)		Response (Colour) (%)	
Run	Catalyst Load (g/L)	Mixing Speed (rpm)	Exposure Time (minutes)	Actual	Predicted	Actual	Predicted	Actual	Predicted
1	2	90	60	39.74	37.70	55.59	54.76	22.86	23.36
2	2	60	35	41.54	40.11	55.48	55.85	28.65	28.42
3	1.5	90	35	26.56	26.45	59.17	59.10	31.57	31.33
4	1	60	35	40.30	39.98	70.39	69.84	42.23	41.63
5	1.5	60	10	25.19	26.52	64.93	64.62	37.51	38.86
6	1	90	60	31.89	31.63	63.74	63.81	34.26	35.13
7	2	120	35	46.75	47.07	73.39	73.88	45.47	46.59
8	1.5	90	35	23.91	26.45	58.85	59.10	30.37	31.33
9	1.5	90	35	28.87	26.45	59.39	59.10	31.00	31.33
10	2	90	10	36.62	39.77	69.58	69.56	44.19	42.80
11	1.5	120	10	31.16	27.54	69.14	68.70	42.89	42.90
12	1.5	120	60	23.59	25.47	62.54	62.91	38.02	36.14
13	1.5	60	60	24.03	24.45	50.49	50.99	25.62	25.09
14	1	120	35	33.62	35.05	68.24	67.82	37.80	38.55
15	1	90	10	34.54	33.70	67.54	68.43	37.22	36.21

4.4.2 Model fitting and statistical analysis

The experimental data for contaminant removal in actual form (Table4-2) was fitted to reduced quadratic models represented by Equations (4-3)-(4-5) and their statistical significance and validity were tested via the analysis of variance (ANOVA) detailed under Section 4.4.4. The model reduction and modification were necessary to enhance the predictability of the response variables. The models present a direct relationship between the dependent variables (COD, turbidity, and colour removal) and the independent variables (catalyst dosage (A), mixing speed (B), and exposure time (C)). With these models, COD, turbidity, and colour removal were predicted within the designed space.

The model Equations (4-3)-(4-5) are expressed with the actual values of the input parameters (A, B, and C), their interaction (AB, AC, and BC), and quadratic terms (A^2, B^2, and C^2) as a function of the responses (Y1, Y2, and Y3). The real or actual factor equations were used to make predictions about the response for given levels of each factor. The model equations were useful for identifying the relative impact of the factors by comparing the factor coefficients. The extent to which terms of the models can affect the response or contaminant removal is associated with the positive and negative coefficients of the terms. The negative coefficients represent undesirable effects (antagonistic effect) of the factors, whereas positive coefficients show that a factor or combination of factors contributes favourably (synergistic effect) to the contaminant removal (response). The magnitudes of the coefficients correlate with the degree to which the response variable is affected.

$$\mathrm{COD\ (Y1)} = 165.7 - 154.6\mathrm{A} - 0.720\mathrm{B} + 0.256\mathrm{C} + 0.198\mathrm{AB} + 47.63\mathrm{A}^2 + 0.002\mathrm{B}^2 - 0.004\mathrm{C}^2 \quad (4\text{-}3)$$

$$\mathrm{Turbidity\ (Y2)} = 172.2 - 87.42\mathrm{A} + -1.001\mathrm{B} - 0.124\mathrm{C} + 0.334\mathrm{AB} - 0.204\mathrm{AC} + +0.003\mathrm{BC} + 20.17\mathrm{A}^2 + 0.003\mathrm{B}^2 \quad (4\text{-}4)$$

$$\mathrm{Colour\ (Y3)} = 134.2 - 58.18\mathrm{A} - 1.372\mathrm{B} + 0.135\mathrm{C} + 0.354\mathrm{AB} - 0.367\mathrm{AC} + 0.002\mathrm{BC} + 12.19\mathrm{A}^2 + 0.005\mathrm{B}^2 \quad (4\text{-}5)$$

4.4.3 Predicted vs Actual

Figure 4-8 shows good correlation plots of the predicted and experimental values, with the data points evenly distributed around the straight line. Hence, the response models reflected the experiments well within the design space. Furthermore, in response surface methodology (RSM), the colours blue, green, yellow, and red in a predicted versus actual plot indicate the value of the data points, from lowest to highest: (i) Blue: The lowest value; (2) Green: Moderately low value; (3) Yellow: Moderately high value; (4) Red: The highest value. Therefore, as depicted in Figure 4-8a, the lowest value was 23.6% and the highest value was 46.8% for COD removal. For Figure 4-8b, the lowest value was 50.5% and the highest value was 73.4% for turbidity removal. For Figure 4-8c, the lowest value was 22.9% and the highest value was 45.5% colour removal.

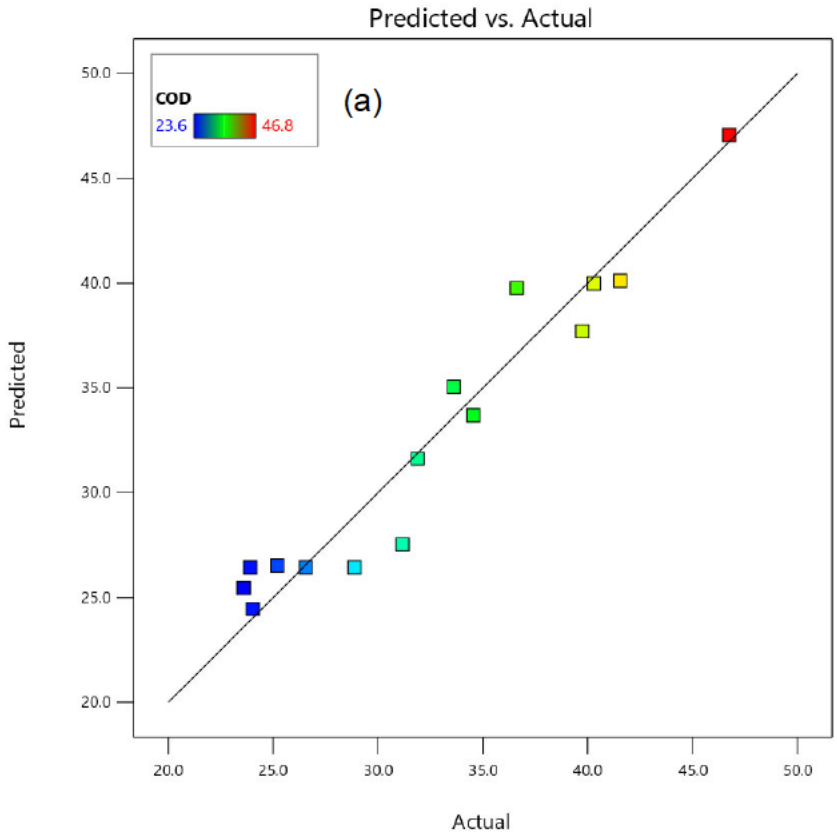
Predicted vs. Actual
COD
23.6
46.8
(a)
Predicted
Actual
50.0
45.0
40.0
35.0
30.0
25.0
20.0
20.0
25.0
30.0
35.0
40.0
45.0
50.0

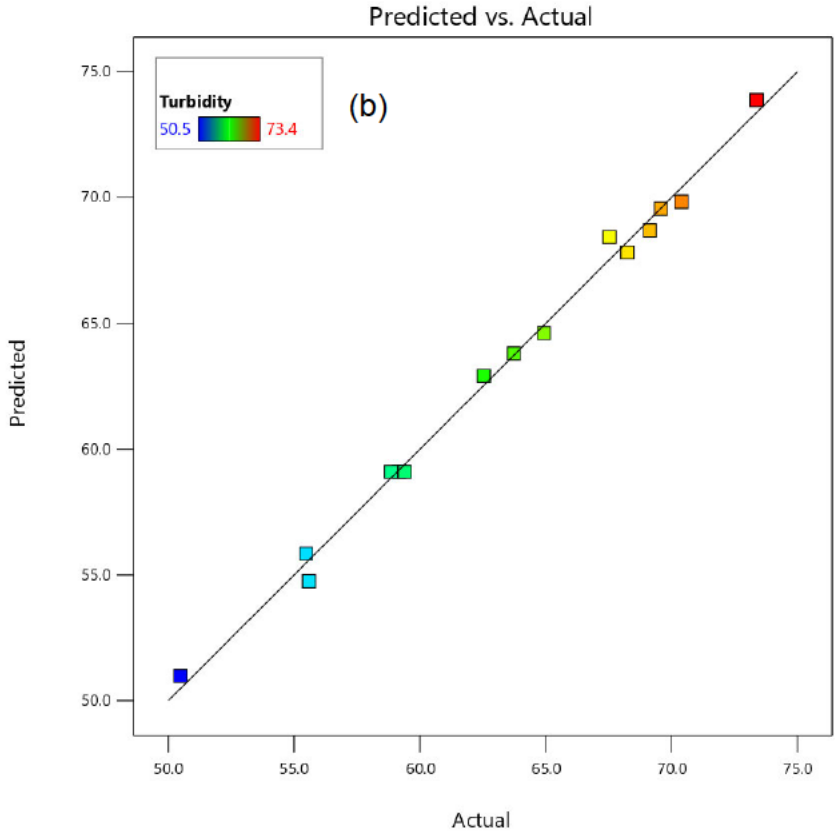
Predicted vs. Actual
Turbidity
50.5
73.4
(b)
Predicted
Actual
75.0
70.0
65.0
60.0
55.0
50.0
50.0
55.0
60.0
65.0
70.0
75.0

(c)

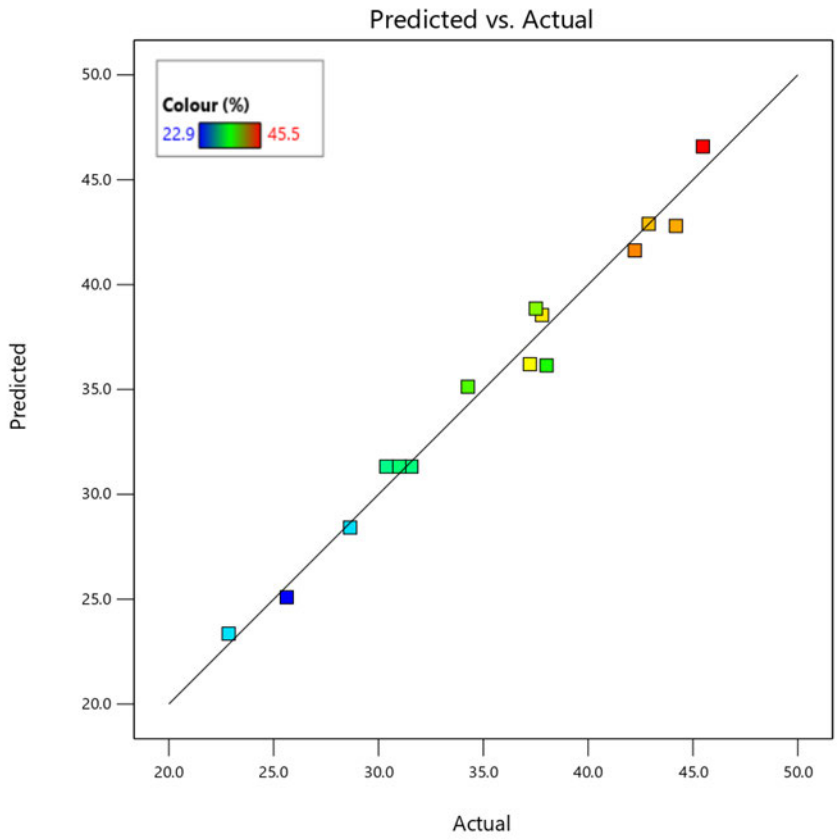

Figure 4-8: Predicted vs Actual graphs (a) COD, (b) turbidity, and (c) colour

4.4.4 Analysis of variance (ANOVA)

Analysis of variance (ANOVA) was used to check the statistical validity and accuracy of each of the fitted models, as shown in Table 4-3, Table 4-4, and Table 4-5. Typical features of ANOVA are the F-values, P-values, R^2, and Predicted R^2 values. These values reveal whether the model is statistically valid or not. As shown in the tables, for all models, the F-values (13.96, 142.32, and 37.71) for COD, turbidity, and colour respectively, were greater than their respective p-values (0.0013, 0.0001, and 0.0001) for each term in the model, implying the models are significant. There is only a 0.13% chance that an F-value this large could occur due to noise for COD and a 0.01% chance of both turbidity and colour. Furthermore, P-values less than 0.05 indicate model terms are significant. For COD, A^2 is a significant model term. Values greater than 0.1 indicate the model terms are not significant. However, AB, $B^{2,}$ and C^2 model terms are significant and required to support hierarchy. For turbidity and colour, the model terms AB, AC, BC, A^2, and B^2 are significant. For colour, the model term BC was significant and required to support the hierarchy.

For COD, turbidity, and colour, the Lack of Fit F-values of 1.23, 10.17, and 8.46 respectively suggested that the Lack of Fit is not significant in relation to the pure error. The Lack of Fit F-value has a 50.63%, 9.15%, and 10.85% chance of occurring due to noise, respectively. It is required that the model fits precisely, thus a non-significant lack of Fit is good.

A data set's proximity to the fitted regression line is shown by its correlation coefficient (R^2). This value provides a clear indication of how well a dataset fits a model (Tetteh et al. 2020). A model is considered more relevant when its R^2 value approaches 1. The R^2 values (0.9332, 0.9948, 0.9805) and their corresponding Adjusted R^2 values (0.8663, 0.9878, and 0.9545) were close to 1, as indicated in Tables 4-3 to 4-5, suggesting that the developed statistical model fit the data collected well. Furthermore, since the difference between the Predicted and Adjusted R^2 values is less than 0.2, there is an acceptable degree of agreement between the two.

As an alternative, one can assess a model's significance by calculating its coefficient of variation (CV) along with its adequate precision (Adeq. Pr). The range of the predicted response in relation to the corresponding error is measured by the signal-to-noise ratio, which indicates adequate precision. Generally speaking, an adequate precision of at least 4 is preferred. From the tables above, the values obtained for adequate precision at COD (11.58), turbidity (40.54), and colour (20.46) indicate an adequate signal greater than 4 and prove the adequacy of the models. Therefore, this model can be used to navigate the design space. The standard deviation to mean ratio is known as the CV. This number indicates the degree of dispersion around the mean and is expressed as a percentage. The CV values for COD, turbidity, and colour as 8.22, 1.15, and 4.15% respectively were all less than 15% indicating the accuracy of the model (Tetteh et al. 2020).

Table 4-3: ANOVA for COD removal by CuS— Reduced Quadratic model

Source	Sum of Squares	df	Mean Square	F-value	p-value	
Model	699.41	7	99.92	13.96	0.0013	significant
A-Catalyst Load	73.85	1	73.85	10.32	0.0148	
B-Mixing Speed	2.07	1	2.07	0.2886	0.6078	
C-Exposure Time	8.54	1	8.54	1.19	0.3108	
AB	35.31	1	35.31	4.93	0.0618	
A^2	523.42	1	523.42	73.14	< 0.0001	
B^2	17.87	1	17.87	2.50	0.1581	
C^2	26.04	1	26.04	3.64	0.0981	
Residual	50.10	7	7.16			
Lack of Fit	37.77	5	7.55	1.23	0.5063	not significant
Pure Error	12.32	2	6.16			
Cor Total	749.51	14				
R^2	**Adjusted R^2**	**C.V.%**	**Predicted R^2**	**Adeq Precision**	**Mean**	**Std. Dev.**
0.9332	0.8663	8.22	0.6926	11.5786	32.56	2.68

Table 4-4: ANOVA for Turbidity removal by CuS— Reduced Quadratic model

Source	Sum of Squares	df	Mean Square	F-value	p-value	
Model	604.88	8	75.61	142.32	< 0.0001	significant
A-Catalyst Load	31.48	1	31.48	59.25	0.0003	
B-Mixing Speed	128.16	1	128.16	241.23	< 0.0001	
C-Exposure Time	188.50	1	188.50	354.82	< 0.0001	
AB	100.54	1	100.54	189.26	< 0.0001	
AC	25.90	1	25.90	48.76	0.0004	
BC	15.36	1	15.36	28.92	0.0017	
A^2	94.40	1	94.40	177.69	< 0.0001	
B^2	27.19	1	27.19	51.18	0.0004	
Residual	3.19	6	0.5313			
Lack of Fit	3.04	4	0.7596	10.17	0.0915	not significant
Pure Error	0.1493	2	0.0747			
Cor Total	608.07	14				
R^2	**Adjusted R^2**	**C.V.%**	**Predicted R^2**	**Adeq Precision**	**Mean**	**Std. Dev.**
0.9948	0.9878	1.15	0.9469	40.5435	63.23	0.7289

Table 4-5: ANOVA for Colour removal by CuS— Reduced Quadratic model

Source	Sum of Squares	df	Mean Square	F-value	p-value	
Model	647.89	8	80.99	37.71	0.0001	significant
A-Catalyst Load	13.40	1	13.40	6.24	0.0467	
B-Mixing Speed	113.83	1	113.83	52.99	0.0003	
C-Exposure Time	210.56	1	210.56	98.03	< 0.0001	
AB	112.95	1	112.95	52.59	0.0003	
AC	84.34	1	84.34	39.27	0.0008	
BC	12.29	1	12.29	5.72	0.0539	
A^2	34.48	1	34.48	16.05	0.0071	
B^2	72.68	1	72.68	33.84	0.0011	
Residual	12.89	6	2.15			
Lack of Fit	12.17	4	3.04	8.46	0.1085	not significant
Pure Error	0.7195	2	0.3597			
Cor Total	660.78	14				
R^2	**Adjusted R^2**	**C.V.%**	**Predicted R^2**	**Adeq Precision**	**Mean**	**Std. Dev**
0.9805	0.9545	4.15	0.8085	20.4645	35.31	1.47

4.4.5 Interactive effects of parameters

The cross-factor interactive effects of the factors (catalyst dosage, exposure time, and mixing speed) on the response (COD, turbidity, and colour removal) were studied. Figure 4-9 represents the 3D (surface) plots resulting from the cross-factor interactions on the contaminant removal by the photocatalysts. It illustrates the interaction between catalyst load and mixing speed (AB). The combined effects of these two parameters have a significant effect on the contaminant removal by CuS. Figure 4-9(a) represents the plots for cross-factor interactive effects on COD removal by CuS. As shown with a catalyst load of 1.9-2 g/L and a mixing speed of 95-120 rpm, an optimum COD removal efficiency of 40-50% was achieved. As catalyst dosage increased, the removal efficiency increased. Figure 4-9(b) represents the plots for cross-factor interactive effects on turbidity removal by CuS. As depicted, with a catalyst load of 1.8-2 g/L and a mixing speed of 100-120 rpm, an optimum turbidity removal efficiency of 70-75% was achieved. Figure 4-9(c) represents the plots for cross-factor interactive effects on colour removal by CuS. As illustrated, with a catalyst load of 1.5-2 g/L and with a mixing speed of 95-120 rpm, an optimum colour removal efficiency of 40-50% was achieved. This corresponding increase in mixing speed enhanced the proper homogenizing of the catalyst in the reacting media. Therefore, a

higher removal efficiency was achieved. This could be attributed to CuS having higher stability, which required higher mixing speeds (Wang et al. 2020; Deng et al. 2021). Moreover, the high agitation develops more surface area contact interactions between particles of the catalyst and the water molecules (Govindaraj and Pattabhi 2015). These results also correlate to experimental results obtained in Objective 1 Figure 4-1 (a), (b), and (c) for COD, turbidity, and colour.

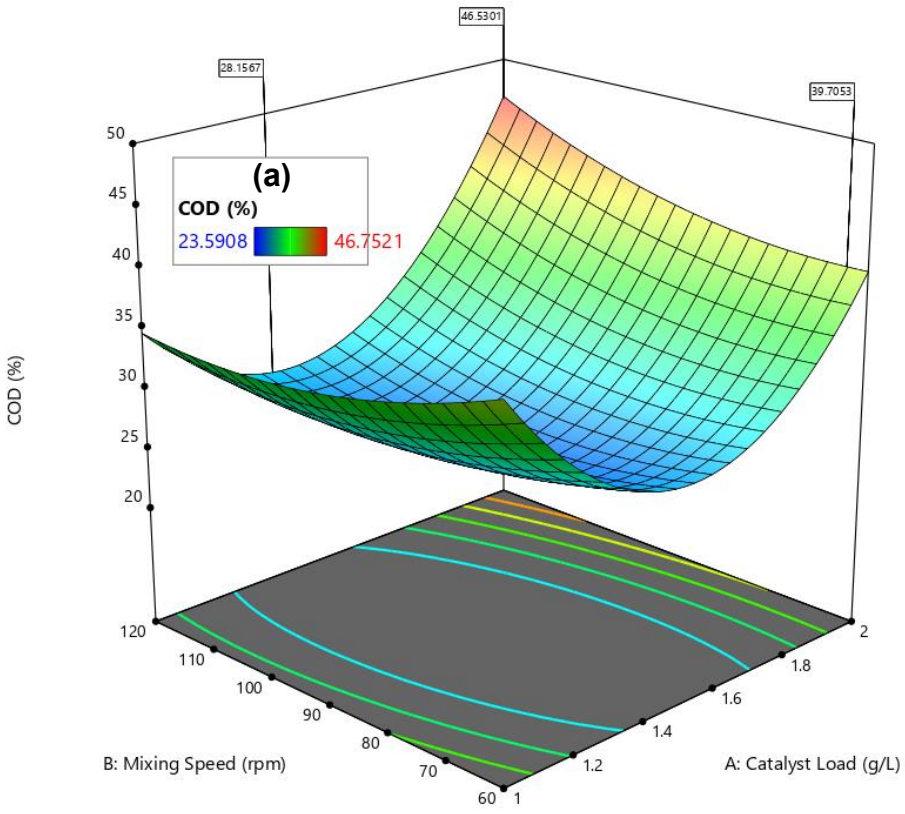

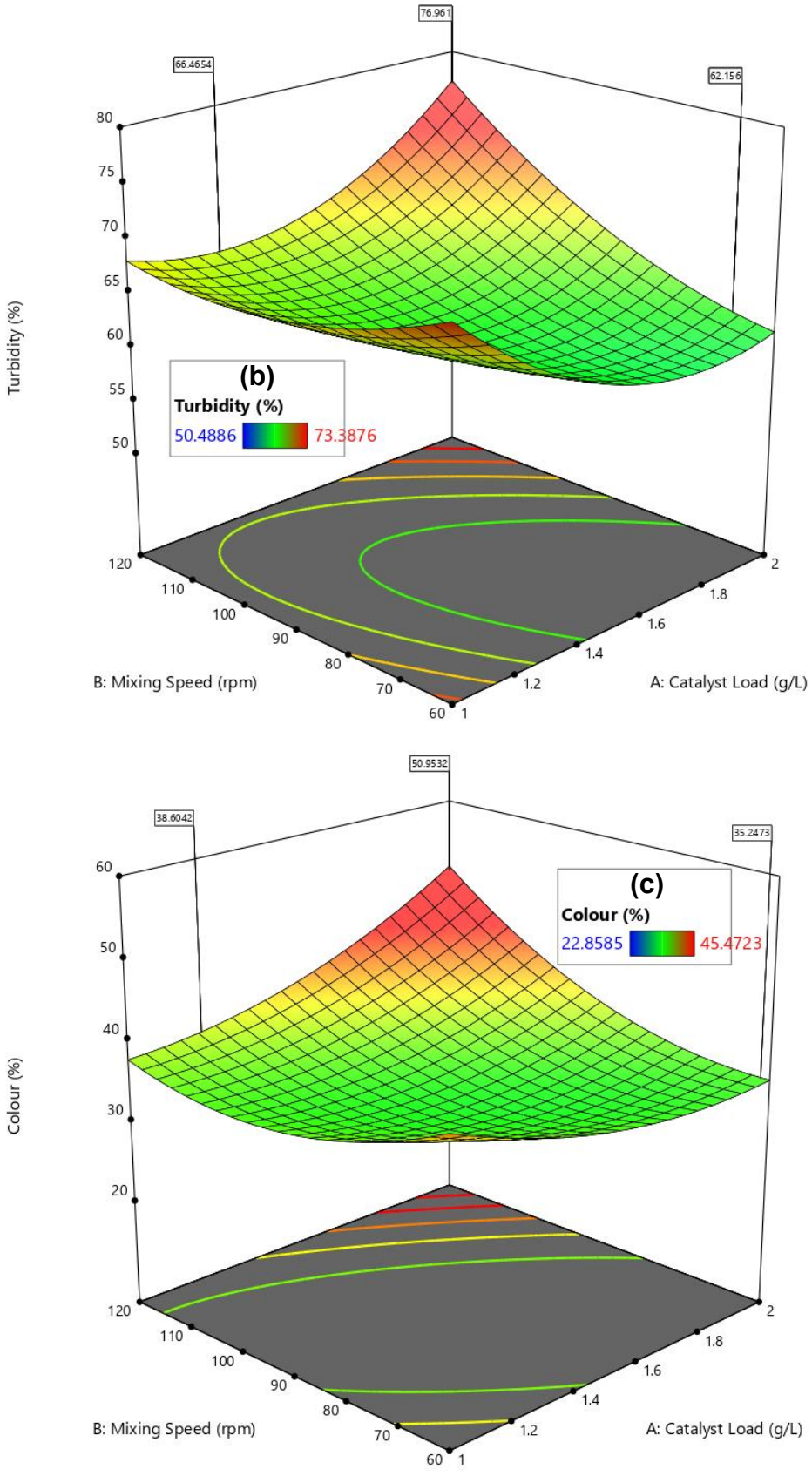

Figure 4-9: 3D plots representing the cross-factor interactive effects of the interaction between catalyst load and mixing speed (AB) on (a) COD removal, (b) turbidity removal, and (c) colour removal by CuS

4.4.6 Optimum conditions (Numerical optimization)

The numerical optimization was done to determine the optimum conditions of the three parameters for contaminant removal. The numerical optimization technique assesses the complete design space based on the developed models to detect the optimum factor conditions for the given range (constraints) shown in Table 4-6. Equations (4-3)-(4-5) served as the objective functions, whereas the three independent variables (input factors) served as constraints (Table 4-6). These constraints were set within the given range. The goal for the optimization was to achieve maximum contaminant removal (output factors). Consequently, all input factors were kept in range, and output responses were maximized.

This generated 10 solutions (Table 4-7) and one was selected as the optimal solution (Figure 4-10) as it presented the highest desirability of 96% removal efficiency. Figure 4-10 represents a ramp plot showing the optimum conditions for the operating parameters and the desirability obtained. The optimal solution suggests a COD, turbidity, and colour removal of 47.2%, 75.1%, and 48.3%, respectively, at a catalyst load of 2 g/L CuS, mixing speed of 120 rpm, and an exposure time of 30 minutes. This translates into minimum catalyst load and cost-effectiveness at a short time interval to achieve the set goal of contaminant removal for the given range of factors.

Table 4-6: Constraints

Name	Goal	Lower Limit	Upper Limit	Lower Weight	Upper Weight	Importance
A: Catalyst Load	is in range	1	2	1	1	3
B: Mixing Speed	is in range	60	120	1	1	3
C: Exposure Time	is in range	10	60	1	1	3
COD	maximize	23.5908	50	1	1	1
Turbidity	maximize	50.4886	73.3876	1	1	3
Colour	maximize	22.8585	45.4723	1	1	3

Table 4-7: Solutions generated

Number	Catalyst Load	Mixing Speed	Exposure Time	COD	Turbidity	Colour	Desirability	
1	**2.000**	**119.999**	**29.557**	**47.172**	**75.062**	**48.323**	**0.963**	**Selected**
2	2.000	119.998	29.762	47.172	75.017	48.257	0.963	
3	2.000	120.000	30.263	47.174	74.909	48.099	0.963	
4	2.000	120.000	30.795	47.172	74.793	47.929	0.963	
5	2.000	120.000	28.291	47.159	75.338	48.727	0.963	
6	2.000	120.000	26.812	47.126	75.660	49.199	0.962	
7	2.000	119.606	29.630	47.070	74.863	48.071	0.962	
8	2.000	119.621	30.331	47.073	74.717	47.855	0.962	
9	2.000	119.571	30.261	47.061	74.709	47.849	0.962	
10	2.000	120.000	23.889	47.008	76.296	50.131	0.962	

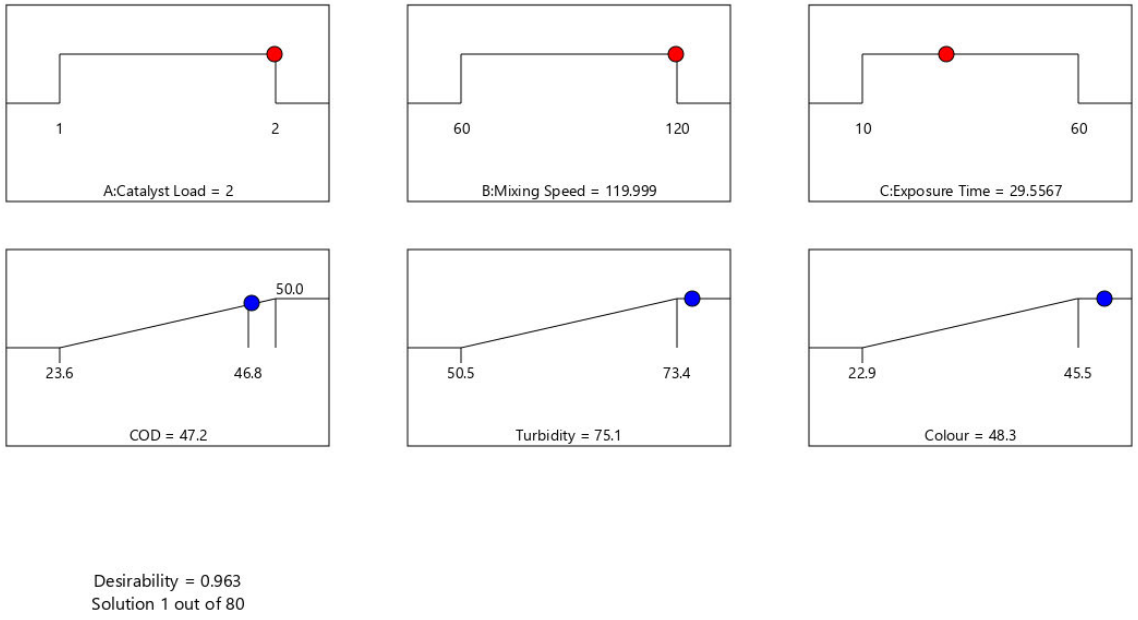

Figure 4-10: Ramp plot with optimum operating conditions for CuS

4.4.7 Validation of optimized conditions

The optimal solution selected (Figure 4-10) was validated and confirmed experimentally (Table 4-8) and was in good agreement with the predicted values as the difference between the predicted and actual values was minimal (<5%). This suggests the model's predictability was consistent ($p < 0.05$) at 95% confidence levels. This is agreeable to other studies that suggested that RSM is economically viable for experimental optimizations based on their predictability with precision (Chaker *et al.*

2021; Hussain *et al.* 2021; Nayeemuddin *et al.* 2023; Pravina, Uthayakumar and Sivasamy 2023).

Table 4-8: Modified RSM-BBD optimum conditions experimental validation

Response (%)	Synthetic wastewater		Difference (%)
	Photocatalyst (CuS)		
	Predicted (%)	Actual (%)	
COD (%)	47.2	46.8	0.4
Turbidity (%)	75.1	73.4	1.7
Colour (%)	48.3	45.5	2.8

4.4.8 Comparative study of CuS and conventional TiO_2 semiconductor photocatalyst under UV-visible light irradiation

Finally, once the optimal operating parameters were verified, a comparative study was performed whereby the same experiment was conducted for CuS and TiO_2 using synthetic wastewater (SW) and raw wastewater (RW). As shown in Figure 4-11, the Actual CuS (SW) follows the same trend as that of the Predicted CuS (SW). The optimum Predicted values for CuS were 47.2%, 75.1%, and 48.2% for COD, turbidity, and colour, respectively. The Actual values for CuS (SW) were 46.8%, 73.4%, and 45.5% for COD, turbidity, and colour, respectively, with a minimal difference as discussed in section 4.4.7, which correlates to that of the predicted results. The optimum contaminant removal efficiencies for COD, turbidity, and colour using CuS (RW) were 45.10%, 90.03%, and 59.58%, respectively, and correlated to a similar trend to that of the Predicted CuS (SW) and Actual CuS (RW). The COD removal of 45.10% for CuS (RW) is similar to that of Actual CuS (SW) at 46.8% and is in good agreement.

The removal efficiencies obtained for CuS are higher in comparison to that of the conventional TiO_2 for both synthetic wastewater (SW) and raw wastewater (RW). Therefore, with desirable performance at 40%, among CuS and TiO_2 catalysts examined, CuS was considered superior to that of the conventional TiO_2.

The primary focus of this research was to primarily degrade the organics, and the results showed an optimum COD removal efficiency at 47% which equates to 4749 mg/L remaining and therefore met the maximum permitted discharge limits of <5000 mg/L according to Table 2-1 (City of Cape Town 2014). However, the turbidity and

colour removal efficiency at 73% and 46% equated to 83 NTU and 1471 Pt.Co which did not meet the maximum permitted discharge limits of <5 NTU and <15 Pt.Co for turbidity and colour, respectively, according to the South Africa Bureau of Standards (2015) for drinking water (Table 2-1). This is due to the vacuum pump not being able to completely filter all photocatalyst nanoparticles. Consequently, a post-treatment process is required to enhance the improvement of the water quality (colour and turbidity).

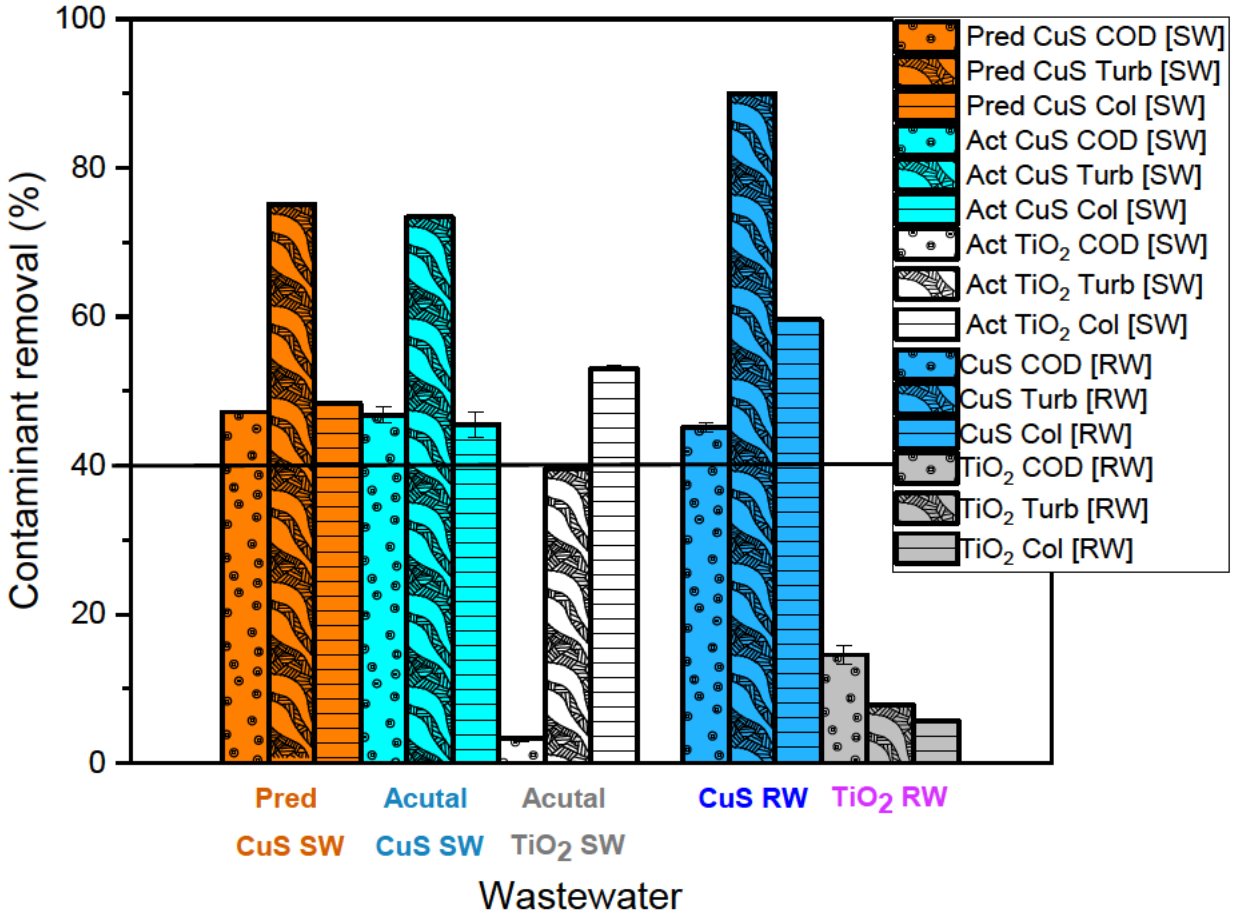

Figure 4-11: Comparative study between CuS and TiO_2 using synthetic (SW) and raw wastewater (RW) for contaminant removal efficiency (%)

4.5 Summary

The optimization utilizing RSM proved to be economically viable and required fewer trial runs. For the use of CuS, the optimal solution suggests a COD, turbidity, and colour removal of 47.2%, 75.1%, and 48.3%, respectively, at a catalyst load of 2 g/L CuS, mixing speed of 120 rpm, and an exposure time of 30 minutes, and highest desirability of 96% removal efficiency. This translated into minimum catalyst load and cost-effectiveness at a short time interval to achieve the set goal of contaminant removal for the given range of factors.

The optimal solution selected was then validated and confirmed experimentally and was in good agreement with the predicted values as the difference between the predicted and actual values was minimal. This suggests the model's predictability was significant ($p < 0.05$) at 95% confidence levels. This is agreeable to other studies suggesting RSMs to be economically viable for experimental optimizations based on their predictability with precision. Finally, a comparative study was performed whereby the same experiment was conducted for CuS and TiO_2 using synthetic wastewater and raw wastewater. The Actual CuS (SW) and raw wastewater for CuS (RW) follow the same trend as that of the Predicted CuS (SW). The optimum contaminant removal efficiencies for COD, turbidity, and colour using Actual CuS SW were 46.8%, 73.4%, and 45.5%, and the optimum efficiencies for CuS RW are 45,1%, 90,03%, and 59,58%, respectively. The removal efficiencies obtained for CuS are higher in comparison to that of TiO_2 for both synthetic wastewater (SW) and raw wastewater (RW). Therefore, with desirable performance at 40%, among CuS and TiO_2 catalysts examined, CuS was considered superior to that of the conventional TiO_2.

CHAPTER FIVE
CONCLUSION AND RECOMMENDATION

The study focused on optimizing the photocatalytic degradation of wastewater using oxide and non-oxide photocatalysts. This chapter presents the major findings obtained from the research based on the following specific objectives and provides recommendations for future research.

Specific objectives:

1. To investigate the applicability and performance of oxide (TiO_2 and Fe_2O_3) and non-oxide (CuS and ZnS) transition metal photocatalysts for municipal wastewater treatment. The parameters investigated were catalyst load (0.5-2.5 g/L) at increments of 0.5 g/L, mixing speed (30-150 rpm) at increments of 30 rpm, and exposure time (60 minutes) at 10-minute time intervals.
2. To investigate the effect of light sources (UV, UV-visible, and natural sunlight) on the performance of photocatalytic degradation of municipal wastewater.
3. To optimize the operating conditions of the photocatalytic process using the best catalyst and light source with response surface methodology (RSM). The input parameters investigated were catalyst load, mixing rate, and exposure time.

5.1 Conclusion

Insufficient research has been conducted on optimizing multiple parameters in the photocatalytic degradation process. Consequently, there is limited information on simulating experimental data to establish a relationship between the input parameters as a function of the response water quality metrics, depending on the water source. Thus, a strategy for optimization in the wastewater treatment process to improve the performance of the end usage of water is necessary. Furthermore, the above-mentioned objectives were met, and their main findings are summarized below:

- Firstly, at a catalyst loading of 1.5 g/L, mixing speed of 90 rpm, and UV exposure time of 45 minutes, CuS displayed the best results overall for COD removal, whilst ZnS was efficient in removing turbidity and colour. Low catalyst load and mixing speed enhanced the aggregation and inter-particle surface contact time between the catalyst's active surface and

water molecules. Considering the desirability performance of reducing COD, turbidity, and colour by 50%, the increasing order of the estimated cost at 1.5 g catalyst load was CuS < ZnS < Fe_2O_3 < TiO_2. Hence, CuS was considered the most cost-effective alternative semiconductor photocatalyst to degrade the high organic content of wastewater in comparison to the conventional TiO_2, which has been the most widely used photocatalyst. Therefore, the prospect of CuS as a photocatalyst under an optimized photocatalytic process condition is viable for wastewater treatment.

- Secondly, the UV-visible light source favoured the UV-visible absorption wavelength for Fe_2O_3 and ZnS, with the optimum COD removal efficiency of 72.25% and 70.87% at 10 and 50 minutes, respectively. CuS's best COD removal efficiency was 70.20% at 20 minutes which precisely illustrated its compatibility with the UV-visible light source favouring its visible absorption wavelength. The comparative study revealed UV-visible irradiation to be the most effective. The light intensity (Lux) under UV-visible irradiation was noted as 1910x100 (191 000) Lux, which was found to be the highest amongst the light sources examined. Sunlight was shown to be more effective than UV light irradiation as most of the sunlight on the earth's surface falls within the visible region (400-700 nm). Consequently, this could justify the Sunlight's superiority over UV light in correspondence with the favorable visible absorbance wavelength of photocatalysts and their respective band gaps. The shorter wavelength of UV light and relatively higher energy than visible light may have caused phototoxicity or photodamage as well as lower penetrability in the samples.
- Finally, the BBD adapted from the RSM was successful, due to its ability to incorporate multiple interaction factors in the experimental design, modeling and optimization, and analysis of the results. It has been established that a good correlation exists between the input variables and the responses. Thus, the optimum condition experimental results were in good agreement with the response model predicted results. Comparatively, it was established that CuS was considered superior to that of the conventional TiO_2 for synthetic and raw wastewater.

Conclusively, this finding provides notable insight into the optimization of photocatalytic degradation of wastewater using oxide (Fe_2O_3) and non-oxide (CuS) photocatalysts with high applicability performance for municipal wastewater treatment. Furthermore, it will drive swift progress on developing photocatalysis novel materials into the forefront of sustainable wastewater treatments and contribute to green and sustainable technology for wastewater treatment and mitigation of the OMP environmental challenges in the South African water sector.

5.2 Prospects and recommendations

The research findings were based on the following recommendations:

- The considerable cost, particularly on chemicals and energy consumption, is the main barrier to the adoption of AOPs in real-world wastewater treatment settings even in the bioenergy sector.
    - AOPs should be further investigated since they have the potential to reduce the overall costs associated with treating organic wastewater, particularly when combined with traditional methods like physical-chemical or biological ones. The synergistic effects of combining various AOPs, in contrast to using standalone AOPs, can improve the degradation of pollutants whilst reducing the overall expenses of treatment. As a result, the technology is more competitive and economical.
    - Furthermore, life cycle assessments and techno-economic studies are still needed to direct the research community's future efforts toward the critical cost elements that are most likely to improve overall economic efficiency and the environment.

- The environmental impact and contamination of hazardous substances into the environment is vital to be investigated since some semiconductor photocatalysts are small nanoparticles and may accumulate in nature over an extended period. Hence, future research must be given to the separation and recovery of photocatalysts as well as the design of large-scale photocatalytic reactors, which are important considerations.

- Exploring magnetic separation technology as a recovery technique, together with engineering and synthesizing green photocatalysts, has great economic potential to add value to organic waste. The photocatalyst's recoverability potential for reuse will also reduce operational costs and mitigate the detrimental effect of trace element pollution in wastewater settings.
- Ensuring that no catalyst or adsorbent component leaks into the water is crucial. Consequently, as cellulose is a conductive substance, a critical examination of the circular economy of recycled cellulosic nanocomposites should be taken into account while creating supercapacitors. Indeed, cellulose-supported photocatalytic materials have proven to be an excellent way to break down dangerous contaminants. Their untapped potential lies in energy conversion and production, which includes processes such as CO_2 reduction, H_2 production, and O_2 evolution. Beyond pollutant degradation, these cellulose-based polymers have potential use in the energy and environmental domains.

❖ Large and concentrated pollutants are challenging to treat using photocatalysis due to their low quantum efficiency. Reaction activity can be greatly impacted by modifications to the experimental setup as well as the high selectivity of catalysts for particular pollutants.

- Therefore, it is necessary to investigate the compatibility of photocatalysts with specified organic micropollutants (OMP) (phenols, antibiotics, pesticides, microplastics, etc.), to provide maximum degradation efficiency.
- Furthermore, the detrimental impacts of intermediate byproducts on overall production efficiency during the reaction process must be eliminated.
- More sophisticated experimental methods, including atom probe tomography, combine electron tomographic and spectroscopic instruments to provide a more accurate characterization of individual particles.

- Photocatalyst performance, synthesis efficiency, and stable application of photocatalysts are still improving and require further work to be improved. A thorough grasp of the photocatalyst's physicochemical characteristics is crucial, as is the development of better preparation techniques and materials with greater light responsiveness, more robust charge transfer pathways, and increased catalytic activity, with a longer lifetime. Addressing the constraints of the experiments and enhancing processing are also crucial, such as a post-treatment process to enhance the improvement of the water quality (colour and turbidity).

References

Abdullah, A. H., Moey, H. J. M. and Yusof, N. A. 2012. Response surface methodology analysis of the photocatalytic removal of Methylene Blue using bismuth vanadate prepared via polyol route. *Journal of Environmental Sciences*, 24 (9): 1694-1701.

Adams, E. A., Sambu, D. and Smiley, S. L. 2019. Urban water supply in Sub-Saharan Africa: historical and emerging policies and institutional arrangements. *International Journal of Water Resources Development*, 35 (2): 240-263.

Adeel, M., Saeed, M., Khan, I., Muneer, M. and Akram, N. 2021. Synthesis and characterization of Co–ZnO and evaluation of its photocatalytic activity for photodegradation of methyl orange. *ACS Omega*, 6 (2): 1426-1435.

Adom, R. K., Simatele, M. D. and Reid, M. 2023. Assessing the social and economic implications on water security in the Nelson Mandela Bay Metropolitan Municipality, Eastern Cape of South Africa. *Journal of Water and Health*, 21 (7): 939-955.

Agbajor, F. D. and Mewomo, M. C. 2024. Green building research in South Africa: A scoping review and future roadmaps. *Energy and Built Environment*, 5 (2): 316-335.

Ahmad, I., Shukrullah, S., Naz, M. Y., Ahmed, E., Ahmad, M., Obaidullah, A. J., Alkhouri, A., Mahal, A. and Ghadi, Y. Y. 2024. An aimed review of current advances, challenges, and future perspectives of TiO_2-based S-scheme heterojunction photocatalysts. *Materials Science in Semiconductor Processing*, 172: 108088.

Ahmad, I., Zou, Y., Yan, J., Liu, Y., Shukrullah, S., Naz, M. Y., Hussain, H., Khan, W. Q. and Khalid, N. R. 2023. Semiconductor photocatalysts: A critical review highlighting the various strategies to boost the photocatalytic performances for diverse applications. *Advances in Colloid and Interface Science*, 311: 102830.

Aisien, F., Amenaghawon, N. and Urhobotie, O. 2015. Potential application of a locally sourced photocatalyst for the photocatalytic decolourisation of methyl orange in aqueous solution. *Journal of Engineering Science and Technology*, 10: 1641-1653.

Aislen, E. and Aislen, F. A. 2021. Photodegradation and kinetics of edible oil refinery wastewater using titanium dioxide. *South African Journal of Science*, 117 (11-12): 1-9.

Ajibade, P. A. and Oluwalana, A. E. 2021. Enhanced photocatalytic degradation of ternary dyes by copper sulfide nanoparticles. *Nanomaterials*, 11 (8): 2000.

Akpan, U. and Hameed, B. 2010. The advancements in sol–gel method of doped-TiO_2 photocatalysts. *Applied Catalysis A: General*, 375 (1): 1-11.

Al-Nuaim, M. A., Alwasiti, A. A. and Shnain, Z. Y. 2023. The photocatalytic process in the treatment of polluted water. *Chemical Papers*, 77 (2): 677-701.

Alijani, M., Kaleji, B. K. and Rezaee, S. 2017. Highly visible-light active with Co/Sn co-doping of TiO_2 nanoparticles for degradation of methylene blue. *Journal of Materials Science: Materials in Electronics*, 28: 15345-15353.

Amano, F., Yamakata, A., Nogami, K., Osawa, M. and Ohtani, B. 2008. Visible light responsive pristine metal oxide photocatalyst: enhancement of activity by crystallization under hydrothermal treatment. *Journal of the American Chemical Society*, 130 (52): 17650-17651.

Ammar, S. H. and Abdulnabi, W. A. 2020. Synthesis, characterization and environmental remediation applications of polyoxometalates-based magnetic zinc oxide nanocomposites (Fe_3O_4@ ZnO/PMOs). *Environmental Nanotechnology, Monitoring & Management*, 13: 100289.

Ammar, S. H., Elaibi, A. I. and Mohammed, I. S. 2020. Core/shell Fe_3O_4@ Al_2O_3-PMo magnetic nanocatalyst for photocatalytic degradation of organic pollutants in an internal loop airlift reactor. *Journal of Water Process Engineering*, 37: 101240.

Ammar, S. H., Salman, M. D. and Shafi, R. F. 2021. Keggin-and Dawson-type polyoxotungstates immobilized on poly (3, 4-ethylenedioxythiophene)-coated zerovalent iron nanoparticles: Synthesis, characterization and their catalytic oxidative desulfurization activity. *Journal of Environmental Chemical Engineering*, 9 (1): 104904.

Anekwe, I. M. S., Zhou, H., Mkhize, M. M. and Akpasi, S. O. 2024. Addressing Climate Change Challenges in South Africa: A Study in KwaZulu Natal Province. *Climate Crisis: Adaptive Approaches and Sustainability*, Article ID: 475-496.

AoPs Online. 2023. *Electromagnetic spectrum*. Available: https://artofproblemsolving.com/wiki/index.php/Electromagnetic_spectrum (Accessed 16 February 2024).

Archer, E., Wolfaardt, G. M. and Van Wyk, J. H. 2017. Pharmaceutical and Personal Care Products (PPCPS) as Endocrine Disrupting Contaminants (EDCS) in South African Surface Waters. *Water SA*, 43 (4): 684-706.

Ates, N., Kaplan-Bekaroglu, S. S. and Dadaser-Celik, F. 2024. Membrane-based processes for the removal of micropollutants from wastewater. In: Bahadir, A. M., Haarstrick, A., Beduk, F. and Aydin, S. eds. *Pollutants and recent trends in wastewater treatment*. Springer, 227-241.

Aziz, N. A. A., Palaniandy, P., Aziz, H. A. and Dahlan, I. 2016. Review of the Mechanism and Operational Factors Influencing the Degradation Process of Contaminants in Heterogenous Photocatalysis. *Journal of Chemical Research*, 40 (11): 704-712.

Azmoon, P., Farhadian, M., Pendashteh, A. and Tangestaninejad, S. 2023. Adsorption and photocatalytic degradation of oilfield produced water by visible-light driven superhydrophobic composite of MIL-101(Cr)/Fe_3O_4-SiO_2: Synthesis, characterization and optimization. *Applied Surface Science*, 613: 155972.

Ba-Abbad, M. M., Kadhum, A. A. H., Mohamad, A. B., Takriff, M. S. and Sopian, K. 2012. Synthesis and catalytic activity of TiO_2 nanoparticles for photochemical oxidation of concentrated chlorophenols under direct solar radiation. *Int. J. Electrochem. Sci*, 7 (6): 4871-4888.

Barasarathi, J., Abdullah, P. S. and Uche, E. C. 2022. Application of magnetic carbon nanocomposite from agro-waste for the removal of pollutants from water and wastewater. *Chemosphere*, 305: 135384.

Bayan, E., Pustovaya, L. and Volkova, M. 2021. Recent advances in TiO_2-based materials for photocatalytic degradation of antibiotics in aqueous systems. *Environmental Technology & Innovation*, 24: 101822.

Bessekhouad, Y., Robert, D. and Weber, J. 2004. Bi_2S_3/TiO_2 and CdS/TiO_2 heterojunctions as an available configuration for photocatalytic degradation of organic pollutant. *Journal of Photochemistry and Photobiology A: Chemistry*, 163 (3): 569-580.

Bi, Z., Wang, W., Zhao, L., Wang, X., Xing, D., Zhou, Y., Lee, D.-J., Ren, N. and Chen, C. 2024. The generation and transformation mechanisms of reactive oxygen species in the environment and their implications for pollution control processes: a review. *Environmental Research*, Article ID: 119592.

Bio-Sol. 2021. The challenge of wastewater treatment around the world. *Bio-Sol* (Blog). Available: https://www.bio-sol.ca/blog/en/the-challenge-of-wastewater-treatment-around-the-world/ (Accessed 01 December 2023).

Boretti, A. and Rosa, L. 2019. Reassessing the projections of the world water development report. *NPJ Clean Water*, 2 (1): 15.

Bozzi, A., Yuranova, T. and Kiwi, J. 2005. Self-cleaning of wool-polyamide and polyester textiles by TiO_2-rutile modification under daylight irradiation at ambient temperature. *Journal of Photochemistry and Photobiology A: Chemistry*, 172 (1): 27-34.

Cabot, A., Marsal, A., Arbiol, J. and Morante, J. 2004. Bi_2O_3 as a selective sensing material for NO detection. *Sensors and Actuators B: Chemical*, 99 (1): 74-89.

Cai and Kisch, H. 2008. Visible light induced photoelectrochemical properties of n-$BiVO_4$ and n-$BiVO_4$/p-Co_3O_4. *The Journal of Physical Chemistry C*, 112 (2): 548-554.

Canizares, P., Paz, R., Sáez, C. and Rodrigo, M. A. 2009. Costs of the electrochemical oxidation of wastewaters: a comparison with ozonation and Fenton oxidation processes. *Journal of Environmental Management*, 90 (1): 410-420.

Cedeño, E., Plazas-Saldaña, J., Gordillo-Delgado, F., Bedoya, A. and Marín, E. 2018. In-situ monitoring by thermal lens microscopy of a photocatalytic reduction process of hexavalent chromium. *Revista Mexicana De Física*, 64 (5): 507-511.

Chaker, H., Ameur, N., Saidi-Bendahou, K., Djennas, M. and Fourmentin, S. 2021. Modeling and Box-Behnken design optimization of photocatalytic parameters for efficient removal of dye by lanthanum-doped mesoporous TiO_2. *Journal of Environmental Chemical Engineering*, 9 (1): 104584.

Chanathaworn, J., Bunyakan, C., Wiyaratn, W. and Chungsiriporn, J. 2012. Photocatalytic decolorization of basic dye by TiO_2 nanoparticle in photoreactor. *Songklanakarin Journal of Science & Technology*, 34 (2).

Chang, L., He, X., Chen, L. and Zhang, Y. 2017. Mercaptophenylboronic acid-capped Mn-doped ZnS quantum dots for highly selective and sensitive fluorescence detection of glycoproteins. *Sensors and Actuators B: Chemical*, 243: 72-77.

Chen, D., Cheng, Y., Zhou, N., Chen, P., Wang, Y., Li, K., Huo, S., Cheng, P., Peng, P. and Zhang, R. 2020a. Photocatalytic degradation of organic pollutants using TiO_2-based photocatalysts: A review. *Journal of Cleaner Production*, 268: 121725.

Chen, D., Cheng, Y., Zhou, N., Chen, P., Wang, Y., Li, K., Huo, S., Cheng, P., Peng, P., Zhang, R., Wang, L., Liu, H., Liu, Y. and Ruan, R. 2020b. Photocatalytic

degradation of organic pollutants using TiO_2-based photocatalysts: A review. *Journal of Cleaner Production*, 268: 121725.

Chen, X., Wang, J., Wu, H., Zhu, Z., Zhou, J. and Guo, H. 2023. Trade-off effect of dissolved organic matter on degradation and transformation of micropollutants: A review in water decontamination. *Journal of Hazardous Materials*, 450: 130996.

Cheng, J., Pan, Y., Zhu, J., Li, Z., Pan, J. and Ma, Z. 2014. Hybrid network CuS monolith cathode materials synthesized via facile in situ melt-diffusion for Li-ion batteries. *Journal of Power Sources*, 257: 192-197.

Chong, M. N., Zhu, H. and Jin, B. 2010. Response surface optimization of photocatalytic process for degradation of Congo Red using H-titanate nanofiber catalyst. *Chemical Engineering Journal*, 156 (2): 278-285.

Chun, W.-J., Ishikawa, A., Fujisawa, H., Takata, T., Kondo, J. N., Hara, M., Kawai, M., Matsumoto, Y. and Domen, K. 2003. Conduction and valence band positions of Ta_2O_5, TaON, and Ta_3N_5 by UPS and electrochemical methods. *The Journal of Physical Chemistry B*, 107 (8): 1798-1803.

City of Cape Town. 2014. *Wastewater and Industrial Effluent By-law, 2013*. Cape Town: Law Library South Africa. Available: https://openbylaws.org.za/akn/za-cpt/act/by-law/2013/wastewater-industrial-effluent/eng@2014-02-07 (Accessed 20 November 2023).

Coleman, H., Vimonses, V., Leslie, G. and Amal, R. 2007. Degradation of 1, 4-dioxane in water using TiO_2 based photocatalytic and H_2O_2/UV processes. *Journal of Hazardous Materials*, 146 (3): 496-501.

Connor, R. 2015. *The United Nations world water development report 2015: water for a sustainable world*. UNESCO publishing.

Córdova, R., Gómez, H., Schrebler, R., Cury, P., Orellana, M., Grez, P., Leinen, D., Ramos-Barrado, J. R. and Río, R. D. 2002. Electrosynthesis and electrochemical characterization of a thin phase of Cu x S (x→ 2) on ITO electrode. *Langmuir*, 18 (22): 8647-8654.

Cui, Y., Tang, Y. and Wang, X. 2015. Template-free synthesis of graphitic carbon nitride hollow spheres for photocatalytic degradation of organic pollutants. *Materials Letters*, 161: 197-200.

Das, A., Adak, M. K., Mahata, N. and Biswas, B. 2021. Wastewater treatment with the advent of TiO_2 endowed photocatalysts and their reaction kinetics with scavenger effect. *Journal of Molecular Liquids*, 338: 116479.

de Jongh, P. E., Vanmaekelbergh, D. and Kelly, J. J. 1999. Cu_2O: a catalyst for the photochemical decomposition of water? *Chemical Communications*, Article ID(12): 1069-1070.

de Mello Peters, R. F., dos Santos, P. A. M., Machado, T. C., Lopez, D. A. R., Machado, Ê. L. and Rodriguez, A. d. A. L. 2018. Photocatalytic degradation of methylene blue using TiO_2 supported in ceramic material. *Eclética Química*, 43 (1): 26-32.

Deng, F., Shi, H., Guo, Y., Luo, X. and Zhou, J. 2021. Engineering paths of sustainable and green photocatalytic degradation technology for pharmaceuticals and organic contaminants of emerging concern. *Current Opinion in Green and Sustainable Chemistry*, 29: 100465.

Dong, F., Xiong, T., Yan, S., Wang, H., Sun, Y., Zhang, Y., Huang, H. and Wu, Z. 2016. Facets and defects cooperatively promote visible light plasmonic photocatalysis with Bi nanowires@BiOCl nanosheets. *Journal of Catalysis*, 344: 401-410.

Doshi, J. and Reneker, D. H. 1995. Electrospinning process and applications of electrospun fibers. *Journal of Electrostatics*, 35 (2-3): 151-160.

du Plessis, A. 2023a. South Africa's Impending Freshwater Crises. In: *South Africa's Water Predicament*. Springer, 41-65.

du Plessis, A. 2023b. South Africa's Impending Water Crises: Transforming Water Crises into Opportunities and the Way Forward. In: *South Africa's Water Predicament: Freshwater's Unceasing Decline*. Springer, 143-170.

Edokpayi, J. N., Makungo, R., Mathivha, F., Rivers, N., Volenzo, T. and Odiyo, J. O. 2020. Influence of global climate change on water resources in South Africa: toward an adaptive management approach. In: *Water Conservation and Wastewater Treatment in BRICS Nations*. Elsevier, 83-115.

Eniola, J. O., Ansari, M. O., Barakat, M. A. and Kumar, R. 2021. Aerogels in photocatalysis. In: Khan, A. A. P., Ansari, M. O., Khan, A. and Asiri, A. M. eds. *Advances in aerogel composites for environmental remediation*. Elsevier, 87-108. Available: https://www.sciencedirect.com/science/article/pii/B9780128207321000060 (Accessed 11 January 2025).

Ensaldo-Rentería, M., Ramírez-Robledo, G., Sandoval-González, A., Pineda-Arellano, C., Álvarez-Gallegos, A., Zamudio-Lara, Á. and Silva-Martínez, S. 2018. Photoelectrocatalytic oxidation of acid green 50 dye in aqueous solution using Ti/TiO_2-NT electrode. *Journal of Environmental Chemical Engineering*, 6 (1): 1182-1188.

Ercan, Ö., Deniz, S., Yetimoğlu, E. K. and Aydın, A. 2015. Degradation of reactive dyes using advanced oxidation method. *CLEAN–Soil, Air, Water*, 43 (7): 1031-1036.

Escobar, B. M., Nieto, M. G. and García, E. H. 2005. Simple tertiary treatment systems. *Water Science and Technology: Water Supply*, 5 (3-4): 35-41.

Fallahizadeh, S., Gholami, M., Rahimi, M. R., Esrafili, A., Farzadkia, M. and Kermani, M. 2023. Enhanced photocatalytic degradation of amoxicillin using a spinning disc photocatalytic reactor (SDPR) with a novel Fe_3O_4@void@CuO/ZnO yolk-shell thin film nanostructure. *Scientific Reports*, 13 (1): 16185.

Fawzi Suleiman Khasawneh, O. and Palaniandy, P. 2021. Removal of organic pollutants from water by Fe_2O_3/TiO_2 based photocatalytic degradation: A review. *Environmental Technology & Innovation*, 21: 101230.

Feng, X., Zhang, W., Deng, H., Ni, Z., Dong, F. and Zhang, Y. 2017. Efficient visible light photocatalytic NOx removal with cationic Ag clusters-grafted (BiO) $2CO_3$ hierarchical superstructures. *Journal of Hazardous Materials*, 322: 223-232.

Fernández-López, C., Guillén-Navarro, J. M., Padilla, J. J. and Parsons, J. R. 2016. Comparison of the removal efficiencies of selected pharmaceuticals in wastewater treatment plants in the region of Murcia, Spain. *Ecological Engineering*, 95: 811-816.

Fina, F., Callear, S. K., Carins, G. M. and Irvine, J. T. 2015. Structural investigation of graphitic carbon nitride via XRD and neutron diffraction. *Chemistry of Materials*, 27 (7): 2612-2618.

Finlayson, M. F., Wheeler, B. L., Kakuta, N., Park, K. H., Bard, A. J., Campion, A., Fox, M. A., Webber, S. E. and White, J. M. 1985. Determination of flat-band position of cadmium sulfide crystals, films, and powders by photocurrent and impedance techniques, photoredox reaction mediated by intragap states. *The Journal of Physical Chemistry*, 89 (26): 5676-5681.

Forest, P. 2012. Transferring bulk water between Canada and the United States: More than a century of transboundary inter-local water supplies. *Geoforum*, 43 (1): 14-24.

Gao, M.-J., Wang, X.-D., Guo, M. and Zhang, M. 2011. Contrast on COD photo-degradation in coking wastewater catalyzed by TiO_2 and TiO_2–TiO_2 nanorod arrays. *Catalysis Today*, 174 (1): 79-87.

Gao, M., Zhang, D., Pu, X., Ding, K., Li, H., Zhang, T. and Ma, H. 2015. Combustion synthesis of Bi/BiOCl composites with enhanced electron–hole separation and excellent visible light photocatalytic properties. *Separation and Purification Technology*, 149: 288-294.

Ghamarpoor, R., Fallah, A. and Jamshidi, M. 2023. Investigating the use of titanium dioxide (TiO_2) nanoparticles on the amount of protection against UV irradiation. *Scientific Reports*, 13 (1): 9793.

Gogoi, A., Mazumder, P., Tyagi, V. K., Chaminda, G. T., An, A. K. and Kumar, M. 2018. Occurrence and fate of emerging contaminants in water environment: a review. *Groundwater for Sustainable Development*, 6: 169-180.

Gomez Cortes, L., Marinov, D., Sanseverino, I., Navarro Cuenca, A., Niegowska, M., Porcel Rodriguez, E., Stefanelli, F. and Lettieri, T. 2022. Selection of substances for the 4th Watch List under the Water Framework Directive. *Publications Office of the European Union: Luxembourg*, Article ID.

Goodarzi, N., Ashrafi-Peyman, Z., Khani, E. and Moshfegh, A. Z. 2023. Recent progress on semiconductor heterogeneous photocatalysts in clean energy production and environmental remediation. *Catalysts*, 13 (7): 1102.

Gorai, S., Ganguli, D. and Chaudhuri, S. 2005. Synthesis of copper sulfides of varying morphologies and stoichiometries controlled by chelating and nonchelating solvents in a solvothermal process. *Crystal Growth & Design*, 5 (3): 875-877.

Gottfried, A., Shepard, A., Hardiman, K. and Walsh, M. 2008. Impact of recycling filter backwash water on organic removal in coagulation–sedimentation processes. *Water Research*, 42 (18): 4683-4691.

Govindaraj, M. and Pattabhi, S. 2015. Electrochemical Treatment of Endocrine-Disrupting Chemical from Aqueous Solution. *Desalination and Water Treatment*, 53 (10): 2664-2674.

GracePavithra, K., Jaikumar, V., Kumar, P. S. and SundarRajan, P. 2019. A review on cleaner strategies for chromium industrial wastewater: Present research and future perspective. *Journal of Cleaner Production*, 228: 580-593.

Groeneveld, I., Kanelli, M., Ariese, F. and van Bommel, M. R. 2023. Parameters that affect the photodegradation of dyes and pigments in solution and on substrate – An overview. *Dyes and Pigments,* 210: 110999. Available: https://doi.org/10.1016/j.dyepig.2022.110999 (Accessed 13 January 2025).

Guo, Y., Zhu, S., Wang, B., Huang, J., Deng, S., Yu, G. and Wang, Y. 2019. Modelling of emerging contaminant removal during heterogeneous catalytic ozonation using chemical kinetic approaches. *Journal of Hazardous Materials*, 380: 120888.

Guo, Z., Kodikara, D., Albi, L. S., Hatano, Y., Chen, G., Yoshimura, C. and Wang, J. 2023. Photodegradation of organic micropollutants in aquatic environment: Importance, factors and processes. *Water Research*, 231: 118236.

Hameed, A., Montini, T., Gombac, V. and Fornasiero, P. 2008. Surface phases and photocatalytic activity correlation of Bi_2O_3/Bi_2O_4-x nanocomposite. *Journal of the American Chemical Society*, 130 (30): 9658-9659.

Haq, I. and Kalamdhad, A. S. 2021. *Emerging treatment technologies for waste management*. Springer.

Hardee, K. L. and Bard, A. J. 1977. Semiconductor electrodes: X. Photoelectrochemical behavior of several polycrystalline metal oxide electrodes in aqueous solutions. *Journal of the Electrochemical Society*, 124 (2): 215.

Hisatomi, T., Kubota, J. and Domen, K. 2014. Recent advances in semiconductors for photocatalytic and photoelectrochemical water splitting. *Chemical Society Reviews*, 43 (22): 7520-7535.

Hitam, C. N. C. and Jalil, A. A. 2020. A review on exploration of Fe_2O_3 photocatalyst towards degradation of dyes and organic contaminants. *Journal of Environmental Management*, 258: 110050.

Hong, P., Liu, J., Qin, K. X., Tian, R., Peng, L. Y., Su, Y. S., Gan, Z., Yu, X. X., Ye, L. and Zhu, M. Q. 2024. Towards Optical Information Recording: A Robust Visible-Light-Driven Molecular Photoswitch with the Ring-Closure Reaction Yield Exceeding 96.3%. *Angewandte Chemie International Edition*, 63 (8): e202316706.

Hoque, M. A. and Guzman, M. I. 2018. Photocatalytic activity: experimental features to report in heterogeneous photocatalysis. *Materials*, 11 (10): 1990.

Huang, M., Xu, C., Wu, Z., Huang, Y., Lin, J. and Wu, J. 2008. Photocatalytic discolorization of methyl orange solution by Pt modified TiO_2 loaded on natural zeolite. *Dyes and Pigments*, 77 (2): 327-334.

Huang, M., Yu, J., Li, B., Deng, C., Wang, L., Wu, W., Dong, L., Zhang, F. and Fan, M. 2015. Intergrowth and coexistence effects of TiO_2–SnO_2 nanocomposite with excellent photocatalytic activity. *Journal of Alloys and Compounds*, 629: 55-61.

Huang, Y., Wang, W., Zhang, Q., Cao, J.-j., Huang, R.-j., Ho, W. and Lee, S. C. 2016. In situ fabrication of α-Bi_2O_3/$(BiO)_2CO_3$ nanoplate heterojunctions with tunable optical property and photocatalytic activity. *Scientific Reports*, 6 (1): 23435.

Hussain, S., Khan, H., Gul, S., Steter, J. R. and Motheo, A. J. 2021. Modeling of photolytic degradation of sulfamethoxazole using boosted regression tree (BRT), artificial neural network (ANN) and response surface methodology (RSM); energy consumption and intermediates study. *Chemosphere,* 276: 130151. Available: https://doi.org/10.1016/j.chemosphere.2021.130151 (Accessed 13 January 2025).

Inturi, S. N. R., Boningari, T., Suidan, M. and Smirniotis, P. G. 2014. Visible-light-induced photodegradation of gas phase acetonitrile using aerosol-made transition metal (V, Cr, Fe, Co, Mn, Mo, Ni, Cu, Y, Ce, and Zr) doped TiO_2. *Applied Catalysis B: Environmental*, 144: 333-342.

Issakhov, A., Alimbek, A. and Abylkassymova, A. 2023. Numerical modeling of water pollution by products of chemical reactions from the activities of industrial facilities at variable and constant temperatures of the environment. *Journal of Contaminant Hydrology*, 252: 104116.

Jabbar, Z. H. and Ebrahim, S. E. 2021. Highly efficient visible-light-driven photocatalytic degradation of organic pollutants by using magnetically separable supported heterogeneous nanocomposites (SiO_2/Fe_3O_4/Ag_2WO_4). *Environmental Nanotechnology, Monitoring & Management*, 16: 100554.

Jabbar, Z. H. and Graimed, B. H. 2022. Recent developments in industrial organic degradation via semiconductor heterojunctions and the parameters affecting the photocatalytic process: A review study. *Journal of Water Process Engineering*, 47: 102671.

Jablonski, M., Ranicke, H., Qureshi, A., Purohit, H. and Reisel, J. 2016. Novel photo-fenton oxidation with sand and carbon filtration of high concentration reactive dyes both with and without biodegradation. *J. Text. Sci. Eng*, 6: 2-17.

Jallouli, N., Pastrana-Martínez, L. M., Ribeiro, A. R., Moreira, N. F., Faria, J. L., Hentati, O., Silva, A. M. and Ksibi, M. 2018. Heterogeneous Photocatalytic Degradation of Ibuprofen in Ultrapure Water, Municipal and Pharmaceutical Industry Wastewaters Using a TiO_2/UV-LED System. *Chemical Engineering Journal*, 334: 976-984.

Jiang, D., Otitoju, T. A., Ouyang, Y., Shoparwe, N. F., Wang, S., Zhang, A. and Li, S. 2021. A review on metal ions modified TiO_2 for photocatalytic degradation of organic pollutants. *Catalysts*, 11 (9): 1039.

Jiang, J.-Q., Zhou, Z. and Sharma, V. 2013. Occurrence, transportation, monitoring and treatment of emerging micro-pollutants in waste water—A review from global views. *Microchemical Journal*, 110: 292-300.

Kakavandi, B. and Ahmadi, M. 2019. Efficient treatment of saline recalcitrant petrochemical wastewater using heterogeneous UV-assisted sono-Fenton process. *Ultrasonics Sonochemistry*, 56: 25-36.

Kanemoto, M., Shiragami, T., Pac, C. and Yanagida, S. 1992. Semiconductor photocatalysis. 13. Effective photoreduction of carbon dioxide catalyzed by zinc sulfide quantum crystallites with low density of surface defects. *The Journal of Physical Chemistry*, 96 (8): 3521-3526.

Kannan, K., Radhika, D., Sadasivuni, K. K., Reddy, K. R. and Raghu, A. V. 2020. Nanostructured metal oxides and its hybrids for photocatalytic and biomedical applications. *Advances in Colloid and Interface Science*, 281: 102178.

Kassegn Weldegebrieal, G. and Kassegn Sibhatu, A. 2022. 5 Photocatalytic degradation of organic contaminants in wastewater treatment. In: *Environmental Microbiology*. 113-136.

Kaur, A. and Kansal, S. K. 2016. Bi_2WO_6 nanocuboids: an efficient visible light active photocatalyst for the degradation of levofloxacin drug in aqueous phase. *Chemical Engineering Journal*, 302: 194-203.

Khatri, K., Klein, J. A., White, M. R., Grant, O. C., Leymarie, N., Woods, R. J., Hartshorn, K. L. and Zaia, J. 2016. Integrated omics and computational glycobiology reveal structural basis for influenza A virus glycan microheterogeneity and host interactions. *Molecular & Cellular Proteomics*, 15 (6): 1895-1912.

Khodabandeloo, F., Shahsavarifar, S., Nayebi, B., Niavol, K. P., Nayebi, B., Varma, R. S., Cha, J. H., Jang, H. W., Kim, D. and Shokouhimehr, M. 2023. Applications of

nanostructured semiconductor photocatalysts for the decontamination of assorted pollutants from wastewater. *Inorganic Chemistry Communications*, 157: 111357.

Khodadoost, S., Hadi, A., Karimi-Sabet, J., Mehdipourghazi, M. and Golzary, A. 2017. Optimization of hydrothermal synthesis of Bismuth titanate nanoparticles and application for photocatalytic degradation of Tetracycline. *Journal of Environmental Chemical Engineering*, 5 (6): 5369-5380.

Kim, H. G., Hwang, D. W. and Lee, J. S. 2004. An undoped, single-phase oxide photocatalyst working under visible light. *Journal of the American Chemical Society*, 126 (29): 8912-8913.

Kim, T.-H., Lee, Y., Han, S.-H. and Hwang, S.-J. 2013. The effects of wavelength and wavelength mixing ratios on microalgae growth and nitrogen, phosphorus removal using Scenedesmus sp. for wastewater treatment. *Bioresource Technology*, 130: 75-80.

Kleywegt, S., Pileggi, V., Yang, P., Hao, C., Zhao, X., Rocks, C., Thach, S., Cheung, P. and Whitehead, B. 2011. Pharmaceuticals, hormones and bisphenol A in untreated source and finished drinking water in Ontario, Canada—occurrence and treatment efficiency. *Science of The Total Environment*, 409 (8): 1481-1488.

Kneissl, M., Seong, T.-Y., Han, J. and Amano, H. 2019. The emergence and prospects of deep-ultraviolet light-emitting diode technologies. *Nature Photonics*, 13 (4): 233-244.

Koe, W. S., Lee, J. W., Chong, W. C., Pang, Y. L. and Sim, L. C. 2020. An overview of photocatalytic degradation: photocatalysts, mechanisms, and development of photocatalytic membrane. *Environmental Science and Pollution Research,* 27 (3): 2522-2565. Available: 10.1007/s11356-019-07193-5 (Accessed 13 December 2022).

Kong, Z., Li, L., Xue, Y., Yang, M. and Li, Y.-Y. 2019. Challenges and prospects for the anaerobic treatment of chemical-industrial organic wastewater: A review. *Journal of Cleaner Production*, 231: 913-927.

Kretzmann, S. 2022. *Municipalities are failing to provide clean water. citizens are stepping in to fix the problem*. Available: https://www.groundup.org.za/article/water-in-two-thirds-municipalities-does-not-meet-minimum-standards/ (Accessed 6 March 2023).

Kudo, A. and Miseki, Y. 2009. Heterogeneous photocatalyst materials for water splitting. *Chemical Society Reviews*, 38 (1): 253-278.

Kumar, A. and Pandey, G. 2017a. The Photocatalytic Degradation of Methyl Green in Presence of Visible Light with Photoactive $Ni_{0.10}$:$La_{0.05}$:TiO_2 Nanocomposites. *IOSR Journal of Applied Chemistry*, 10 (9): 31-44.

Kumar, A. and Pandey, G. 2017b. A review on the factors affecting the photocatalytic degradation of hazardous materials. *Material Science & Engineering International Journal,* 1 (3): 106-114. Available: https://medcraveonline.com/MSEIJ/a-review-on-the-factors-affecting-the-photocatalytic-degradation-of-hazardous-materials.html#:~:text=Size%20and%20structure%20of%20the,surface%20coverage%20of%20the%20photocatalyst. (Accessed 28 May 2023).

Kumar, A. and Pandey, G. 2017c. A review on the factors affecting the photocatalytic degradation of hazardous materials. *Mater. Sci. Eng. Int. J*, 1 (3): 1-10.

Kumar, N., Jung, U., Jung, B., Park, J. and Naushad, M. 2023. Zinc hydroxystannate/zinc-tin oxide heterojunctions for the UVC-assisted photocatalytic degradation of methyl orange and tetracycline. *Environmental Pollution*, 316: 120353.

Kusiak-Nejman, E. and Morawski, A. W. 2019. TiO_2/graphene-based nanocomposites for water treatment: A brief overview of charge carrier transfer, antimicrobial and photocatalytic performance. *Applied Catalysis B: Environmental*, 253: 179-186.

Lamidi, S., Olaleye, N., Bankole, Y., Obalola, A., Aribike, E. and Adigun, I. 2022. Applications of response surface methodology (RSM) in product design, development, and process optimization. *Response Surface Methodology-Research Advances and Applications*, Article ID.

Landrigan, P. J., Fuller, R., Acosta, N. J. R., Adeyi, O., Arnold, R., Basu, N., Baldé, A. B., Bertollini, R., Bose-O'Reilly, S., Boufford, J. I., Breysse, P. N., Chiles, T., Mahidol, C., Coll-Seck, A. M., Cropper, M. L., Fobil, J., Fuster, V., Greenstone, M., Haines, A., Hanrahan, D., Hunter, D., Khare, M., Krupnick, A., Lanphear, B., Lohani, B., Martin, K., Mathiasen, K. V., McTeer, M. A., Murray, C. J. L., Ndahimananjara, J. D., Perera, F., Potočnik, J., Preker, A. S., Ramesh, J., Rockström, J., Salinas, C., Samson, L. D., Sandilya, K., Sly, P. D., Smith, K. R., Steiner, A., Stewart, R. B., Suk, W. A., van Schayck, O. C. P., Yadama, G. N., Yumkella, K. and Zhong, M. 2018. The Lancet Commission on pollution and health. *The Lancet*, 391 (10119): 462-512.

Lee, C.-G., Javed, H., Zhang, D., Kim, J.-H., Westerhoff, P., Li, Q. and Alvarez, P. J. 2018. Porous electrospun fibers embedding TiO_2 for adsorption and photocatalytic

degradation of water pollutants. *Environmental Science & Technology*, 52 (7): 4285-4293.

Leonard, L. 2023. Climate change, mining development and residential water security in the uMkhanyakude District Muncipality, KwaZulu-Natal, South Africa: a double catastrophe for local communities. *Local Environment*, 28 (3): 331-346.

Li, D., Song, H., Meng, X., Shen, T., Sun, J., Han, W. and Wang, X. 2020. Effects of particle size on the structure and photocatalytic performance by alkali-treated TiO_2. *Nanomaterials*, 10 (3): 546.

Li, X., Wen, J., Low, J., Fang, Y. and Yu, J. 2014. Design and fabrication of semiconductor photocatalyst for photocatalytic reduction of CO_2 to solar fuel. *Science China Materials*, 57: 70-100.

Li, Z.-Q., Chen, X.-T. and Xue, Z.-L. 2013. Microwave-assisted synthesis and photocatalytic properties of flower-like Bi_2WO_6 and Bi_2O_3–Bi_2WO_6 composite. *Journal of Colloid and Interface Science*, 394: 69-77.

Lim, W. P., Wong, C. T., Ang, S. L., Low, H. Y. and Chin, W. S. 2006. Phase-selective synthesis of copper sulfide nanocrystals. *Chemistry of Materials*, 18 (26): 6170-6177.

Liu, C.-C., Hsieh, Y.-H., Lai, P.-F., Li, C.-H. and Kao, C.-L. 2006. Photodegradation treatment of azo dye wastewater by UV/TiO_2 process. *Dyes and Pigments*, 68 (2-3): 191-195.

Liu, H. and Qiu, H. 2020. Recent advances of 3D graphene-based adsorbents for sample preparation of water pollutants: A review. *Chemical Engineering Journal*, 393: 124691.

Liu, H., Zhang, Z.-G., He, H.-W., Wang, X.-X., Zhang, J., Zhang, Q.-Q., Tong, Y.-F., Liu, H.-L., Ramakrishna, S. and Yan, S.-Y. 2018. One-step synthesis heterostructured g-C_3N_4/TiO_2 composite for rapid degradation of pollutants in utilizing visible light. *Nanomaterials*, 8 (10): 842.

Liu, S., Jaffrezic, N. and Guillard, C. 2008. Size effects in liquid-phase photo-oxidation of phenol using nanometer-sized TiO_2 catalysts. *Applied Surface Science*, 255 (5): 2704-2709.

Lv, Q., Si, W., He, J., Sun, L., Zhang, C., Wang, N., Yang, Z., Li, X., Wang, X. and Deng, W. 2018. Selectively nitrogen-doped carbon materials as superior metal-free catalysts for oxygen reduction. *Nature Communications*, 9 (1): 3376.

Lv, R., Cao, C., Guo, Y. and Zhu, H. 2004. Preparation of ZnS nanotubes via surfactant micelle-template inducing reaction. *Journal of Materials Science*, 39: 1575-1578.

Ma, D., Yi, H., Lai, C., Liu, X., Huo, X., An, Z., Li, L., Fu, Y., Li, B. and Zhang, M. 2021. Critical review of advanced oxidation processes in organic wastewater treatment. *Chemosphere*, 275: 130104.

Madikizela, L. M., Ncube, S. and Chimuka, L. 2020. Analysis, occurrence and removal of pharmaceuticals in African water resources: A current status. *Journal of Environmental Management*, 253: 109741.

Maeda, K., Kuriki, R., Zhang, M., Wang, X. and Ishitani, O. 2014. The effect of the pore-wall structure of carbon nitride on photocatalytic CO_2 reduction under visible light. *Journal of Materials Chemistry A*, 2 (36): 15146-15151.

Maluleke, L. 2023. South Africa's water security crisis worsens. *The Mail & Guardian*, 27 September. Available: https://mg.co.za/thoughtleader/2023-09-27-south-africas-water-security-crisis-worsens/#:~:text=Disappointingly%2C%20the%202023%20Blue%20Drop,poor%20and%2For%20critical%20condition. (Accessed 08 November 2023).

Manikandan, G., Senthil Kumar, P. and Saravanan, A. 2018. Modelling and analysis on the removal of methylene blue dye from aqueous solution using physically/chemically modified Ceiba pentandra seeds. *Journal of Industrial and Engineering Chemistry*, 62: 446-461.

Matamoros, V., Arias, C. A., Nguyen, L. X., Salvadó, V. and Brix, H. 2012. Occurrence and behavior of emerging contaminants in surface water and a restored wetland. *Chemosphere*, 88 (9): 1083-1089.

Mecha, A. C., Onyango, M. S., Ochieng, A., Fourie, C. J. S. and Momba, M. N. B. 2016. Synergistic Effect of UV–vis and Solar Photocatalytic Ozonation on the Degradation of Phenol in Municipal Wastewater: A Comparative Study. *Journal of Catalysis*, 341: 116-125.

Medeiros, R. C., de M. N. Fava, N., Freitas, B. L. S., Sabogal-Paz, L. P., Hoffmann, M. T., Davis, J., Fernandez-Ibañez, P. and Byrne, J. A. 2020. Drinking water treatment

by multistage filtration on a household scale: Efficiency and challenges. *Water Research*, 178: 115816.

Memar, A., Phan, C. M. and Tade, M. O. 2012. Influence of surfactants on Fe_2O_3 nanostructure photoanode. *International Journal of Hydrogen Energy*, 37 (22): 16835-16843.

MERCK. 2024a. *Copper (II) sulfide*. Available: https://www.sigmaaldrich.com/ZA/en/product/aldrich/342467 (Accessed 24 April 2024).

MERCK. 2024b. *Iron (III) oxide*. Available: https://www.sigmaaldrich.com/ZA/en/product/sigald/310050 (Accessed 24 April 2024).

MERCK. 2024c. *Titanium (IV) oxide*. Available: https://www.sigmaaldrich.com/ZA/en/product/sigald/14021 (Accessed 24 April 2024).

MERCK. 2024d. *Zinc sulfide*. Available: https://www.sigmaaldrich.com/ZA/en/product/sial/14459 (Accessed 24 April 2024).

Mills, A., O'Rourke, C. and Moore, K. 2015. Powder semiconductor photocatalysis in aqueous solution: An overview of kinetics-based reaction mechanisms. *Journal of Photochemistry and Photobiology A: Chemistry*, 310: 66-105.

Mirzaei, A., Yerushalmi, L., Chen, Z. and Haghighat, F. 2018. Photocatalytic degradation of sulfamethoxazole by hierarchical magnetic ZnO@g-C_3N_4: RSM optimization, kinetic study, reaction pathway and toxicity evaluation. *Journal of Hazardous Materials*, 359: 516-526.

Mishra, R. K., Mentha, S. S., Misra, Y. and Dwivedi, N. 2023. Emerging pollutants of severe environmental concern in water and wastewater: A comprehensive review on current developments and future research. *Water-Energy Nexus*, Article ID.

Mishra, S. and Sundaram, B. 2023. A review of the photocatalysis process used for wastewater treatment. *Materials Today: Proceedings*, Article ID.

Mittal, A., Brajpuriya, R. and Gupta, R. 2023. Solar steam generation using hybrid nanomaterials to address global environmental pollution and water shortage crisis. *Materials Today Sustainability*, 21: 100319.

Mohadesi, M., Sanavi Fard, M. and Shokri, A. 2022. The application of modified nano-TiO_2 photocatalyst for wastewater treatment: A review. *International Journal of Environmental Analytical Chemistry*, Article ID: 1-22.

Morshedy, A. S., El-Fawal, E. M., Zaki, T., El-Zahhar, A. A., Alghamdi, M. M. and El Naggar, A. M. A. 2024. A review on heterogeneous photocatalytic materials: Mechanism, perspectives, and environmental and energy sustainability applications. *Inorganic Chemistry Communications*, 163: 112307.

Mortazavi, S., Bakhtiari, A. R., Sari, A. E., Bahramifar, N. and Rahbarizade, F. 2012. Phenolic endocrine disrupting chemicals (EDCs) in Anzali Wetland, Iran: Elevated concentrations of 4-nonylphenol, octhylphenol and bisphenol A. *Marine Pollution Bulletin*, 64 (5): 1067-1073.

Munien, C., Tetteh, E. K., Govender, T., Jairajh, S., Mguni, L. L. and Rathilal, S. 2023. Turbidity and COD removal from municipal wastewater using a TiO_2 photocatalyst—a comparative study of UV and visible light. *Applied Sciences*, 13 (8): 4766.

Murtaza, S. Z. M., Alqassem, H. T., Sabouni, R. and Ghommem, M. 2023. Degradation of micropollutants by metal organic framework composite-based catalysts: A review. *Environmental Technology & Innovation*, 29: 102998.

Murty, M. N. and Kumar, S. 2011. Water pollution in India: an economic appraisal. *India Infrastructure Report*, 19: 285-298.

Muscetta, M., Ganguly, P. and Clarizia, L. 2024. Solar-powered photocatalysis in water purification: applications and commercialization challenges. *Journal of Environmental Chemical Engineering,* 12 (3): 113073. Available: https://doi.org/10.1016/j.jece.2024.113073 (Accessed 13 January 2025).

Mutono, N., Wright, J. A., Mutembei, H., Muema, J., Thomas, M. L., Mutunga, M. and Thumbi, S. M. 2021. The nexus between improved water supply and water-borne diseases in urban areas in Africa: a scoping review. *AAS Open Research*, 4.

Muyambo, F., Belle, J., Nyam, Y. S. and Orimoloye, I. R. 2023. Climate-change-induced weather events and implications for urban water resource management in the free state province of South Africa. *Environmental Management*, 71 (1): 40-54.

Nadeem, N., Zahid, M., Rehan, Z., Hanif, M. and Yaseen, M. 2021. Improved photocatalytic degradation of dye using coal fly ash-based zinc ferrite ($CFA/ZnFe_2O_4$) composite. *International journal of Environmental Science and Technology*, Article ID: 1-16.

Nayeemuddin, M., Palaniandya, P., Shaik, F. and Mewada, H. 2023. Experimental and computational analysis for optimization of seawater biodegradability using photo catalysis. *IIUM Engineering Journal*, 24 (2): 11-33.

Neppolian, B., Choi, H., Sakthivel, S., Arabindoo, B. and Murugesan, V. 2002. Solar/UV-induced photocatalytic degradation of three commercial textile dyes. *Journal of Hazardous Materials*, 89 (2-3): 303-317.

Ng, K. H., Cheng, Y. W., Khan, M. R. and Cheng, C. K. 2016. Optimization of photocatalytic degradation of palm oil mill effluent in UV/ZnO system based on response surface methodology. *Journal of Environmental Management*, 184: 487-493.

NuWater. 2023. *Addressing South Africa's Municipal Water Treatment Challenges*. Available: https://nuwater.com/addressing-south-africas-municipal-water-treatment-challenges/ (Accessed 08 November 2023).

Offenloch, J. T., Gernhardt, M., Blinco, J. P., Frisch, H., Mutlu, H. and Barner-Kowollik, C. 2019. Contemporary photoligation chemistry: the visible light challenge. *Chemistry–A European Journal*, 25 (15): 3700-3709.

Okolie, J. A., Epelle, E. I., Nanda, S., Castello, D., Dalai, A. K. and Kozinski, J. A. 2021. Modeling and process optimization of hydrothermal gasification for hydrogen production: A comprehensive review. *The Journal of Supercritical Fluids*, 173: 105199.

Onu, M. A., Ayeleru, O. O., Oboirien, B. and Olubambi, P. A. 2023. Challenges of wastewater generation and management in sub-Saharan Africa: A Review. *Environmental Challenges*, 11: 100686.

Opoku, F., Govender, K. K., van Sittert, C. G. C. E. and Govender, P. P. 2017. Recent progress in the development of semiconductor-based photocatalyst materials for applications in photocatalytic water splitting and degradation of pollutants. *Advanced Sustainable Systems,* 1 (7): 1-24. Available: 10.1002/adsu.201700006 (Accessed 23 September 2022).

Otitoju, T. A., Okoye, P. U., Chen, G., Li, Y., Okoye, M. O. and Li, S. 2020. Advanced ceramic components: Materials, fabrication, and applications. *Journal of Industrial and Engineering Chemistry*, 85: 34-65.

Pal, A., He, Y., Jekel, M., Reinhard, M. and Gin, K. Y.-H. 2014. Emerging contaminants of public health significance as water quality indicator compounds in the urban water cycle. *Environment International*, 71: 46-62.

Papageorgiou, M., Kosma, C. and Lambropoulou, D. 2016. Seasonal occurrence, removal, mass loading and environmental risk assessment of 55 pharmaceuticals and personal care products in a municipal wastewater treatment plant in Central Greece. *Science of The Total Environment*, 543: 547-569.

Parkavan, D., Viswanathan, K. K. and Prabakar, K. 2014. CuS nano flakes and nano platelets as counter electrode for quantum dots sensitized solar cells. *Electrochimica Acta*, 149: 364-369.

Pejman, A. H., Bidhendi, G. R. N., Karbassi, A. R., Mehrdadi, N. and Bidhendi, M. E. 2009. Evaluation of spatial and seasonal variations in surface water quality using multivariate statistical techniques. *International Journal of Environmental Science & Technology*, 6 (3): 467-476.

Philip, J. M., Aravind, U. K. and Aravindakumar, C. T. 2018. Emerging contaminants in Indian environmental matrices–a review. *Chemosphere*, 190: 307-326.

Pirsaheb, M., Moradi, S., Shahlaei, M. and Farhadian, N. 2018. Application of carbon dots as efficient catalyst for the green oxidation of phenol: kinetic study of the degradation and optimization using response surface methodology. *Journal of Hazardous Materials*, 353: 444-453.

Pravina, R., Uthayakumar, H. and Sivasamy, A. 2023. Hybrid approach based on response surface methodology and artificial neural networks coupled with genetic algorithm (RSM-GA-ANN) for the Prediction and optimization for the Photodegradation of dye using nano ZnO anchored glass fiber under solar light irradiation. *Journal of the Taiwan Institute of Chemical Engineers,* 153: 105248. Available: https://doi.org/10.1016/j.jtice.2023.105248 (Accessed 13 January 2025).

Pulido-Velazquez, M. and Ward, F. 2017. Comparison of water management institutions and approaches in the United States and Europe—What can we learn from each other? In: *Competition for Water Resources*. Elsevier, 423-441.

Qian, X., Yue, D., Tian, Z., Reng, M., Zhu, Y., Kan, M., Zhang, T. and Zhao, Y. 2016. Carbon quantum dots decorated Bi_2WO_6 nanocomposite with enhanced photocatalytic oxidation activity for VOCs. *Applied Catalysis B: Environmental*, 193: 16-21.

Qu, J., Meng, X. and You, H. 2016. Multi-stage ranking of emergency technology alternatives for water source pollution accidents using a fuzzy group decision making tool. *Journal of Hazardous Materials*, 310: 68-81.

Quansah, A., Ntaryamira, T. and Rwemera, J. 2018. Sludge wastewater management by conventional treatment process: case study-Bujumbura municipal sewage. *Int. J. Sci*, 4: 52-65.

Rajendran, H. K., Fakrudeen, M. A. D., Chandrasekar, R., Silvestri, S., Sillanpää, M. and Padmanaban, V. C. 2022. A comprehensive review on analytical and equation derived multivariate chemometrics for the accurate interpretation of the degradation of aqueous contaminants. *Environmental Technology & Innovation*, Article ID: 102827.

Rakić, T., Kasagić-Vujanović, I., Jovanović, M., Jančić-Stojanović, B. and Ivanović, D. 2014. Comparison of full factorial design, central composite design, and box-behnken design in chromatographic method development for the determination of fluconazole and its impurities. *Analytical Letters*, 47 (8): 1334-1347.

Ram, C., Zaman, B., Jena, R. K. and Kumar, A. 2021. Recent trends in solar photocatalytic degradation of organic pollutants using TiO_2 nanomaterials. In: Kumar, A. and Ram, C. eds. *Nanobiotechnology for Green Environment*. CRC Press, 165-194.

Ramalingam, G., Perumal, N., Priya, A. K. and Rajendran, S. 2022. A review of graphene-based semiconductors for photocatalytic degradation of pollutants in wastewater. *Chemosphere,* 300: 134391. Available: 10.1016/j.chemosphere.2022.134391 (Accessed 12 November 2022).

Rani, A., Reddy, R., Sharma, U., Mukherjee, P., Mishra, P., Kuila, A., Sim, L. C. and Saravanan, P. 2018. A review on the progress of nanostructure materials for energy harnessing and environmental remediation. *Journal of Nanostructure in Chemistry*, 8: 255-291.

Rani, M. and Shanker, U. 2017. Removal of carcinogenic aromatic amines by metal hexacyanoferrates nanocubes synthesized via green process. *Journal of Environmental Chemical Engineering*, 5 (6): 5298-5311.

Rao, K. V. S., Subrahmanyam, M. and Boule, P. 2004. Immobilized TiO_2 photocatalyst during long-term use: decrease of its activity. *Applied Catalysis B: Environmental*, 49 (4): 239-249.

Raza, N., Raza, W., Gul, H., Azam, M., Lee, J., Vikrant, K. and Kim, K.-H. 2020. Solar-light-active silver phosphate/titanium dioxide/silica heterostructures for photocatalytic removal of organic dye. *Journal of Cleaner Production*, 254: 120031.

Reddy, P. L., Deshmukh, K., Chidambaram, K., Ali, M. M. N., Sadasivuni, K. K., Kumar, Y. R., Lakshmipathy, R. and Pasha, S. K. 2019. Dielectric properties of polyvinyl alcohol (PVA) nanocomposites filled with green synthesized zinc sulphide (ZnS) nanoparticles. *Journal of Materials Science: Materials in Electronics*, 30: 4676-4687.

Ren, G., Han, H., Wang, Y., Liu, S., Zhao, J., Meng, X. and Li, Z. 2021. Recent advances of photocatalytic application in water treatment: A review. *Nanomaterials,* 11 (7). Available: 10.3390/nano11071804 (Accessed 13 December 2022).

Riga, A., Soutsas, K., Ntampegliotis, K., Karayannis, V. and Papapolymerou, G. 2007. Effect of system parameters and of inorganic salts on the decolorization and degradation of Procion H-exl dyes. Comparison of H_2O_2/UV, Fenton, UV/Fenton, TiO_2/UV and TiO_2/UV/H_2O_2 processes. *Desalination*, 211 (1-3): 72-86.

Riva, F., Castiglioni, S., Fattore, E., Manenti, A., Davoli, E. and Zuccato, E. 2018. Monitoring emerging contaminants in the drinking water of Milan and assessment of the human risk. *International Journal of Hygiene and Environmental Health*, 221 (3): 451-457.

Roger Williams University. n.d. *Introduction to oceanography* Available: https://rwu.pressbooks.pub/webboceanography/chapter/6-5-light/ (Accessed 18 February 2024).

Rosenfeldt, E. J., Chen, P. J., Kullman, S. and Linden, K. G. 2007. Destruction of estrogenic activity in water using UV advanced oxidation. *Science of The Total Environment*, 377 (1): 105-113.

Rozas, O., Baeza, C., Núñez, K., Rossner, A., Urrutia, R. and Mansilla, H. D. 2017. Organic micropollutants (OMPs) oxidation by ozone: Effect of activated carbon on toxicity abatement. *Science of The Total Environment*, 590: 430-439.

Saffari, R., Shariatinia, Z. and Jourshabani, M. 2020. Synthesis and photocatalytic degradation activities of phosphorus containing ZnO microparticles under visible light irradiation for water treatment applications. *Environmental pollution*, 259: 113902.

Sahoo, C. and Gupta, A. 2012. Optimization of photocatalytic degradation of methyl blue using silver ion doped titanium dioxide by combination of experimental design and response surface approach. *Journal of Hazardous Materials*, 215: 302-310.

Sakkas, V. A., Islam, M. A., Stalikas, C. and Albanis, T. A. 2010. Photocatalytic degradation using design of experiments: A review and example of the Congo red degradation. *Journal of Hazardous Materials*, 175 (1): 33-44.

Sanganyado, E. and Gwenzi, W. 2019. Antibiotic resistance in drinking water systems: Occurrence, removal, and human health risks. *Science of The Total Environment*, 669: 785-797.

Sangchay, W. and Kaewjang, S. 2016. SnO_2-doped TiO_2 nanostructured thin films with antibacterial properties. In: Proceedings of *AIP Conference Proceedings*. AIP Publishing,

Saravanan, A., Kumar, P. S., Jeevanantham, S., Karishma, S., Tajsabreen, B., Yaashikaa, P. and Reshma, B. 2021. Effective water/wastewater treatment methodologies for toxic pollutants removal: Processes and applications towards sustainable development. *Chemosphere*, 280: 130595.

Saravanan, R., Gracia, F. and Arumainathan, S. 2017. Basic principles, mechanism, and challenges of photocatalysis. In: Khan, M. M. ed. *Nanocomposites for Visible Light-induced Photocatalysis*. New York: Springer, 19-40.

Saravanan, R., Sacari, E., Gracia, F., Khan, M. M., Mosquera, E. and Gupta, V. K. 2016. Conducting PANI stimulated ZnO system for visible light photocatalytic degradation of coloured dyes. *Journal of Molecular Liquids*, 221: 1029-1033.

Sarwar, T., Shahid, M., Natasha, Khalid, S., Shah, A. H., Ahmad, N., Naeem, M. A., ul Haq, Z., Murtaza, B. and Bakhat, H. F. 2020. Quantification and risk assessment of heavy metal build-up in soil–plant system after irrigation with untreated city wastewater in Vehari, Pakistan. *Environmental Geochemistry and Health*, 42: 4281-4297.

Shafi, R. F., Ammar, S. H. and Rashed, M. K. 2021. Catalytic/photocatalytic oxidative desulfurization activities of heteropolyacid immobilized on magnetic polythiophene nanocatalyst. *Journal of Sulfur Chemistry*, 42 (4): 443-463.

Shahid, M. U., Najam, T., Helal, M. H., Hossain, I., El-Bahy, S. M., El-Bahy, Z. M., Rehman, A. u., Shah, S. S. A. and Nazir, M. A. 2024. Transition metal chalcogenides and phosphides for photocatalytic H_2 generation via water splitting: a critical review. *International Journal of Hydrogen Energy*, 62: 1113-1138.

Shaikh, G. Y., Nilegave, D. S., Girawale, S. S., Kore, K. B., Newaskar, S. R., Sahu, S. A. and Funde, A. M. 2022. Structural, Optical, Photoelectrochemical, and Electronic

Properties of the Photocathode CuS and the Efficient CuS/CdS Heterojunction. *ACS Omega*, 7 (34): 30233-30240.

Sharma, A., Ahmad, J. and Flora, S. 2018. Application of advanced oxidation processes and toxicity assessment of transformation products. *Environmental Research*, 167: 223-233.

Sharma, M., Jain, T., Singh, S. and Pandey, O. P. 2012. Photocatalytic degradation of organic dyes under UV–Visible light using capped ZnS nanoparticles. *Solar Energy*, 86 (1): 626-633.

Shehata, N., Egirani, D., Olabi, A. G., Inayat, A., Abdelkareem, M. A., Chae, K.-J. and Sayed, E. T. 2023. Membrane-based water and wastewater treatment technologies: Issues, current trends, challenges, and role in achieving sustainable development goals, and circular economy. *Chemosphere*, 320: 137993.

Shemer, H. and Linden, K. G. 2007. Aqueous photodegradation and toxicity of the polycyclic aromatic hydrocarbons fluorene, dibenzofuran, and dibenzothiophene. *Water Research*, 41 (4): 853-861.

Shinde, S., Shinde, P., Bhosale, C. and Rajpure, K. 2011. Zinc oxide mediated heterogeneous photocatalytic degradation of organic species under solar radiation. *Journal of Photochemistry and Photobiology B: Biology*, 104 (3): 425-433.

Shirzad-Siboni, M., Jonidi-Jafari, A., Farzadkia, M., Esrafili, A. and Gholami, M. 2017. Enhancement of photocatalytic activity of Cu-doped ZnO nanorods for the degradation of an insecticide: kinetics and reaction pathways. *Journal of Environmental Management*, 186: 1-11.

Shivaraju, H. 2011. Removal of Organic Pollutants in the Municipal Sewage Water by TiO_2 Based Heterogeneous Photocatalysis. *International Journal of Environmental Sciences*, 1 (5): 911-923.

Shu, H.-Y. and Chang, M.-C. 2005. Pre-ozonation coupled with UV/H_2O_2 process for the decolorization and mineralization of cotton dyeing effluent and synthesized CI Direct Black 22 wastewater. *Journal of Hazardous Materials*, 121 (1-3): 127-133.

Silva, M. R. F., Alves, M. F. R. P., Cunha, J. P. G. Q., Costa, J. L., Silva, C. A., Fernandes, M. H. V., Vilarinho, P. M. and Ferreira, P. 2023. Nanostructured transparent solutions for UV-shielding: Recent developments and future challenges. *Materials Today Physics*, 35: 101131.

Smarte Anekwe, I. M., Akpasi, S. O., Mkhize, M. M., Zhou, H., Moyo, R. T. and Gaza, L. 2024. Renewable energy investments in South Africa: Potentials and challenges for a sustainable transition-a review. *Science Progress*, 107 (2): 00368504241237347.

Sobana, N., Muruganandam, M. and Swaminathan, M. 2008. Characterization of AC–ZnO catalyst and its photocatalytic activity on 4-acetylphenol degradation. *Catalysis Communications*, 9 (2): 262-268.

Soleymani, A. R., Saien, J., Chin, S., Le, H. A., Park, E. and Jurng, J. 2015. Modeling and optimization of a sono-assisted photocatalytic water treatment process via central composite design methodology. *Process Safety and Environmental Protection*, 94: 307-314.

Son, D.-J., Kim, W.-Y., Jung, B.-R., Chang, D. and Hong, K.-H. 2020. Pilot-scale anoxic/aerobic biofilter system combined with chemical precipitation for tertiary treatment of wastewater. *Journal of Water Process Engineering*, 35: 101224.

Soni, S. S., Henderson, M. J., Bardeau, J. F. and Gibaud, A. 2008. Visible-light photocatalysis in titania-based mesoporous thin films. *Advanced Materials*, 20 (8): 1493-1498.

South Africa Bureau of Standards. 2015. *Drinking water part 1: microbiological, physical, aesthetic and chemical determinands, SANS 241-1:2015*, Article ID. Pretoria: SABS Standards Division. Available: https://libapp1.dut.ac.za/sabs/documents/SANS241-1.pdf (Accessed 02 May 2023).

Steenkamp, R. M. 2023. City-level law and governance for water security in South Africa. Article IDNorth-West University (South Africa).

Sudhaik, A., Raizada, P., Rangabhashiyam, S., Singh, A., Nguyen, V.-H., Van Le, Q., Khan, A. A. P., Hu, C., Huang, C.-W., Ahamad, T. and Singh, P. 2022. Copper sulfides based photocatalysts for degradation of environmental pollution hazards: A review on the recent catalyst design concepts and future perspectives. *Surfaces and Interfaces*, 33: 102182.

Sun, J., Qiao, L., Sun, S. and Wang, G. 2008. Photocatalytic degradation of Orange G on nitrogen-doped TiO_2 catalysts under visible light and sunlight irradiation. *Journal of Hazardous Materials*, 155 (1-2): 312-319.

Sun, J., Wang, X., Sun, J., Sun, R., Sun, S. and Qiao, L. 2006. Photocatalytic degradation and kinetics of Orange G using nano-sized Sn(IV)/TiO_2/AC photocatalyst. *Journal of Molecular Catalysis A: Chemical*, 260 (1-2): 241-246.

Sun, N., Si, X., He, L., Zhang, J. and Sun, Y. 2024. Strategies for enhancing the photocatalytic activity of semiconductors. *International Journal of Hydrogen Energy*, 58: 1249-1265.

Sun, P., Zhang, J., Liu, W., Wang, Q. and Cao, W. 2018. Modification to LH kinetics model and its application in the investigation on photodegradation of gaseous benzene by nitrogen-doped TiO_2. *Catalysts*, 8 (8): 326.

Sun, Y., Zhou, S., Pan, S.-Y., Zhu, S., Yu, Y. and Zheng, H. 2020. Performance evaluation and optimization of flocculation process for removing heavy metal. *Chemical Engineering Journal*, 385: 123911.

Sun, Z., Li, L., Yang, H., Zhou, D. and Li, H. 2016. Photocatalytic reduction of silver ion probe on nano titanium dioxide. *J. Xinyang Norm. Univ*, 29: 79-83.

Syed, M. A., Mauriya, A. K. and Shaik, F. 2022. Investigation of epoxy resin/nano-TiO_2 composites in photocatalytic degradation of organics present in oil-produced water. *International Journal of Environmental Analytical Chemistry*, 102 (16): 4518-4534.

Tang, C., Yi, Y., Yang, Z. and Sun, J. 2016. Risk analysis of emergent water pollution accidents based on a Bayesian Network. *Journal of Environmental Management*, 165: 199-205.

Tayade, R. J., Natarajan, T. S. and Bajaj, H. C. 2009. Photocatalytic Degradation of Methylene Blue Dye Using Ultraviolet Light Emitting Diodes. *Industrial & Engineering Chemistry Research*, 48 (23): 10262-10267.

Tetteh, E. K. 2022. Wastewater treatment and photo-reduction of CO_2 using an integrated magnetized TiO_2 anaerobic- photocatalytic system. PhD. Engineering & Built Environment, Durban University of Technology Available: https://hdl.handle.net/10321/4323 (Accessed 14 March 2024).

Tetteh, E. K., Ezugbe, E. O. E., Rathilal, S. and Asante-Sackey, D. 2020. Removal of COD and SO_4^{2-} from oil refinery wastewater using a photo-catalytic system—comparing TiO_2 and zeolite efficiencies. *Water*, 12: 5-14.

Tetteh, E. K., Rathilal, S. and Robinson, K. 2017. Treatment of industrial mineral oil wastewater–effects of coagulant type and dosage. *Water Practice and Technology*, 12 (1): 139-145.

Tian, J., Zhao, Z., Kumar, A., Boughton, R. I. and Liu, H. 2014. Recent progress in design, synthesis, and applications of one-dimensional TiO_2 nanostructured surface heterostructures: a review. *Chemical Society Reviews*, 43 (20): 6920-6937.

Torrens, A., de la Varga, D., Ndiaye, A. K., Folch, M. and Coly, A. 2020. Innovative multistage constructed wetland for municipal wastewater treatment and reuse for agriculture in Senegal. *Water*, 12 (11): 3139.

Toxopeüs, M. 2019. *Understanding water issues and challenges ii: municipalities and the delivery of water services*. Available: https://hsf.org.za/publications/hsf-briefs/understanding-water-issues-and-challenges-ii-municipalities-and-the-delivery-of-water-services. (Accessed 01 December 2022).

Toyoda, M., Nanbu, Y., Nakazawa, Y., Hirano, M. and Inagaki, M. 2004. Effect of crystallinity of anatase on photoactivity for methyleneblue decomposition in water. *Applied Catalysis B: Environmental*, 49 (4): 227-232.

Truppi, A., Petronella, F., Placido, T., Margiotta, V., Lasorella, G., Giotta, L., Giannini, C., Sibillano, T., Murgolo, S. and Mascolo, G. 2019. Gram-scale synthesis of UV–vis light active plasmonic photocatalytic nanocomposite based on TiO_2/Au nanorods for degradation of pollutants in water. *Applied Catalysis B: Environmental*, 243: 604-613.

Vaiano, V., Matarangolo, M., Sacco, O. and Sannino, D. 2017. Photocatalytic treatment of aqueous solutions at high dye concentration using praseodymium-doped ZnO catalysts. *Applied Catalysis B: Environmental*, 209: 621-630.

Wang, F., Yu, X., Ge, M., Wu, S., Guan, J., Tang, J., Wu, X. and Ritchie, R. O. 2019. Facile self-assembly synthesis of γ-Fe_2O_3/graphene oxide for enhanced photo-Fenton reaction. *Environmental Pollution*, 248: 229-237.

Wang, J., Zhang, Q., Deng, F., Luo, X. and Dionysiou, D. D. 2020. Rapid toxicity elimination of organic pollutants by the photocatalysis of environment-friendly and magnetically recoverable step-scheme $SnFe_2O_4$/$ZnFe_2O_4$ nano-heterojunctions. *Chemical Engineering Journal*, 379: 122264.

Wang, S., Yun, J.-H., Luo, B., Butburee, T., Peerakiatkhajohn, P., Thaweesak, S., Xiao, M. and Wang, L. 2017. Recent Progress on Visible Light Responsive Heterojunctions for Photocatalytic Applications. *Journal of Materials Science & Technology*, 33 (1): 1-22.

Wang, X., Gao, P., Li, J., Summers, C. J. and Wang, Z. L. 2002. Rectangular porous ZnO–ZnS nanocables and ZnS nanotubes. *Advanced Materials*, 14 (23): 1732-1735.

Wang, X., Maeda, K., Chen, X., Takanabe, K., Domen, K., Hou, Y., Fu, X. and Antonietti, M. 2009a. Polymer semiconductors for artificial photosynthesis: hydrogen evolution by mesoporous graphitic carbon nitride with visible light. *Journal of the American Chemical Society*, 131 (5): 1680-1681.

Wang, X., Maeda, K., Thomas, A., Takanabe, K., Xin, G., Carlsson, J. M., Domen, K. and Antonietti, M. 2009b. A metal-free polymeric photocatalyst for hydrogen production from water under visible light. *Nature Materials*, 8 (1): 76-80.

Wei, S. and Zheng, Q. 2024. Biosynthesis and characterization of zinc sulphide nanoparticles produced by the bacterium Lysinibacillus sp. SH74. *Ceramics International*, 50 (2, Part A): 2637-2642.

Wu, C.-H., Chang, H.-W. and Chern, J.-M. 2006. Basic dye decomposition kinetics in a photocatalytic slurry reactor. *Journal of Hazardous Materials*, 137 (1): 336-343.

Wu, T., Li, X., Zhang, D., Dong, F. and Chen, S. 2016. Efficient visible light photocatalytic oxidation of NO with hierarchical nanostructured 3D flower-like BiOClxBr1− x solid solutions. *Journal of Alloys and Compounds*, 671: 318-327.

Xaba, N. 2023. *The Centrality of the Water-Energy-Food Nexus in Navigating South Africa's Power Crisis*. Available: https://www.dailymaverick.co.za/opinionista/2023-02-27-the-water-energy-food-nexus-and-south-africas-energy-crisis/ (Accessed 10 March 2023).

Xiong, T., Wen, M., Dong, F., Yu, J., Han, L., Lei, B., Zhang, Y., Tang, X. and Zang, Z. 2016. Three dimensional Z-scheme $(BiO)_2CO_3/MoS_2$ with enhanced visible light photocatalytic NO removal. *Applied Catalysis B: Environmental*, 199: 87-95.

Xu, D. and Ma, H. 2021. Degradation of rhodamine B in water by ultrasound-assisted TiO2 photocatalysis. *Journal of Cleaner Production*, 313: 127758.

Yan, B., Dai, Y., Xin, L., Li, M., Zhang, H., Long, H. and Gao, X. 2024. Research progress in the degradation of printing and dyeing wastewater using chitosan based composite photocatalytic materials. *International Journal of Biological Macromolecules,* 263 (2): 130082. Available: https://doi.org/10.1016/j.ijbiomac.2024.130082 (Accessed 13 January 2025).

Yan, S., Lv, S., Li, Z. and Zou, Z. 2010. Organic–inorganic composite photocatalyst of gC_3N_4 and TaON with improved visible light photocatalytic activities. *Dalton Transactions*, 39 (6): 1488-1491.

Yang, D., He, Y., Wu, B., Deng, Y., Li, M., Yang, Q., Huang, L., Cao, Y. and Liu, Y. 2020. Drinking water and sanitation conditions are associated with the risk of malaria among children under five years old in sub-Saharan Africa: a logistic regression model analysis of national survey data. *Journal of Advanced Research*, 21: 1-13.

Yang, X., Zhao, R., Zhan, H., Zhao, H., Duan, Y. and Shen, Z. 2024. Modified Titanium dioxide-based photocatalysts for water treatment: Mini review. *Environmental Functional Materials*, 3 (1): 1-12.

Yi, Z., Ye, J., Kikugawa, N., Kako, T., Ouyang, S., Stuart-Williams, H., Yang, H., Cao, J., Luo, W. and Li, Z. 2010. An orthophosphate semiconductor with photooxidation properties under visible-light irradiation. *Nature Materials*, 9 (7): 559-564.

Yonar, T., Yonar, G. K., Kestioglu, K. and Azbar, N. 2005. Decolorisation of textile effluent using homogeneous photochemical oxidation processes. *Coloration Technology*, 121 (5): 258-264.

Zakaria, R., Youssef, Y., Hassan, I. and Eltawil, Y. 2014. Removal of organic pollutants from wastewater using an agitated batch photocatalytic reactor. *Sci-Afric Journal of Scientific Issues, Research and Essays*, 2: 323-326.

Zare, E. N., Iftekhar, S., Park, Y., Joseph, J., Srivastava, V., Khan, M. A., Makvandi, P., Sillanpaa, M. and Varma, R. S. 2021. An Overview on Non-Spherical Semiconductors for Heterogeneous Photocatalytic Degradation of Organic Water Contaminants. *Chemosphere*, 280: 130907.

Zerbo, A., Delgado, R. C. and González, P. A. 2020. A review of the risk of cholera outbreaks and urbanization in sub-Saharan Africa. *Journal of Biosafety and Biosecurity*, 2 (2): 71-76.

Zhang, F., Wang, X., Liu, H., Liu, C., Wan, Y., Long, Y. and Cai, Z. 2019a. Recent advances and applications of semiconductor photocatalytic technology. *Applied Sciences*, 9 (12): 2489.

Zhang, F., Wang, X., Liu, H., Liu, C., Wan, Y., Long, Y. and Cai, Z. 2019b. Recent advances and applications of semiconductor photocatalytic technology. *Applied Sciences*, 9 (12).

Zhang, J., Chen, X., Takanabe, K., Maeda, K., Domen, K., Epping, J. D., Fu, X., Antonietti, M. and Wang, X. 2010. Synthesis of a carbon nitride structure for visible-

light catalysis by copolymerization. *Angewandte Chemie International Edition*, 49 (2): 441-444.

Zhang, J. and Tian, H. 2018. The endeavor of diarylethenes: new structures, high performance, and bright future. *Advanced Optical Materials*, 6 (6): 1701278.

Zhang, J., Yu, J., Zhang, Y., Li, Q. and Gong, J. R. 2011. Visible light photocatalytic H_2-production activity of CuS/ZnS porous nanosheets based on photoinduced interfacial charge transfer. *Nano Letters*, 11 (11): 4774-4779.

Zhang, Y. and Shen, Y. 2019. Wastewater irrigation: past, present, and future. *Wiley Interdisciplinary Reviews: Water*, 6 (3): e1234.

Zhang, Y. Q., Zhang, B. P., Ge, Z. H., Zhu, L. F. and Li, Y. 2014. Preparation by solvothermal synthesis, growth mechanism, and photocatalytic performance of CuS nanopowders. *European Journal of Inorganic Chemistry*, 2014 (14): 2368-2375.

Zhang, Z., Wang, W., O'Hagan, M., Dai, J., Zhang, J. and Tian, H. 2022. Stepping out of the blue: from visible to near-IR triggered photoswitches. *Angewandte Chemie*, 134 (31): e202205758.

Zheng, N.-C., Ouyang, T., Chen, Y., Wang, Z., Chen, D.-Y. and Liu, Z.-Q. 2019. Ultrathin CdS shell-sensitized hollow S-doped CeO_2 spheres for efficient visible-light photocatalysis. *Catalysis Science & Technology*, 9 (6): 1357-1364.

Zhou, X., Shao, C., Li, X., Wang, X., Guo, X. and Liu, Y. 2018. Three dimensional hierarchical heterostructures of g-C_3N_4 nanosheets/TiO_2 nanofibers: controllable growth via gas-solid reaction and enhanced photocatalytic activity under visible light. *Journal of Hazardous Materials*, 344: 113-122.

Zoschke, K., Börnick, H. and Worch, E. 2014. Vacuum-UV radiation at 185 nm in water treatment–a review. *Water Research*, 52: 131-145.

Zou, Y., Zhang, Y., Hu, Y. and Gu, H. 2018. Ultraviolet detectors based on wide bandgap semiconductor nanowire: A review. *Sensors*, 18 (7): 2072.

Appendices

Appendix A: Analytical Protocols

A1. Turbidity measurement

The HI98703-02 turbidimeter was used to measure the turbidity (HANNA instruments). This equipment had a sample test cell of volume 10 mL.

I. Two (2) sample cells were used, one of which was filled with deionized water (Blank) and the other with the effluent sample to the sample cell mark.

II. The first cell was rinsed adequately with deionized water to eliminate any contaminants and thereafter filled to the sample cell mark. This sample containing deionized water is known as the (Blank).

III. The second cell was rinsed adequately with the effluent sample for reliable results and thereafter filled to the sample cell mark.

IV. The Blank cell was inserted into the meter and zeroed.

V. Thereafter, the effluent sample cell was also inserted into the meter and the reading was taken and recorded (NTU).

The turbidity removal percentages were determined by using [Equation (A-1)]:

$$\text{Turbidty removal} = \frac{T_i - T_f}{T_i} \times 100 \qquad \text{(A-1)}$$

where T_i and T_f are the initial and the final Turbidity concentrations (NTU) before and after treatment, respectively.

Figure A-1: HI98703-02 turbidimeter (HANNA instruments)

A2. Colour measurement

The colour was analyzed by Spectrophotometer DR 3900 (HACH), using the stored programs 125-colour 465 nm. This equipment had a sample test cell of volume 10 mL.

I. Two (2) sample cells were used, one of which was filled with deionized water (Blank) and the other with the effluent sample to the sample cell mark.

II. The first cell was rinsed adequately with deionized water to eliminate any contaminants and thereafter filled to the sample cell mark. This sample containing deionized water is known as the (Blank).

III. The second cell was rinsed adequately with the effluent sample for reliable results and thereafter filled to the sample cell mark.

IV. The Blank cell was inserted into the meter and zeroed.

V. Thereafter, the effluent sample cell was also inserted into the meter and the reading was taken and recorded (Pt.Co). These techniques were carried out for all the samples tested.

The colour removal percentages were determined by using [Equation (A-2)]:

$$\text{Colour removal} = \frac{\text{Cl}_\text{i} - \text{Cl}_\text{f}}{\text{Cl}_\text{i}} \times 100 \qquad \text{(A-2)}$$

where Cl_i and Cl_f are the initial and the final colour (Pt.Co) before and after treatment, respectively.

Figure A-2: Spectrophotometer DR 3900 (HACH)

A3. Chemical Oxygen Demand (COD) measurement

The COD was analyzed by the Spectrophotometer DR 3900 (HACH) illustrated in Figure A-2 above, using the stored programs 435-COD HR. This equipment had a sample test cell of volume 10 mL.

The following procedure was followed:

I. The digestor block was preheated to 150°C.
II. The caps from each COD vial were removed.
III. The vial was marked with the effluent sample ID and the other as Blank.
IV. The vial marked with the effluent sample ID was held at a 45-degree angle. Pipette 2 mL of effluent sample in the case of low range and 0.2 mL for high range, into each vial. However, a dilution factor can be used where necessary. (Note: contents of vials will become hot).
V. The reagent blank was prepared by removing the COD vial cap, repeating the above step 4, by substituting (pipetting deionized water rather than sample into the vial) the effluent sample with the reagent blank.
VI. The caps on each COD vial were secured (Note be sure not to over-tighten).
VII. Each vial was immediately inverted ten (10) times while holding it by the cap to enhance the proper mixing of the contents (Note: since again the vials will become very hot).
VIII. The vials were wiped with a damp towel and placed in the preheated digestor (Note: At least one reagent Blank must be run with each set of samples and with each new lot number of COD vials. Use a Blank vial from the same lot as the test COD vials).
IX. The vials were allowed to heat in the digestor at 150°C for 2 hours.
X. Once the time has expired, the digestor was turned off.
XI. The vials remained in the unit for 15-20 minutes to cool.
XII. Thereafter each vial was removed from the digestor using caution since the vials were still very hot.
XIII. each vial was again inverted several times while still warm (Note: Be aware that hot vials may shatter if dropped or cooled rapidly).
XIV. The vials were then placed in a rack where the vials were stored in the dark for at least 30 minutes and allowed to be cooled to room temperature.

XV. The COD program was selected on the Spectrophotometer DR 3900 (HACH) depending on the range (program 430 for Low Range or 435 for High Range).

XVI. The vials were wiped again until they were clean and dry.

XVII. The reagent Blank vial was first inserted into the sample cell compartment, and the instrument was zeroed. Thereafter, the vial was removed, the effluent sample vial was inserted, and the test reading was obtained.

The COD removal percentages were determined by using [Equation (A-3)]:

$$\text{COD removal} = \frac{C_i - C_f}{C_i} \times 100 \qquad \text{(A-3)}$$

where C_i and C_f are the initial and the final COD concentrations (mg/L) before and after treatment, respectively.

A4. Light intensity measurement

The MT940 handheld Lux meter is an accurate and delicate instrument with a durable structure. It was utilized to measure the light intensity within an environment. It provides an accurate display of light levels in terms of Lux over a wide range. This versatile meter can measure light up to 20,000 Lux. The light sensor is connected through an extension cable to the meter, providing fast measurements in the allocated environment.

I. Press the POWER button to turn on the meter.

II. Choose a suitable range and display unit.

III. Open the sensor cover, and horizontally place the sensor under the light source.

IV. Read the measurement result on the LCD.

I. If “1” is displayed on the top digit, it means overload, a higher range should be selected.

II. Press the HOLD button, the “H” symbol appears, and the current value will be held. Press HOLD again to exist in HOLD mode. Press the PEAK button, the “P-H” symbol appears, the light impulse signal can be measured, and its peak value will be held. Press the PEAK button again to exist in PEAK mode.

III. If the measurement is completed, cover the light sensor and press the POWER button to turn off the meter.

Figure A-3: Handheld Digital Lux Meter Major Tech (MT940)

A5. Sampling the municipal wastewater

Figure A-4: Sampling the municipal wastewater

Appendix B: Raw Data: Objective 1

Table B-1: Effect of catalyst load on photocatalytic treatment - Titanium Dioxide

Photocatalyst: Titanium Dioxide (TiO_2)					
	Run 1	**Run 2**	**Run 3**	**Run 4**	**Run 5**
Catalyst Load	**0.5**	**1**	**1.5**	**2**	**2.5**
pH	**7.07**	**7.14**	**7.12**	**7.02**	**6.98**
Colour	698	861	653	627	767
	708	857	658	629	769
	704	862	662	629	771
Colour Average	**703.3**	**860.0**	**657.7**	**628.3**	**769.0**
Colour % removal	**61.2**	**52.6**	**63.7**	**65.3**	**57.6**
Colour Standard Deviation	**1.7**	**0.9**	**1.5**	**0.4**	**0.7**
Turbidity	106	114	148	118	165
	107	114	151	119	166
	108	112	147	117	166
Turbidity Average	**107.0**	**113.3**	**148.7**	**118.0**	**165.7**
Turbidity % removal	**78.9**	**77.6**	**70.6**	**76.7**	**67.3**
Turbidity Standard Deviation	**0.3**	**0.4**	**0.7**	**0.3**	**0.2**
COD	1457	1545	1367	1497	1503
	1457	1554	1367	1487	1480
	1440	1530	1350	1476	1480
COD Average	**1451.3**	**1543.0**	**1361.3**	**1486.7**	**1487.7**
COD % removal	**24.5**	**19.8**	**29.2**	**22.7**	**22.6**
COD Standard Deviation	**3.3**	**4.0**	**3.3**	**3.5**	**4.4**

Table B-2: Effect of catalyst load on photocatalytic treatment - Iron (III) Oxide

Photocatalyst: Iron (III) Oxide (Fe_2O_3)					
	Run 1	**Run 2**	**Run 3**	**Run 4**	**Run 5**
Catalyst Load	**0.5**	**1**	**1.5**	**2**	**2.5**
pH	**7.19**	**7.15**	**7.13**	**7.23**	**7.16**
Colour	1013	738	775	695	773
	1003	743	778	703	783
	1005	743	781	707	791
Colour Average	**1007.0**	**741.3**	**778.0**	**701.7**	**782.3**
Colour % removal	**44.4**	**59.1**	**57.1**	**61.3**	**56.8**
Colour Standard Deviation	**1.8**	**1.0**	**1.0**	**2.0**	**3.0**
Turbidity	129	132	126	99.5	123
	128	135	127	98	126
	127	133	125	100	127
Turbidity Average	**128.0**	**133.3**	**126.0**	**99.2**	**125.3**
Turbidity % removal	**74.7**	**73.7**	**75.1**	**80.4**	**75.2**
Turbidity Standard Deviation	**0.3**	**0.5**	**0.3**	**0.3**	**0.7**
COD	1180	1355	580	1100	1240
	1168	1357	570	1093	1235
	1168	1335	585	1093	1215
COD Average	**1172.0**	**1349.0**	**578.3**	**1095.3**	**1230.0**
COD % removal	**39.1**	**29.8**	**69.9**	**43.0**	**36.0**
COD Standard Deviation	**2.3**	**4.1**	**2.5**	**1.3**	**4.4**

Table B-3: Effect of catalyst load on photocatalytic treatment - Zinc Sulphide

Photocatalyst: Zinc Sulphide (ZnS)					
	Run 1	**Run 2**	**Run 3**	**Run 4**	**Run 5**
Catalyst Load	**0.5**	**1**	**1.5**	**2**	**2.5**
pH	7	7.03	6.93	6.71	6.58
Colour	686	611	621	491	522
	703	618	617	492	525
	704	616	617	491	524
Colour Average	**697.7**	**615.0**	**618.3**	**491.3**	**523.7**
Colour % removal	**61.5**	**66.1**	**65.9**	**72.9**	**71.1**
Colour Standard Deviation	**3.4**	**1.2**	**0.8**	**0.2**	**0.5**
Turbidity	81.8	156	110	71.4	85.4
	81.4	155	103	77.1	86.9
	81.2	157	106	77.1	87.8
Turbidity Average	**81.5**	**156.0**	**106.3**	**75.2**	**86.7**
Turbidity % removal	**83.9**	**69.2**	**79.0**	**85.1**	**82.9**
Turbidity Standard Deviation	**0.1**	**0.3**	**1.2**	**1.1**	**0.4**
COD	1400	1020	1457	1580	1320
	1420	1000	1470	1580	1330
	1420	1020	1457	1572	1330
COD Average	**1413.3**	**1013.3**	**1461.3**	**1577.3**	**1326.7**
COD % removal	**26.5**	**47.3**	**24.0**	**18.0**	**31.0**
COD Standard Deviation	**3.8**	**3.8**	**2.5**	**1.5**	**1.9**

Table B-4: Effect of catalyst load on photocatalytic treatment - Copper Sulphide

Photocatalyst: Copper Sulphide (CuS)					
	Run 1	**Run 2**	**Run 3**	**Run 4**	**Run 5**
Catalyst Load	**0.5**	**1**	**1.5**	**2**	**2.5**
pH	**6.74**	**6.84**	**6.74**	**6.62**	**6.62**
Colour	**1498**	**1476**	**1138**	**1129**	**1029**
	1510	**1483**	**1136**	**1136**	**1034**
	1514	**1489**	**1137**	**1140**	**1042**
Colour Average	**1507.3**	**1482.7**	**1137.0**	**1135.0**	**1035.0**
Colour % removal	**16.8**	**18.2**	**37.3**	**37.4**	**42.9**
Colour Standard Deviation	**2.8**	**2.2**	**0.3**	**1.9**	**2.2**
Turbidity	**300**	**304**	**190**	**221**	**153**
	300	**305**	**200**	**220**	**153**
	300	**305**	**202**	**222**	**153**
Turbidity Average	**300.0**	**304.7**	**197.3**	**221.0**	**153.0**
Turbidity % removal	**40.8**	**39.8**	**61.0**	**56.4**	**69.8**
Turbidity Standard Deviation	**0.0**	**0.2**	**2.1**	**0.3**	**0.0**
COD	**765**	**530**	**526**	**337**	**490**
	790	510	522	343	486
	785	504	540	343	469
COD Average	780.0	514.7	529.3	341.0	481.7
COD % removal	**59.4**	**73.2**	**72.5**	**82.3**	**75.0**
COD Standard Deviation	**4.4**	**4.5**	**3.2**	**1.2**	**3.7**

Appendix C: Raw Data: Objective 2

Table C-1: Comparative study for UV, UV-visible, and Sunlight

Comparative study - UV, UV-visible, and Sunlight								
Light Source	TiO_2	TiO_2 SD	Fe_2O_3	Fe_2O_3 SD	ZnS	ZnS SD	CuS	CuS SD
UV	29.7	0.5	30.1	0.4	29.9	1.0	30.2	1.1
UV-visible	37.0	0.6	42.8	0.3	56.2	0.5	42.6	0.4
Sunlight	37.6	1.4	35.8	2.3	35.6	0.9	32.5	0.5

Appendix D: Raw Data: Objective 3

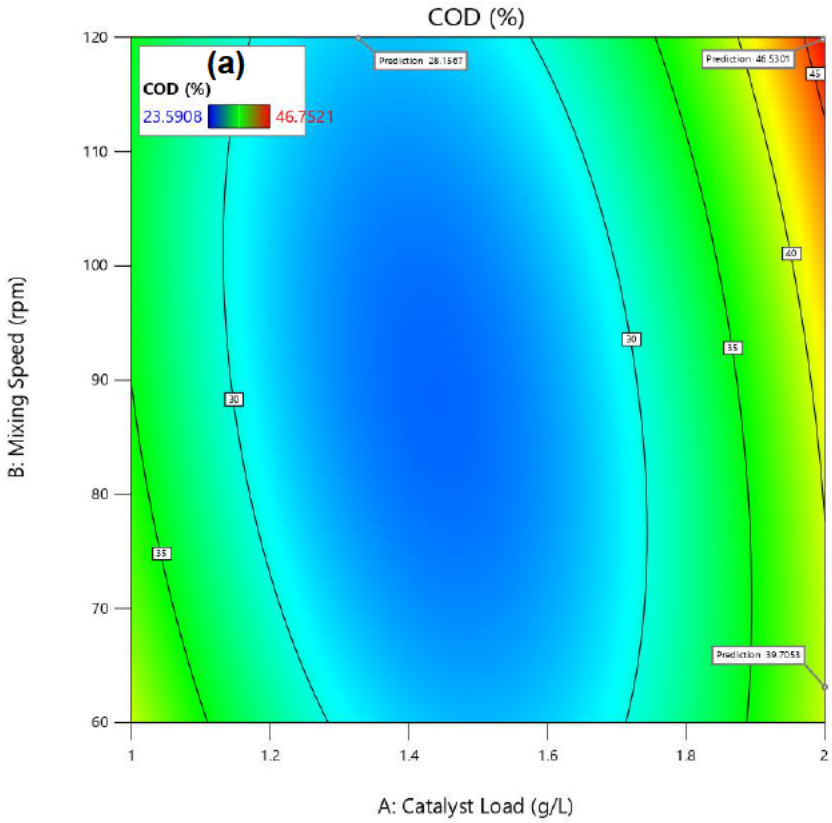

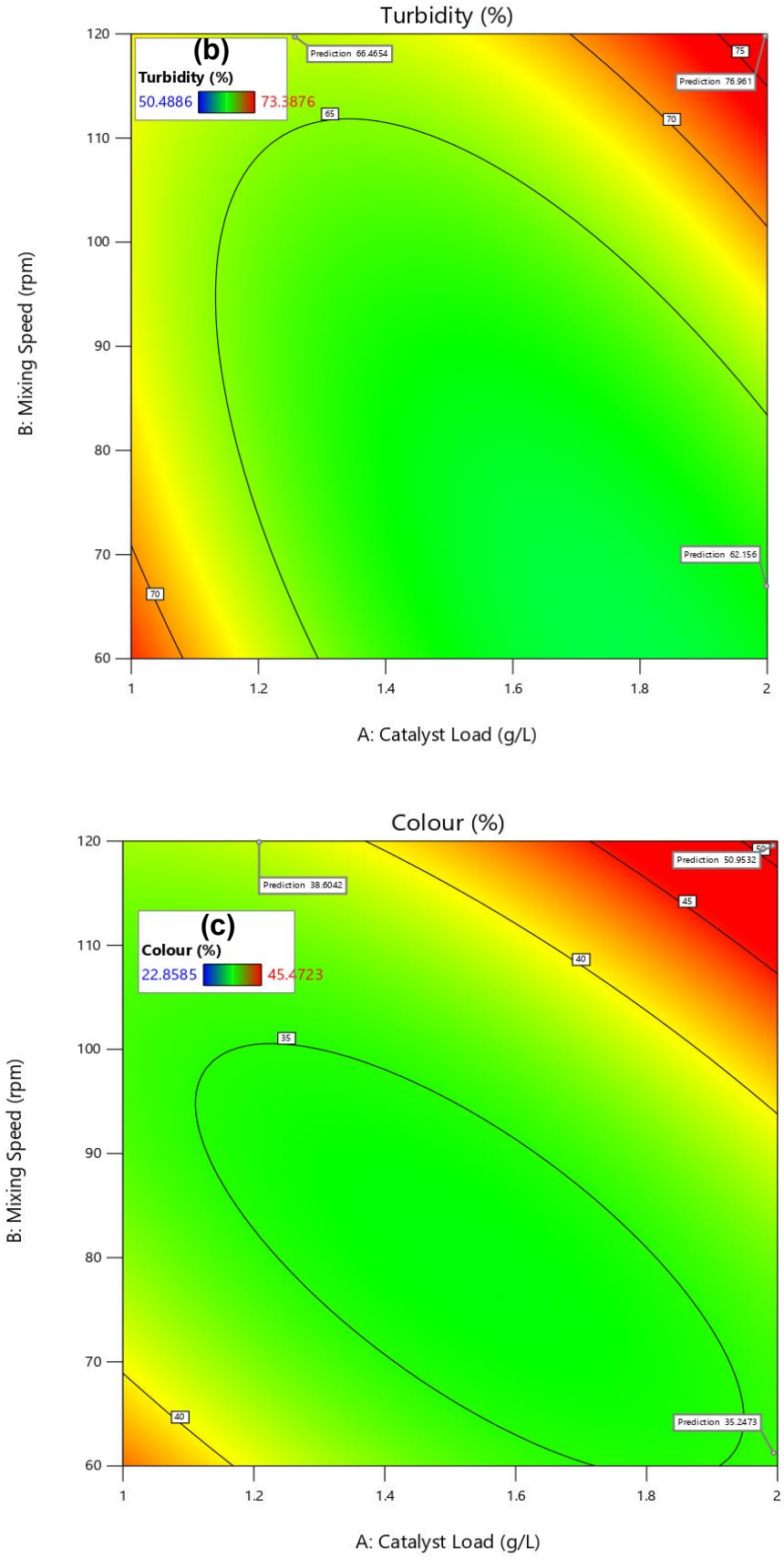

Figure D-1: 2D plot representing the cross-factor interactive effects of the interaction between catalyst load and mixing speed (AB) on (a) COD, (b) turbidity, and (c) colour removal by CuS